Examining the impact of methionine availability on T cell epigenetics

Jocelyn Chen
Master of Science

Department of Physiology
Faculty of Medicine
McGill University
Montreal, Quebec, Canada

Submitted December 2017

A thesis submitted to McGill University in
partial fulfillment of the requirements of the degree of Master of Science

Table of Contents

Abstract 3

Acknowledgements 7

Preface and Contribution of Authors 8

List of Abbreviations 9

List of Tables 13

List of Figures 14

Introduction 15

1.1 T cell biology and epigenetics 15
1.1.1 Role of T cells in immune response 15
1.1.2 $CD4^+$ T helper cell differentiation 17
1.1.3 Epigenetic regulation of T helper cell subsets 21
1.2 Metabolic pathways in T cells 27
1.2.1 Glycolysis and oxidative phosphorylation 27
1.2.2 One-carbon metabolism 31
1.2.3 Methionine cycle 34
1.2.4 Relationship between epigenetic remodeling and metabolism 35
1.3 Technical aspects of thesis 38
1.3.1 ChIP-seq 38
1.3.2 T cell intracellular cytokine staining 39
1.3.3 *In vivo* models 41
1.3.4 *Listeria monocytogenes* clearance by $CD8^+$ T cells 41
1.3.5 Induction of colitis in *Rag2*$^{-/-}$ mice 42
1.3.6 Homeostatic proliferation assay 44
1.3.7 Experimental autoimmune encephalomyelitis 46

Materials and Methods 48

Mice 48
T cell purification and culture 48
Immunoblotting 49
Histology 49
Flow cytometry 49
Infection with *L. monocytogenes* 50
Induction of colitis and homeostatic proliferation in *Rag2*$^{-/-}$ mice 50
ELISA 51
qPCR 51
Metabolomics experiments 52
LC-MS 52
GC-MS 54
Statistical analysis 55

Results 56

SAM biosynthesis is enhanced upon T cell activation 56
Methionine cycle dynamics in T cells 58

Glucose and serine contribute to SAM production, but not methionine production 59
Reduced SAM production under methionine restriction leads to decreased histone methylation 61
Methionine restriction impairs T cell growth 63
Differentiation in low methionine limits lineage-specific factors in Th17 cells 65
Acute methionine restriction decreases cytokine production, but not lineage identity 69
..... 72
Dietary methionine affects the serum levels of methionine cycle metabolites 72
Low methionine diet does not alter immune cell proportions in secondary lymphoid organs 74
..... 75
Low methionine *in vivo* does not attenuate OT-I response to *L. monocytogenes* 76
Low dietary methionine led to earlier clinical endpoints in colitic *Rag2*$^{-/-}$ mice 79
Low dietary methionine is protective for experimental autoimmune encephalomyelitis 84
Discussion 86
Serine and methionine feed different pools for one-carbon metabolism 87
Methionine availability influences T cell epigenetics 88
Regulation of SAM biosynthesis in T cells 90
Methionine availability and control of T cell epigenetics 92
Dietary methionine availability and immune responses 93
Concluding Thoughts 95

Abstract

Epigenetic modifications on DNA and histones activate or repress gene transcription by modulating chromatin accessibility to transcription machinery. This is linked to cellular metabolic state and nutrient availability through the dependence of chromatin-modifying enzymes on metabolic intermediates that serve as cofactors and substrates. The methionine cycle is particularly implicated in epigenetic control due to the production of S-adenosyl-L-methionine (SAM), the universal methyl donor for methyltransferases that modify chromatin as well as other macromolecules. As such, methionine restriction and depletion of SAM have been shown to alter epigenetic status.

Differentiated $CD4^+$ T cells with intermediate or mixed phenotypes have recently been described; these mixed cell lineages are attributed to the presence of epigenetic modifications at the loci encoding lineage-specific transcription factors and signature cytokines. Thus, we aim to establish a link between one-carbon metabolism and downstream epigenetic control of T cell phenotype to better understand lineage plasticity in T cells.

Using metabolomics approaches, we show that methionine is rapidly taken up by activated T cells and is converted to SAM. Moreover, reducing extracellular methionine decreases SAM in T cells, which translates to decreased global histone H3 methylation as shown by Western blotting. We use flow cytometry to demonstrate that methionine restriction limits T cell proliferation and differentiation to the Th17 lineage. Furthermore, acute restriction diminishes signature cytokine expression in differentiated cells. We test whether there is a defect in T cell effector function *in vivo* in C57BL/6 mice fed control or low methionine diets. Expansion of adoptively transferred $CD8^+$ OT-I T cells after infection with *Listeria monocytogenes* is not impaired. We examine two animal models of $CD4^+$ T cell-driven disease, colitis in immunodeficient mice and experimental autoimmune encephalomyelitis, to determine whether low methionine diet impacts disease onset and severity. Overall our data suggest that decreased methionine availability impacts epigenetic modifications in T cells, which is associated with impaired T cell

proliferation and differentiation *in vitro,* and dietary methionine *in vivo* may affect Th1- and Th17-mediated disease outcome.

Abrégé

Les modifications épigénétiques sur l'ADN et les histones activent ou répriment la transcription génique en modulant l'accessibilité de la chromatine aux mécanismes de transcription. Ceci est lié à l'état métabolique cellulaire et la disponibilité des nutriments par le besoin des enzymes qui modifier la chromatine pour les intermédiaires métaboliques comme les cofacteurs et les substrats. Le cycle de la méthionine est impliqué particulièrement dans le contrôle épigénétique grâce à la production du S-adénosyl-L-méthionine (SAM), le donneur universel de groupes méthyle, utilisé par les méthyltransférases qui modifient la chromatine ainsi que d'autres macromolécules. Par conséquent, la restriction de méthionine et l'épuisement du SAM ont été montrés à modifier l'état épigénétique.

Les lymphocytes T $CD4^+$ différenciés avec des phénotypes intermédiaires ou mixtes ont été décrits récemment; ces lignées cellulaires mixtes sont attribuées à la présence de modifications épigénétiques sur les loci codant pour des facteurs de transcription spécifiques ou les cytokines signatures pour chaque lignée. Donc, on tente d'établir un lien entre le métabolisme d'un-carbone et le contrôle épigénétique du phénotype des lymphocytes T afin de mieux comprendre la plasticité entre les lignées des lymphocytes T.

En utilisante des approches métabolomiques, on montre que la méthionine est importée rapidement par les lymphocytes T activées et elle est convertie au SAM. D'ailleurs, réduisant la méthionine extracellulaire diminue le SAM dans les lymphocytes T, menant à la diminution globale de la méthylation d'histone H3, comme montré par immunoblot. On utilise la cytométrie en flux pour démonstrer que la restriction de méthionine limite la prolifération des cellules T et la différenciation à la lignée Th17. En plus, restriction de méthionine aiguë diminue l'expression de cytokine signature dans les cellules différenciées. On teste s'il y a un défaut de fonction d'effecteur des lymphocytes T *in vivo* chez les souris C57BL/6 nourries les régimes contrôle ou pauvre en méthionine. L'expansion de cellules OT-I T $CD8^+$ transférées adoptivement après l'infection avec *Listeria monocytogenes* n'a pas été abîmée.

On examine l'apparition et gravité de la colite à l'induction de la maladie chez les souris immunodéficientes et dans l'encéphalomyélite autoimmune expérimentale. De bout à l'autre, les données suggèrent que la disponibilité de méthionine diminuée influe les modifications épigénétiques dans les lymphocytes T, lequel est associé avec la proliferation et la différenciation abîmées *in vitro* et la méthionine alimentaire *in vivo* peut déranger le résultat des maladies qui sont médiatisées par les cellules Th1 et Th17.

Acknowledgements

I would like to thank my supervisor, Dr. Russell Jones, for giving me the opportunity to work in his lab and for his guidance and support over the last three years. I would also like to thank my committee, Dr. Connie Krawcyzk, Dr. John White, and Dr. Vincent Giguère for their feedback at my progress meetings.

My gratitude extends to all the members of the Jones lab for teaching me and for sharing ideas and laughter through the years. Thank you to Bozena Samborska, Eric Ma, Maya Poffenberger, Said Izreig, and Takla Griss for teaching me, and to past Jones lab member Julianna Blagih for developing protocols that I used extensively. I would especially like to thank Mark Verway for his help during my undergraduate research project. Thank you also to Emma Vincent, Rebecca Rabinovitch, Alexandra Garièpy, Alison Wong, Dominic Roy, Lisa Kellenberger, and Thomas Carlo Raissi for advice, fun conversations, and moral support.

Thank you to Julien Leconte for training me in flow cytometry, for coming to the rescue when the Fortessa clogged, and for sharing his expertise in designing flow panels; to the animal care staff; and to Gaëlle Bridon for her extremely helpful, kind, and efficient instruction in metabolomics. I humbly acknowledge that my skills and knowledge are built on the contributions of others.

Of course, thank you to my friends and family outside of science who put up with my ramblings about my experiments and who supported me through this experience.

Preface and Contribution of Authors

The experiments and analysis were performed by Jocelyn Chen, Eric Ma, Mya Steadman, Radia Johnson, Maya Poffenberger, and Catherine Larochelle. Specifically, the data in Figure 7 were obtained and analyzed by Eric Ma, Mya Steadman, and Radia Johnson. I performed the experiments in Figures 8-9, with assistance from Eric Ma for GC-MS sample preparation and machine operation as well as data analysis. I obtained and analyzed the data for Figures 10-13. Maya Poffenberger assisted with dissections for the immunophenotyping experiment in Figures 14-15 and Tables 1-6. Eric Ma assisted with experiment design, tail vein injections and dissections for Figure 16 (Lm-OVA experiment) and Figure 18 (homeostatic proliferation assay). Maya Poffenberger assisted with experiment design, *in vivo* manipulations (i.p. injections), and sample collection for the colitis experiment in Figure 17. Catherine Larochelle performed the EAE experiment in Figure 19.

Samples for LC-MS were run by Gaëlle Bridon (formerly associated with the Metabolomics Core Facility) and cell sorting was performed by Julien Leconte and Vinicius Motta from the Flow Cytometry Core Facility.

List of Abbreviations

3-PG, 3-phosphoglycerate

3-PHP, 3-phosphohydroxypyruvate

3-PS, 3-phosphoserine

Acetyl-CoA, acetyl-coenzyme A

ACL, ATP citrate lyase

AMP, adenosine monophosphate

AMPK, AMP-activated protein kinase

AP-1, activator protein 1

APC, antigen-presenting cell

ATP, adenosine triphosphate

BCL6, B cell lymphoma 6

ChIP-seq, chromatin immunoprecipitation-sequencing

ChIP-PCR, chromatin immunoprecipitation-polymerase chain reaction

CNS, central nervous system

CTL, cytotoxic T lymphocyte

DC, dendritic cell

DNA, deoxyribonucleic acid

DSS, dextran sodium sulfate

EAE, experimental autoimmune encephalomyelitis

ELISA, enzyme-linked immunosorbent assay

EZH2, enhancer of zeste homolog 2

FOXO1, forkhead box O1

FoxP3, forkhead box P3

Glc, glucose

Glut1, glucose transporter 1

GSH, glutathione

HMT, histone methyltransferase

IBD, inflammatory bowel disease

ICS, intracellular cytokine staining

IFN-γ, interferon-gamma

IRF4, interferon regulatory factor 4

JAK/STAT, Janus kinase/signal transducer and activator of transcription

JHDM, Jumonji domain-containing histone demethylase

KDM, histone lysine demethylase

α-KG, alpha-ketoglutarate

LCMV, lymphocytic choriomeningitis virus

LKB1, liver kinase B1

Lm-OVA, *Listeria monocytogenes* expressing OVA

lncRNA, long non-coding RNA

MAPK, mitogen-activated protein kinase

Met, methionine

MHC, major histocompatibility complex

MID, mass isotopomer distribution

miRNA, microRNA

MLL1, mixed-lineage leukemia 1

MLN, mesenteric lymph node

MOG, myelin oligodendrocyte glycoprotein

MS, multiple sclerosis

mTORC1, mammalian target of rapamycin complex 1

NADH, nicotinamide adenine dinucleotide

NADPH, nicotinamide adenine dinucleotide phosphate

NFAT, nuclear factor of activated T cells

NF-κB, nuclear factor kappa B

NK cell, natural killer cell

OVA, ovalbumin

OXPHOS, oxidative phosphorylation

PAMP, pathogen-associated molecular pattern

PHGDH, phosphoglycerate dehydrogenase

PKC, protein kinase C

PLN, peripheral lymph node

PMA, phorbol myristate acetate

PRR, pattern recognition receptor

PSAT1, phosphoserine aminotransferase 1

PSPH, phosphoserine phosphatase

RAG, recombination activating gene

RNA, ribonucleic acid

RORγt, retinoic acid receptor-related orphan receptor gamma t

ROS, reactive oxygen species

RUNX1, runt-related transcription factor 1

SAM, S-adenosyl-L-methionine

SAH, S-adenosyl-L-homocysteine

SCID, severe combined immunodeficiency

Ser, serine

SGOC, serine, glycine, one-carbon

SHMT1/2, serine hydroxymethyltransferase 1/2

SLC7A5, solute carrier family 7 member 5

TCA, tricarboxylic acid

TCR, T cell receptor

TGF-β, transforming growth factor-beta

THF, tetrahydrofolate

TLR, toll-like receptor

TMEVPG1, Theiler's murine encephalitis virus possible gene 1

TNF-α, tumor necrosis factor-alpha

List of Tables

Table 1: Splenic immune cell composition by cell number for mice on control or low methionine feed 96

Table 2: Splenic immune cell composition by percentage for mice on control or low methionine feed 97

Table 3: Peripheral lymph node immune cell composition by cell number for mice on control or low methionine feed 98

Table 4: Peripheral lymph node immune cell composition expressed as a percentage for mice on control or low methionine feed 99

Table 5: Mesenteric lymph node immune cell composition by cell number for mice on control or low methionine feed 100

Table 6: Mesenteric lymph node immune cell composition expressed as a percentage for mice on control or low methionine feed 101

List of Figures

Figure 1. Classical T helper cell lineages 18
Figure 2. Covalent modifications on histone tails 23
Figure 3. Bivalent histone methylation facilitates T helper cell plasticity 26
Figure 4. Glycolysis and serine biosynthesis pathways 28
Figure 5: Schematic of the folate and methionine cycles 32
Figure 6. Histone demethylases depend on TCA cycle intermediates 36
Figure 7: Differential metabolite expression between naïve and activated T cells 57
Figure 8: Extracellular methionine is rapidly incorporated into the methionine cycle 58
Figure 9: Glucose and serine are incorporated into SAM 60
Figure 10: Methionine restriction decreases global histone methylation 62
Figure 11: Impaired T cell growth and cytokine production in low methionine 64
Figure 12: Low extracellular methionine reduces capacity to differentiate to Th17 lineage 68
Figure 13: Acute methionine restriction impairs production of lineage-specific cytokines 71
Figure 14: Circulating methionine levels are decreased on low methionine diet 73
Figure 15: Low methionine diet does not alter immune cell composition in secondary lymphoid organs 75
Figure 16: In vivo $CD8^+$ T_{eff} response to *L. monocytogenes* is not impaired in low methionine 78
Figure 17: Induction of colitis in *Rag2*$^{-/-}$ mice 80
Figure 18: Homeostatic proliferation assay in *Rag2*$^{-/-}$ mice 83
Figure 19: Reduced EAE severity in mice on low methionine diet 85
Figure 20: Summary of the effect of methionine cycle dynamics on T cell function 87
Figure 21: Balance between HMT and KDM activity regulates chromatin epigenetic state 91

Introduction

1.1 T cell biology and epigenetics

1.1.1 Role of T cells in immune response

The immune system is the host's defense against pathogenic microbes, toxins, and allergens. It possesses the unique ability to distinguish "self" from "non-self" in order to mount a response to eliminate foreign substances. The immune system is subdivided into the innate and adaptive immune systems, with the innate system being the fast-acting first line of defense while the adaptive response is the antigen-specific response to infection [5]. The innate and adaptive immune systems are not independent; rather, they signal to one another via cytokines and physical interactions to convey information about particular challenges to the host to potentiate the immune response.

The innate immune system consists of physical and mucosal barriers that prevent entry by foreign microbes, as well as circulating complement proteins that recognize pathogen-associated molecular patterns (PAMP) and either directly lyse microbes or recruit immune cells. The cells of the innate immune system comprise macrophages, dendritic cells (DC), neutrophils, eosinophils, natural killer cells, and others. Since the innate immune response is not antigen-specific, it is able to act rapidly, and is still able to distinguish self from non-self through the expression of pattern-recognition receptors (PRR) [6]. Macrophages and dendritic cells are phagocytic, produce cytokines and chemokines, and have PRRs, including toll-like receptors (TLR), for recognizing PAMPs. Pathogen interaction with TLRs stimulates DCs [7], consequently leading to DC maturation and migration to lymphoid tissue for antigen presentation [8]. This is the process by which antigen is taken up and processed by proteolysis to present the peptide fragments bound to major histocompatibility complex (MHC) class I or class II molecules. Dendritic cells are potent T cell activators through antigen presentation, and macrophages and monocytes are also capable of presenting antigen [5].

The adaptive immune system is antigen-specific, due to adaptive immune cells having undergone V(D)J recombination to generate unique antigen-specific receptors with broad diversity. One arm of the adaptive immune system is the humoral response, which is mediated by B lymphocytes. B cells express the B cell receptor and upon encounter and recognition of foreign antigen, they are activated and proliferate. This process is also known as clonal selection and expansion. Unlike innate immune cells, there are few adaptive immune cells that are specific for a particular pathogen, so the cells that respond (clonal selection) must proliferate (clonal expansion) to reach a sufficient cell count for effective pathogen clearance [5]; as a result, it is slower to mount a response. B cells then differentiate to plasma cells that secrete soluble antigen-specific immunoglobulins (also known as antibodies) that neutralize pathogens and toxins [6]. B cells are further subcategorized into subsets that differ in the types of antibodies that they can produce [5]. B cells are also capable of internalizing the foreign antigen that they encounter, processing it, and presenting antigen to T cells.

Antigen-presenting cells (APC) are central regulators of the adaptive immune system since they are required to activate T lymphocytes. T cells are the cell-mediated component of the adaptive immune system. They circulate the body, acting as sentinels that recognize foreign antigen presented by APCs. If a T cell is specific for antigen, it is activated and responds by blasting, proliferating, and differentiating into a lineage suited to combat the pathogen encountered [7]. This usually occurs in lymphoid tissue such as the spleen or lymph nodes [6]. Besides exerting their immediate effector functions, T cells are also critical for establishing long-term immunity through the generation of a small pool of memory T cells at the conclusion of an immune response [9, 10]. These memory cells are in a quiescent state until future encounters with the same foreign pathogen, upon which they rapidly re-express effector functions for more efficient pathogen elimination [5].

T cells express the T cell receptor and a CD4 or CD8 coreceptor. $CD8^+$ T cells are the cytotoxic T lymphocytes (CTL) which kill infected cells and recognize antigen bound to a MHC class I molecule.

$CD4^+$ T cells are the precursors to T helper cells that regulate cellular and humoral responses and respond to antigen on a MHC class II molecule [5]. There are three signals for activation. The first signal is antigen presentation of peptide bound to a self-MHC molecule to the T cell receptor. The second signal is costimulation in which CD28 on the T cell binds to B7 molecules (CD80/CD86) on the APC. In the absence of this signal, the T cell becomes anergic. Downstream of TCR interaction with the antigen peptide-MHC complex is a signaling cascade that includes phospholipase C activation, calcium signaling, protein kinase C activity, and p21, MAPK, Ras, and Rac activation which ultimately lead to lymphocyte proliferation and differentiation [5, 11]. The third signal promotes $CD8^+$ T cell expansion and tunes effector functions, and instructs $CD4^+$ T cells to differentiate. Dendritic cells secrete cytokines, or chemical messengers, that bind to cell surface receptors, dictating signaling that initiates differentiation to a particular lineage [8]. The fate that is induced is tailored to the pathogen stimulus. Thus, differentiation gives rise to an effector cell type that delivers a response to specifically target the pathogen.

1.1.2 $CD4^+$ T helper cell differentiation

$CD4^+$ T cells differentiate to specialized lineages in response to stimuli from the milieu, mediating defense against diverse pathogens. There are 4 classically defined subsets of $CD4^+$ T helper cells: Th1, Th2, Th17, and Treg cells (Figure 1). Each lineage is characterized by expression of a master regulator transcription factor that controls cytokine and receptor expression, as well as an upstream STAT protein that initiates the differentiation program [12]. Accordingly, T helper cells arise in response to different pathogens based on the cytokine profile produced by each cell type, allowing for a targeted response.

Cytokines bind to Type I/II transmembrane cytokine receptors on the cell surface and signal through the Janus kinase/signal transducer and activator of transcription (JAK/STAT) pathway [13]. The 7 members of the STAT family are important signal transducers that sense the cytokine stimulus and

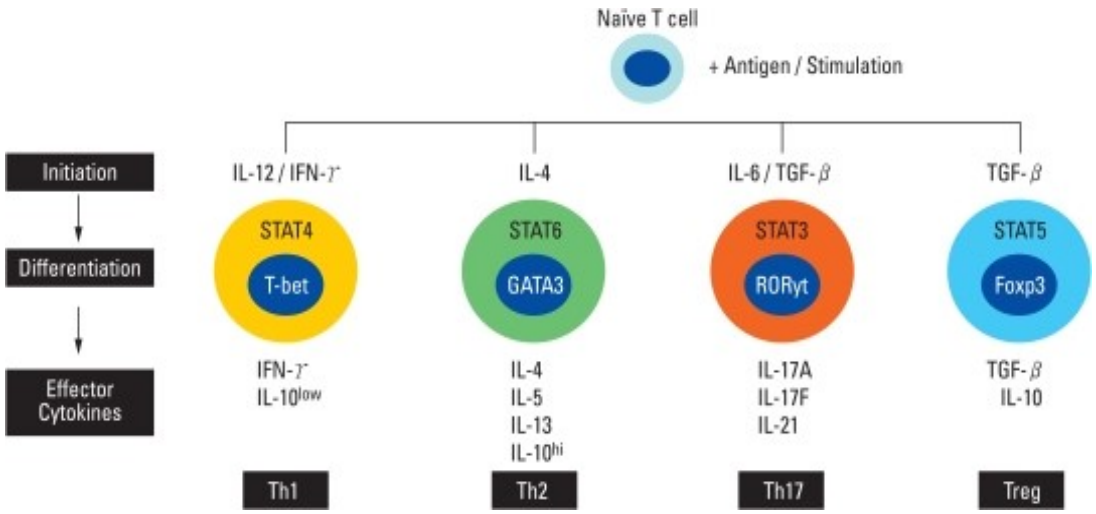

Figure 1. Classical T helper cell lineages

Naïve $CD4^+$ T helper cells initiate differentiation to a particular cell fate in response to instructive environmental stimuli. Differentiated $CD4^+$ T cells express a STAT family protein, lineage-specific transcription factor, and produce a set of signature cytokines to carry out effector functions in an antigen-specific response [2].

direct polarization to the appropriate cell fate by binding to specific sites in the genome. The STAT proteins turn on transcription of "master regulator" transcription factors, which in turn play a key role in controlling gene expression of lineage-specific signature cytokines. Upon differentiation, $CD4^+$ T cells generate a distinct cytokine response, orchestrated by the master regulator, while inhibiting production of non-lineage cytokines [14].

Th1 cells protect the host against intracellular pathogens such as bacteria and viral infections. Th1 polarization is initiated in response to IL-12, which activates STAT4. STAT4 translocates to the nucleus and turns on Th1-associated factors, including interferon-gamma (IFN-γ). IFN-γ activates and induces phosphorylation of STAT1, leading to activation of IL12Rβ as well as T box transcription factor

(T-bet, which is encoded by *Tbx21*), the master regulator for Th1 cells. T-bet induces production of the cytokines IFN-γ, tumour necrosis factor-alpha (TNF-α), and IL-2 [13]. Thus, Th1 differentiation operates on a positive feedback loop by increasing sensitivity to extracellular IL-12 and producing IFN-γ to further drive polarization. In addition to controlling production of signature cytokine IFN-γ, T-bet also cooperates with other transcription factors such as RUNX1 and BCL6 to restrict differentiation to alternate fates. Similarly, T-bet inhibits interferon regulatory factor 4 (IRF4) expression, leading to repression of Th17 signature genes. Therefore, a complex of transcription factors that interact with or that are regulated by T-bet antagonizes Th2 and Th17 differentiation by inhibiting their lineage-specific master regulators, cytokines, and other contributing factors, and thereby reinforces Th1 polarization [13, 15].

Th2 cells are induced in response to extracellular parasites such as helminths and in allergic reactions. IL-4 induces this cell fate, with STAT6 strongly driving differentiation. It was discovered in humans that up to 80% of differentially regulated genes in early Th2 polarization are associated with STAT6 [13]. The master regulator transcription factor is GATA-3 (encoded by *Gata3*). Th2 cells produce signature cytokine IL-4, as well as IL-5 and IL-13 [12-14, 16]. Thus, like Th1 cells, differentiation is supported by a positive feedback loop in which the signature cytokine produced also induces the fate of Th2 cells. GATA-3 plays a further role by binding to its own regulatory elements to heighten Th2 polarization, and represses transcription of Th1 gene *Stat4* [13, 15].

Th17 cells are involved in inflammatory immune responses and host defense against extracellular bacteria and fungi [17]. They are induced by IL-6 and transforming growth factor beta (TGF-β). STAT3 induces expression of a splice variant of retinoic acid receptor-related orphan receptor-γ (RORγt, encoded by *Rorc*) which functions as the master regulator, leading to production of signature cytokine IL-17 (IL-17A and IL-17F), as well as IL-21, IL-22, and TNF-α [13]. Th17 cells are pathogenic in several autoimmune disorders, including multiple sclerosis, experimental autoimmune encephalomyelitis [14,

18], rheumatoid arthritis [17, 19], Crohn's disease, ulcerative colitis, and systemic lupus erythematosus [19].

Regulatory T cells (Treg) are necessary to dampen the immune response, playing an important role in preventing autoimmune disease by mediating tolerance to self-antigens. Treg cells are induced by IL-2 and TGF-β, with STAT5a/b driving differentiation. They express the transcription factor forkhead box P3, FOXP3 (encoded by *Foxp3*), which is important for the homeostasis and development of Treg cells. Mutations in this key lineage-specific transcription factor result in the absence of Treg cells, which leads to systemic autoimmunity, illustrating the importance of FOXP3 [14]. FOXP3 is expressed in both natural Treg (nTreg) and induced Treg (iTreg) cells. nTreg cells are derived in the thymus and express CD25 (IL2Rα), while induced Treg cells are derived from differentiation of naïve $CD4^+$ T cells in the periphery. Despite the dominant role of FOXP3, global mapping of its binding sites in the genome suggests that other transcription factors are involved in Treg development. These include a network of EOS, IRF4 and other factors [12-14, 16].

In addition to polarizing cytokines in the milieu, the degree of TCR stimulation also contributes to T cell fate – a stronger TCR signal promotes Th1, Th17, and T follicular helper cell differentiation, while a weak TCR signal promotes Th2 and iTreg cells. Moreover, TCR signaling itself induces transcription factors that affect T helper differentiation. For example, TCR signaling induces NF-κB, NFAT, AP-1, and FOXO1, which can influence Treg development by binding to the *Foxp3* promoter or by making a physical association with the FOXP3 protein [13].

More recently, further lineages have been described. For example, Th9 cells produce IL-9 and are involved in allergic and inflammatory diseases [12]. Th9 cells reuse factors discussed for classical subsets; they are induced by IL-4 and TGF-β, leading to expression of STAT6, IRF4, and PU.1 [13]. Other new subsets are T follicular helper cells that assist B cell maturation, differentiation, and antibody responses [14, 16] and Th22 cells which produce IL-22 and are induced by IL-6 and TNF-α [13]. Along

with the classification of new subsets, recent research provides evidence for plasticity among subsets. Although the phenotype of a cell population is defined at differentiation, it must also be maintained since extrinsic factors can induce reprogramming of differentiated cells.

1.1.3 Epigenetic regulation of T helper cell subsets

Instability of phenotype has been observed after terminal differentiation of T helper cells in several cases. Th2 cells are induced to express T-bet and IFN-γ (characteristic of Th1 cells) upon lymphocytic choriomeningitis virus (LCMV) infection, while still expressing typical Th2 factors GATA-3 and IL-4 [14, 20]. Pathogenic RORγt$^+$ T-bet$^+$ double positive cells have been observed in mouse experimental autoimmune encephalomyelitis and are more pathogenic than RORγt$^+$ T-bet$^-$ cells, while RORγt$^+$ GATA-3$^+$ cells are implicated in experimental asthma [14]. Moreover, besides "double lineage" cells, the switch from one lineage to another has also been reported with the description of Th1-like ex-Th17 cells, wherein Th17 cells no longer express characteristic factors IL-17 and RORγt and instead express the Th1 transcription factor T-bet and signature cytokine IFN-γ [17]. Treg cell transfer was proposed as a therapeutic strategy for autoimmune disease, but based on a fate mapping study, it was shown that Treg cells can lose expression of FOXP3 and produce IL-17 like Th17 cells [14, 21]. Thus, differentiated T helper cells display a considerable amount of plasticity in response to environmental stimuli. It is thought that the mixed phenotype of differentiated T helper cells, having combined properties of alternate lineages, is due to epigenetic regulation.

Epigenetics is defined as heritable changes in phenotype without changes to the sequence (or primary structure) of DNA. The concept of epigenetics is important in understanding developmental biology as it is through this mechanism by which genes are selectively expressed temporally and depending on cell type [22]. Differentiated cells, including CD4$^+$ T cells, maintain their phenotype

without continuous exogenous signaling due to the pattern of epigenetic modifications in the chromatin [14].

Chromatin is the complex of DNA and histones tightly packaged in the nucleus of a cell. Nucleosomes are the "beads on a string," the basic structural unit of chromatin. Each nucleosome consists of an octamer of histones – two copies each of histones H2A, H2B, H3, and H4 – around which DNA is coiled [14]. Both the DNA and N-terminal tails of histones can be modified, affecting chromatin accessibility. A more compact or closed chromatin conformation limits access of transcription machinery to DNA leading to decreased gene expression, while an open chromatin conformation is associated with gene activation [14]. Thus, transcription factors regulate gene expression by binding to DNA and directly or indirectly controlling generation of mRNA, a process that requires epigenetic modulation of chromatin accessibility.

Cis-regulatory elements are regions of DNA, including the promoter, enhancer, silencer, insulator, and locus control regions that can influence gene expression; this can affect both nearby and distant genes due to DNA looping. *Trans*-regulatory elements such as transcription factors will bind and act upon *cis*-regulatory elements. In other words, *cis*-regulatory elements serve as sites under epigenetic control that can modulate gene expression due to modifications from *trans*-regulatory elements [13]. Chromatin modifications include DNA methylation, histone tail modifications, and non-coding RNAs [13, 22].

DNA methylation and hydroxymethylation occur primarily on the cytosine residue at CpG islands [23]. This is found primarily at promoter regions and is associated with gene silencing. The gene repression may be due to steric hindrance or a physical barrier created by the methyl groups limiting transcription machinery access to DNA or due to interaction with proteins that bind to methylated DNA [24, 25]. DNA methylation is involved in embryogenesis and gametogenesis through X-chromosome inactivation [14, 22, 25]. Thus, it is thought that DNA methylation is the most stable epigenetic mark.

Like other epigenetic marks, it is heritable, being inherited in daughter strands via DNA methyltransferase 1 [13].

A variety of covalent groups may be found on histone tails; these epigenetic modifications include acetylation, phosphorylation, and methylation (Figure 2). Serine and threonine residues on histones may be phosphorylated, while lysine residues may be acetylated [23]. Acetylation and phosphorylation directly affect the structure of chromatin: since these groups are negatively charged, electrostatic repulsion of negatively-charged DNA causes the overall structure of chromatin to relax [26]. In contrast, histone methylation, which occurs on lysine and arginine residues [23] does not alter the local charge. Instead, histone "readers" recognize and bind to the marks, and subsequently recruit other proteins to

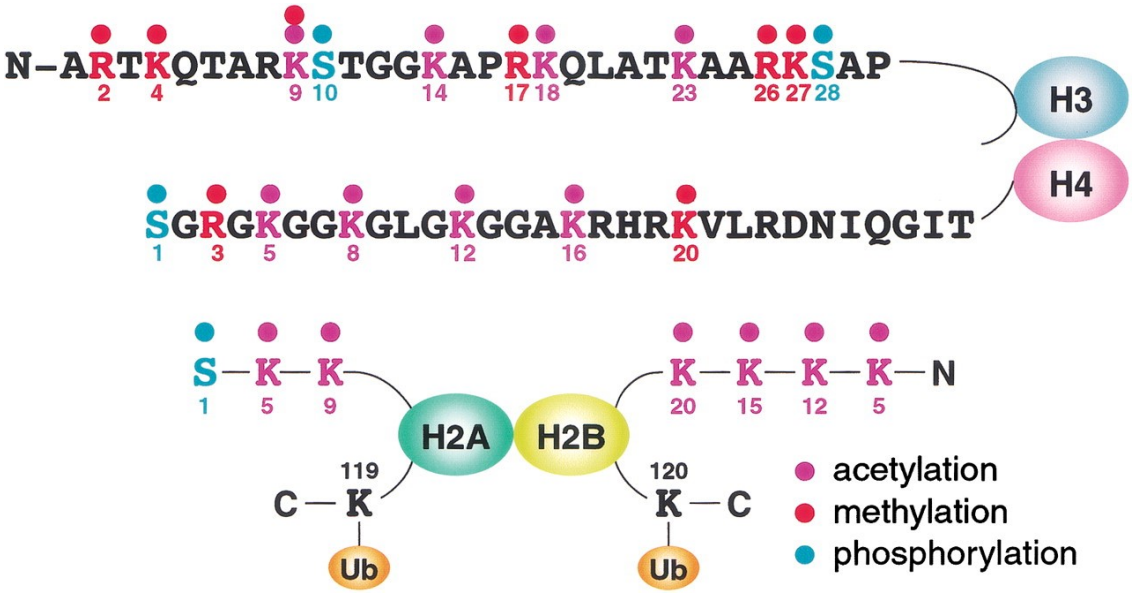

Figure 2. Covalent modifications on histone tails

The N-terminal tails of histones may be modified by acetylation, phosphorylation, and methylation, among other covalent marks. Acetyl groups occur at lysine residues and phosphorylation is found at serine residues; both promote local chromatin openness. Methylation is observed at lysine and arginine residues and serves to recruit chromatin-modifying enzymes, the effect depending on the number of methyl groups and the specific residue [3].

perform chromatin remodeling [22]. Depending on the particular histone methylation mark, the structure of chromatin may be altered to be more permissive or closed. H3K4 mono, di, and trimethylation (H3K4me1/me2/me3) are activating marks, as well as trimethylation of H3K36 and H3K79 (H3K36me3 and H3K79me3) [12]. H3K4me1 is commonly found at enhancer regions, while H3K4me3 is found at gene promoters. Rather than localization to the promoters, H3K36me3, an activating mark, is distributed along the length of gene bodies [13]. H3K9, H3K27, and H4K20 di/trimethylation are generally associated with gene silencing [12, 13, 23], and H3K9me3 is involved in constitutive heterochromatin formation and maintenance [27]. Other modifications on histones include ubiquitination and SUMOylation of lysine and arginine residues [23].

Enzymes known as “writers”, “erasers”, and “readers” are responsible for adding, removing, or detecting epigenetic modifications that lead to chromatin reorganization. These include DNA methyltransferases that add methyl groups onto DNA or DNA demethylases that remove methyl groups. Histone acetyltransferases add acetyl groups onto N-terminal tails of histones, causing the chromatin structure to relax while histone deacetylases remove acetyl groups. Similarly, there are histone methyltransferases and histone demethylases [23]. The activity of these enzymes is regulated by the availability and concentration of co-factors and substrates [23]. Due to the interplay of methyltransferases and demethylases, chromatin regulation is highly dynamic. Moreover, modifications may be made in response to exogenous signals and persist, allowing for maintenance of a differentiated state [14].

Epigenetic changes are necessary for the initial commitment to cell fate and also mediate plasticity between T helper lineages. There is evidence that direct application of epigenetic modifiers causes phenotypic changes in cells. Treatment with 5-azacytidine, a DNA methylation inhibitor, increases IL-2 and IFN-γ secretion by Th1 cells [13, 28]. Similarly, treating Th2 cells with a histone deacetylase inhibitor, which theoretically promotes a more open chromatin conformation, leads to increased IL-4 secretion [13]. These observations imply that pharmacological agents can directly

influence epigenetic remodeling and are sufficient to produce a change in cytokine profile and potentially effector function in T cells.

In naïve T cells, the loci encoding signature cytokines are associated with repressive epigenetic modifications while the "master regulator" transcription factor loci may be regulated with bivalent chromatin marks [12, 13]. Upon differentiation, distinct methylation patterns at these loci are observed, where repressive marks are removed or permissive chromatin modifications are induced, thus activating gene transcription [13]. Several reports support the fact that epigenetics plays a role in T cell differentiation. TGF-β, which induces Treg differentiation, decreases CpG island DNA methylation at the *Foxp3* locus [14] while other transcription factors induce histone acetylation at the enhancer region. Overall, these lead to increased FOXP3 expression. In Th17 cells, H3K4me3 and H3K27ac permissive marks have been observed at the *Il17a* and *Il17f* loci [16].

As mentioned earlier in this section, non-coding RNAs are also epigenetic regulators. MicroRNAs (miRNA) are non-coding short sequences of RNA of ~18-23 nucleotides. They are involved in transcriptional and post-transcriptional regulation of protein-coding genes. By binding to miRNA response elements in the 3' untranslated region of their mRNA targets, gene expression is decreased because translation is inhibited or mRNA is degraded [14, 16]. Like covalent chromatin modifications, there are documented examples of miRNA regulation of T helper differentiation. For example, miR-29 suppresses IFN-γ production and Th1 differentiation both by targeting IFN-γ message and by repressing T-bet expression. The miR-17~92 cluster promotes Th1 responses and prevents Treg differentiation. Similarly, other lineages are targeted by miRNAs through inhibition of master regulators or their cooperating transcription factors [16]. Long non-coding RNAs (lncRNA) serve as scaffolds for transcription factors or chromatin remodelers, thereby impacting expression of adjacent genes [14]. Although many lncRNAs have been revealed by RNA-seq, only few have known function. Of these, Theiler's murine encephalitis virus possible gene 1 (TMEVPG1) is expressed specifically in Th1 cells

and contributes to Th1 differentiation. It is situated near the *Ifng* locus and enhances IFN-γ expression [13, 16].

Histone methylation mapping at the proximal promoter regions of cytokine genes has identified permissive H3K4me3 methylation at lineage-specific cytokine loci along with repressive H3K27me3 methylation at the cytokine genes of opposing lineages [13]. However, for lineage-specific transcription factors, both activating and repressive histone marks are present; this is known as bivalence (Figure 3). Thus, to complete the description of chromatin landscape, there are 3 chromatin states: active, poised, and silent, where bivalence constitutes a poised state [13]. Bivalence was first described in stem cells as a phenomenon that allowed for plasticity and flexibility of gene expression [12]. In T cells, specifically,

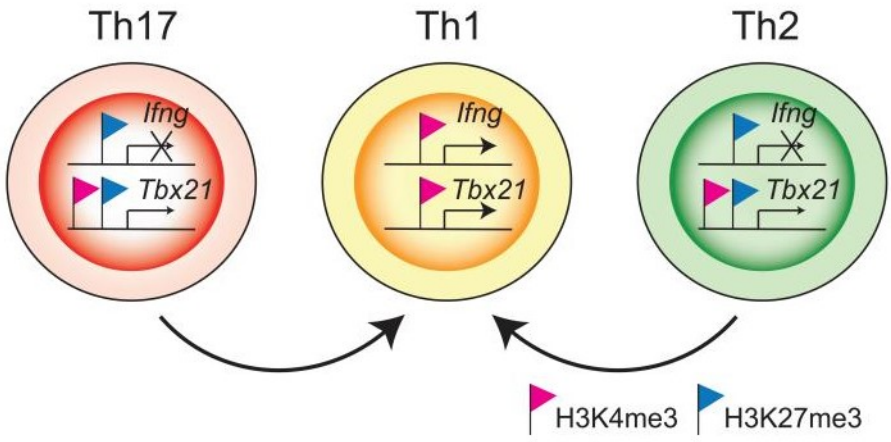

Figure 3. Bivalent histone methylation facilitates T helper cell plasticity

In Th1 cells, the *Ifng* locus encoding the signature cytokine is marked with permissive H3K4me3 histone methylation while the same locus is marked by repressive H3K27me3 methylation in opposing lineages (Th2 and Th17 cells). In contrast, the *Tbx21* locus encoding the Th1 master regulator is active in Th1 cells but possesses both activating and repressive marks in opposing lineages. Due to this bivalence in Th17 and Th2 cells, they are readily induced to expressed T-bet given the appropriate stimulus [4].

this has been reported as colocalization of H3K4me3 and H3K27me3 at promoter regions [13]. Bivalence may explain the mixed phenotypes described at the beginning of this subsection [14]. Since the transcription factor loci are in a poised state, a differentiated T cell may be readily induced to express the transcription factor of an opposing lineage given the appropriate stimulus. The epigenetic modifications that give rise to bivalence at certain loci may be controlled by STAT proteins that act upstream of lineage-specific transcription factors. ChIP-seq analysis identified STAT4 binding sites at the *Ifng* and *Tbx21* loci in Th1 cells and STAT6 binding sites at the *Il4* and *Gata3* loci in Th2 cells. Overall, STAT proteins translate an environmental cue into an appropriate, tailored $CD4^+$ response by reorganizing the epigenetic landscape [12, 14].

1.2 Metabolic pathways in T cells

1.2.1 Glycolysis and oxidative phosphorylation

Cells constantly adjust their metabolism in response to nutrient availability and extracellular signaling [23]. Naïve T cells are quiescent and circulate in a resting state, generally carrying out catabolic processes. They have low glycolytic activity and rely on oxidative phosphorylation (OXPHOS) for ATP generation, completely oxidizing glucose and producing carbon dioxide. However, during immune challenge, naïve T cells are activated by the recognition of foreign antigen and costimulation, transitioning to an activated state. Activated T cells proliferate and differentiate to generate a pool of effector T cells (T_{eff}). Both the rapid proliferation and differentiation demand increased energy expenditure and biosynthesis above the needs of naïve T cells [7, 29, 30]. Thus, the shift from naïve to effector T cells is accompanied by a necessary corresponding shift in metabolic activity in order to meet the demand for growth and to support effector functions [30]. The metabolic state of activated T cells becomes similar to cancer cells which are preferentially glycolytic, consuming large quantities of glucose

and incompletely oxidizing it to lactate [23]. Accordingly, glycolytic and glutaminolytic enzymes are upregulated upon T cell activation, while enzymes involved in fatty acid oxidation are downregulated [29, 30].

Glycolysis is the metabolic pathway through which glucose is broken down into pyruvate (Figure 4). This produces two molecules of pyruvate, two units of ATP, and two NADH molecules. The resulting pyruvate may be channeled into the tricarboxylic acid (TCA) cycle to produce NADH for oxidative phosphorylation, or it can be converted to lactate. This first fate is much more energetically efficient

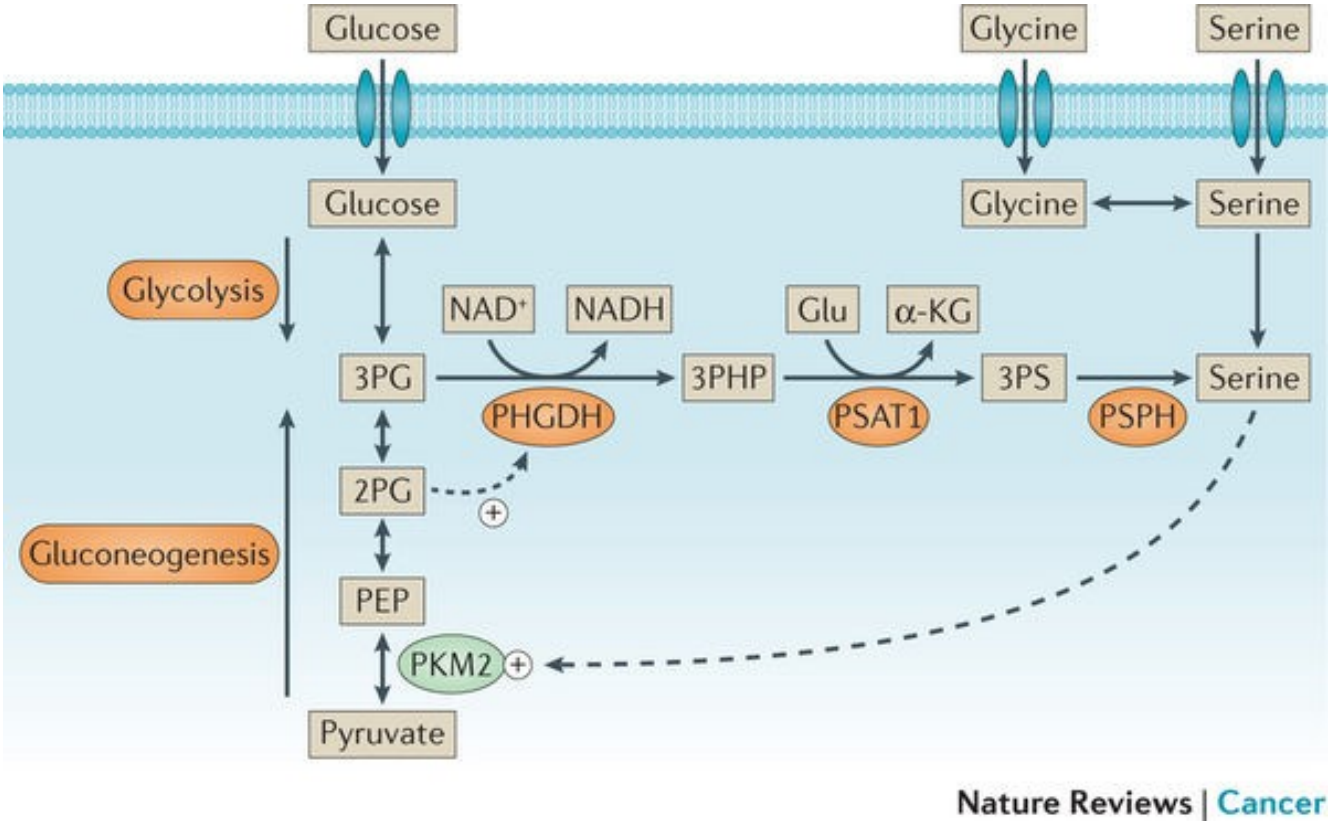

Figure 4. Glycolysis and serine biosynthesis pathways

Glucose is taken up by T cells and broken down via glycolysis to generate pyruvate, which enters the TCA cycle for further oxidation. An intermediate of the glycolytic pathway, 3-phosphoglycerate (3PG) can instead be used to generate serine [1].

since fully oxidizing glucose can produce 36 units of ATP [7, 10]. However, cancer cells preferentially undergo the second fate in the presence of adequate oxygen. This is known as "Warburg" metabolism or aerobic glycolysis. Cancer cells carry out aerobic glycolysis in which pyruvate generated from glucose is converted to and secreted as lactate rather than completely oxidized through OXPHOS using the mitochondrial electron transport chain. Cancer cells may also rely on aerobic glycolysis to prevent production and accumulation of reactive oxygen species (ROS) [31].

This phenomenon is not limited to cancer cells. Rather, it is a feature of proliferating cells, including T cells, to use aerobic glycolysis despite the decreased bioenergetic efficiency [32]. ATP production is reduced compared to glucose oxidation through OXPHOS, so to compensate for inefficient ATP generation, nutrient uptake is increased [7]. T cell receptor ligation triggers upregulation of glucose transporters, particularly Glut1, and amino acid transporters such as SLC7A5 [7, 10, 33]. Mammalian target of rapamycin (mTOR) and c-Myc are activated downstream of amino acid entry through SLC7A5, a transporter for large neutral amino acids. mTOR is a serine/threonine kinase and c-Myc is a transcription factor; both are involved in controlling growth, proliferation, and metabolic reprogramming [7, 34, 35]. Thus, while the upregulation of transporters appears to be a compensatory mechanism to adapt to the new metabolic profile, it also contributes to the effector phenotype.

The decreased bioenergetic efficiency is countered by greater biosynthetic capacity since the biomass is required to sustain generation of new cells. Enzymes that catalyze the biosynthesis of macromolecules are upregulated upon T cell activation [30]. For example, glucose shuttled into the pentose phosphate pathway produces ribose-5-phosphate and NADPH used for nucleotide biosynthesis. Dihydroxyacetone-phosphate is an intermediate of glycolysis that is used to make glycerophospholipids. Another glycolytic intermediate, 3-phosphoglycerate, is used in amino acid or nucleotide biosynthesis. Acetyl coenzyme A (acetyl-CoA) is generated for membrane biosynthesis [7]. Therefore, one of the

advantages of aerobic glycolysis is the increased generation and availability of building blocks used to create daughter cells.

For activated T cells, aerobic glycolysis is the principal pathway for glucose breakdown. Significantly, T cells that do not shift to the proper metabolism are unable to sustain effector function, although they display flexibility in metabolic profile in nutrient-limiting conditions [7, 9]. Despite T cell reliance on aerobic glycolysis upon activation, T cells also increase mitochondrial respiration [10]. OXPHOS may be involved in other processes. Evidence from the literature suggests that mitochondrial ROS generated from the electron transport chain during OXPHOS and *de novo* ATP synthesis in the mitochondria may be important for transition to the effector cell lineage [7, 10]. The balance of glycolysis to OXPHOS applies to both $CD8^+$ and differentiated $CD4^+$ T cells. Th1, Th2, and Th17 cells have high reliance on glycolytic activity, indicated by high surface expression of the glucose transporter, Glut1. In contrast, Treg cells express activated AMPK, which leads to decreased expression of Glut1 and they instead favour lipid oxidation [36]. The divergence between the T helper subsets is exemplified by the observations that Th1 differentiation, measured by T-bet expression and IFN-γ production, is suppressed upon administration of exogenous fatty acids, while Treg cells are favoured when glycolysis is blocked during Th17 differentiation [7, 36].

After carrying out effector functions and clearing pathogens, most effector T cells undergo apoptosis at the end of the immune response. A small population of antigen-specific T cells are maintained for the establishment of immunological memory. Memory T cells are in a resting state, like naïve T cells, and have a lower nutrient uptake relative to T_{eff} cells. Like naïve T cells, memory cells also rely primarily on OXPHOS and fatty acid oxidation [7, 10, 36]. However, both $CD4^+$ and $CD8^+$ memory cells have increased mitochondrial mass and spare respiratory capacity which grant them the capacity to rapidly clear future encounters of the same antigen [7, 10, 37]. One of the factors influencing the generation of $CD8^+$ memory T cells is AMP-activated protein kinase (AMPK), as shown through

treatment with metformin. Metformin is a biguanide commonly prescribed to treat type II diabetes and it activates AMPK via the upstream kinase, liver kinase B1 (LKB1) [38]. Possibly through its effect on AMPK, administration of metformin promotes the generation of $CD8^+$ memory T cells [7]. It is thought that the transition to memory T cells is mediated by the suppression/deactivation of mTOR complex 1 (mTORC1) and the corresponding switch to oxidative metabolism. This supports the correlation between memory T cell generation and AMPK activation, since AMPK is a negative regulator of mTORC1 [36]. Indeed, other suppressors of mTORC1 such as rapamycin also drive memory cell generation [7].

1.2.2 One-carbon metabolism

Besides glycolysis and oxidative phosphorylation, other metabolic pathways are involved in supporting T cell activity, including one-carbon metabolism. This metabolic network consists of the folate and methionine cycles which serve as a source of one-carbon units that are used as building blocks for macromolecules and for methylation reactions [27] (Figure 5). Serine is a non-essential amino acid that feeds into the folate cycle by donating one-carbon units [1]. It is either taken up from the environment using different neutral amino acid transporters or synthesized *de novo* from glucose through the serine biosynthesis pathway (Figure 4).

Glucose is converted to the intermediate, 3-phosphoglycerate (3PG), through glycolysis, which begins the *de novo* serine synthesis pathway. The first step is catalyzed by phosphoglycerate dehydrogenase (PHGDH), a key enzyme in serine biosynthesis because it is rate-limiting. PHGDH converts 3PG to 3-phosphohydroxypyruvate (3PHP), reducing NAD^+ to NADH in the process [1, 7]. Next, 3PHP is converted to phosphoserine (3PS) by phosphoserine aminotransferase 1 (PSAT1), producing α-ketoglutarate as a byproduct. In the third reaction, phosphoserine phosphatase (PSPH) converts 3PS to serine [1, 7, 32].

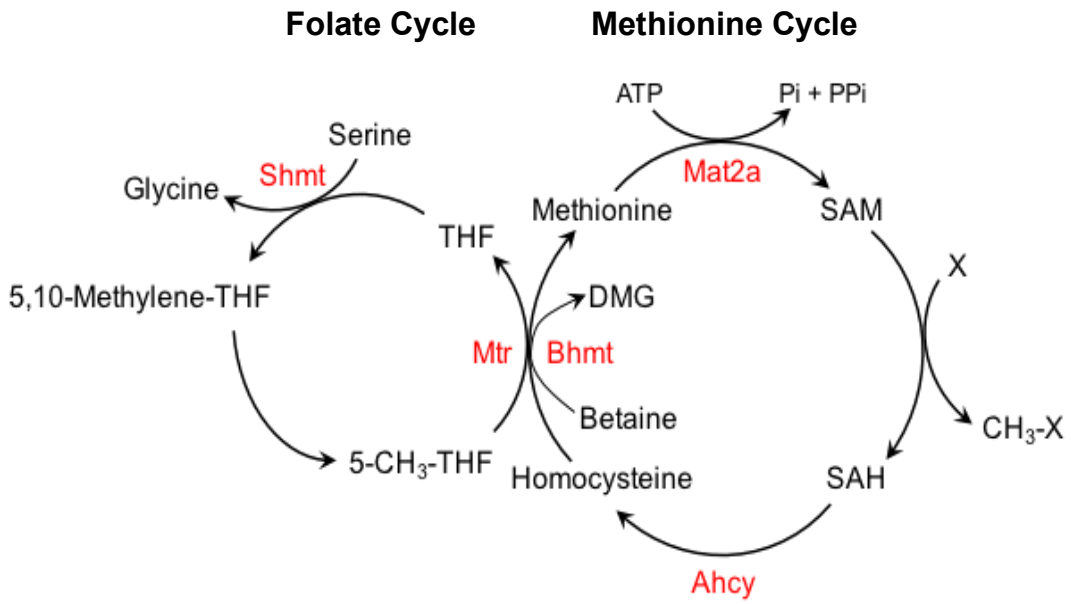

Figure 5: Schematic of the folate and methionine cycles

The folate and methionine cycles are pathways in the one-carbon metabolism network. They are involved in the generation of one carbon units used for methylation reactions or for the biosynthesis of nucleotides. This diagram shows key metabolites (black) and enzymes (red).

Subsequently, using exogenous or *de novo* serine, serine hydroxymethyltransferase (cytoplasmic SHMT1 or mitochondrial SHMT2) catalyzes the interconversion of serine and glycine. In the serine to glycine conversion reaction, tetrahydrofolate is methylated using serine as a methyl donor, producing 5,10-methylene-tetrahydrofolate (5,10-methylene-THF) and glycine. 5,10-methylene-THF, additionally produced by the glycine cleavage system to a small extent, is a folate intermediate used to fuel downstream purine nucleotide biosynthesis and consequently, proliferation [7, 31, 39, 40].

Through its role in supporting biosynthesis, one-carbon metabolism is involved in driving oncogenesis [39]. Indeed, one class of chemotherapeutic agents used in the treatment of acute lymphoblastic leukemia, lymphoma, breast cancer, and bladder cancer acts by antagonizing folate metabolism [39]. Furthermore, many cancer cells are dependent on serine; serine depletion has been

shown to impair cancer cell growth and high glycine inhibits proliferation by depleting one-carbon units needed for nucleotide biosynthesis [1, 31, 40]. The amplification of PHGDH, the first step in *de novo* serine biosynthesis, has been observed in breast cancer and melanoma, and it contributes to cancer cell proliferation [23]. Approximately half of the glucose consumption in cancer is used for serine and glycine biosynthesis, highlighting the importance of this pathway [32]. However, amplification of serine biosynthesis pathway components resulted in lower survival in breast cancer patients. *De novo* generated serine can be further used in biosynthetic reactions – in particular, nucleotide biosynthesis – or used for the production of reduced glutathione (GSH), which is involved in cellular protection against oxidative stress. Moreover, PHGDH produces NADH, which contributes to antioxidant defense along with GSH, allowing cancer cells to cope with the oxidative stress that arises from amino acid biosynthesis. Alternatively, the NADH can be used to generate ATP through mitochondrial OXPHOS, supporting the bioenergetic demands of cancer cells [1, 10, 23].

As both activated T cells and cancer cells are highly proliferative and use aerobic glycolysis, it is hypothesized that the serine biosynthesis pathway plays a similar beneficial role in T cells. Indeed, upon T cell activation, enzymes of the serine, glycine, one-carbon (SGOC) metabolic network are upregulated. Recent work has shown that T cells readily take up the non-essential amino acid serine or synthesize it *de novo* from glucose. Serine is incorporated into the folate cycle but not the methionine cycle. Moreover, serine facilitates T cell proliferation by contributing to the one-carbon pool for nucleotide synthesis, which in turn supports DNA synthesis. In limiting exogenous serine, proliferation is impaired; this is observed *in vitro* even in the presence of full glucose. The proliferation defect is true as well in *in vivo* murine models using a serine/glycine-free diet. Mice that were maintained on a low serine/glycine diet displayed fewer cytokine-producing $CD8^+$ T cells upon infection with *Listeria monocytogenes* and a weakened memory response upon re-challenge [29].

Since one-carbon metabolism also provides substrates for methylation reactions, it has been linked to cellular epigenetic status and genome maintenance [39]. It has been shown by *in vivo* isotope tracing studies that the methyl groups contributing to methionine regeneration from homocysteine are largely derived by serine, but the folate and methionine cycles can become uncoupled [1, 41]. That is, rather than via the re-methylation of homocysteine, serine instead contributes to S-adenosyl-L-methionine (SAM) through the generation of ATP [1, 28]. Thus, nucleotide biosynthesis also serves as the link between the folate and methionine cycles through ATP incorporation into the methionine cycle. ATP is used to adenylate methionine to generate the methionine cycle intermediate and universal methyl donor SAM [27].

Finally, the methionine cycle is linked to a third component of one-carbon metabolism: the transsulfuration pathway. Homocysteine is an intermediate of the methionine cycle and the starting point for the transsulfuration pathway. The combination of homocysteine and serine produces cysteine and glutathione, a tripeptide of cysteine, glycine, and glutamate [1, 39].

1.2.3 Methionine cycle

The methionine cycle is one of the branches of one-carbon metabolism that is involved in synthesizing amino acids and lipids and describes the generation of methyl groups from the essential amino acid, methionine [29]. In this pathway, methionine is converted to S-adenosyl-L-methionine (SAM) through adenylation, or addition of an adenosine monophosphate molecule, by methionine adenosyltransferase (MAT) in an ATP-dependent reaction [27, 28] (Figure 5). SAM is the universal methyl donor in cells used as a substrate for methylation reactions. This includes the methylation of metabolites, nucleic acids, lipids, and proteins. Upon donating a methyl group, SAM is converted to S-adenosylhomocysteine (SAH). SAH is hydrolyzed by S-adenosylhomocysteine hydrolase in a reversible reaction to produce homocysteine and adenine; the reaction is driven forward by the entry of

homocysteine into the transsulfuration pathway or its consumption to regenerate methionine [23, 27]. In the transsulfuration pathway, homocysteine condenses with serine to produce cysteine and glutathione [1].

Methionine is regenerated by the methylation of homocysteine with two possible routes. In the liver and kidney, betaine can be used to donate a methyl group via betaine-homocysteine methyltransferase, producing dimethylglycine as a byproduct. Alternatively, 5-methyltetrahydrofolate methyltransferase catalyzes the transfer of a methyl group from 5-methyltetrahydrofolate to homocysteine, producing tetrahydrofolate as a byproduct [1, 27]. This reaction is dependent on vitamin B_{12} [1].

1.2.4 Relationship between epigenetic remodeling and metabolism

There is an intrinsic link between epigenetic regulation and metabolism since chromatin-modifying enzymes utilize metabolic intermediates as cofactors and substrates [23]. A classic example is the family of histone demethylases known as Jumonji C domain-containing histone demethylases (JHDM) that use α-ketoglutarate (α-KG), oxygen, and iron (II) as co-factors, producing succinate and formaldehyde as reaction by-products (Figure 6). The dependence on α-KG leads to epigenetic aberrations in the case of isocitrate dehydrogenase (IDH) mutants, which are implicated in cancers such as low-grade glioma, AML, and some lymphomas. Normally IDH catalyzes the forward and reverse conversions of isocitrate to α-KG in the tricarboxylic acid cycle. However, when mutated, the enzyme instead produces 2-hydroxyglutarate from α-KG. This inhibits the activity of α-KG-dependent enzymes, including the JHDMs, through competitive inhibition, leading to aberrant hypermethylation (particularly H3K9me3 and H3K27me3) and corresponding DNA hypermethylation. The hypermethylation prevents expression of differentiation genes, generating cancer cells that do not differentiate and instead self-renew [23].

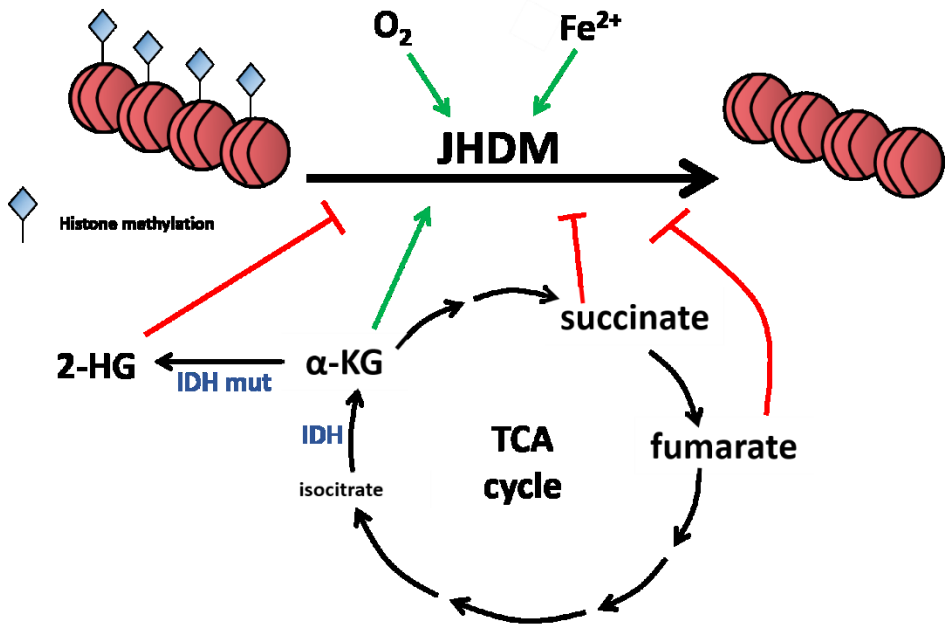

Figure 6. Histone demethylases depend on TCA cycle intermediates

The family of Jumonji domain-containing histone demethylases (JHDM) is an example of the dependence of epigenetic modifiers on cellular metabolism. These histone demethylases are influenced by TCA cycle intermediates, using α-KG as a co-factor and are inhibited by succinate and fumarate. Mutant IDH is implicated in some forms of cancer and leads to the production of 2-HG, also an inhibitor of JHDMs, resulting in a hypermethylated chromatin state.

In summary, JHDMs are dependent on the metabolic intermediate α-KG, as well as oxygen and iron (II), and are inhibited by succinate and fumarate [42] (Figure 6). This example illustrates that modulating metabolite levels (i.e. through the action of mutant IDH) is sufficient to alter the cellular epigenetic status. Enzymatic activity can be manipulated by fluctuations in metabolite concentrations due to physiological stimuli or pathology, leading to alterations in epigenetic marks [23]. The relationship of metabolism regulating epigenetics is true for histone acetylation, phosphorylation, as well as methylation.

Histone acetylation is a process that depends on acetyl-CoA. Histone acetyltransferases transfer the acetyl group from acetyl-CoA to histone lysine residues, releasing CoA as a by-product. The source of this metabolite in mammalian cells is citrate exported from the mitochondria and converted to acetyl-CoA via the activity of ATP-citrate lyase (ACL). When ACL is knocked down, cells exhibit decreased histone acetylation and downregulation of glucose metabolism genes [23, 43]. Thus, this demonstrates that without the production of acetyl-CoA, histone acetyltransferases lack the substrate required to acetylate histones.

Protein kinases can phosphorylate serine, threonine, or tyrosine residues on the N-terminal tails of histones [44]. Histone phosphorylation is dependent on ATP as a substrate, like other phosphorylation events. Given the ATP concentration in the cell and the binding constants of kinases, it is unlikely to limit histone phosphorylation due to low substrate availability. However, it is possible that the kinases are sensitive to other ATP-related stimuli. For example, AMPK is the cellular energy sensor that is activated in response to a low ATP:AMP ratio. Under low energy conditions, it translocates to the nucleus to phosphorylate its target, H2BS36 (serine 36 of histone 2B). Histone phosphorylation can be recognized by "readers" like 14-3-3, leading to downstream effects. Thus, genes involved in cell survival and adaptation to energetic stress are activated downstream of AMPK-mediated phosphorylation of H2BS36 [23].

The methionine cycle is also involved in epigenetic regulation since an intermediate of the pathway is the methyl donor, SAM, which is used in chromatin methylation reactions. Methionine is converted to SAM by the enzyme, methionine adenosyltransferase, which has been detected in chromatin-associated complexes where it provides the substrate for methyltransferases [45]. A methyl group from SAM is transferred to a cytosine residue at a DNA CpG island by a DNA methyltransferase (DNMT), or to an arginine or lysine residue on a histone by a histone methyltransferase (HMT) [23]. The concentration of SAM strongly impacts histone methylation, since small fluctuations in metabolite

level are sufficient to affect enzyme activity [23]. However, the methylation reaction is negatively regulated by SAH; histone methyltransferases are subject to product inhibition by SAH [46]. Thus SAH clearance also plays a role on methyltransferase enzymatic activity [23]. The SAM:SAH ratio directly links methionine metabolism to epigenetic modifications [23, 27, 47]. In fact, it has been shown that manipulating methionine cycle metabolism is sufficient to alter histone methylation, particularly H3K4me3, in human pluripotent stem cells [48]. Similarly, mouse embryonic stem cells rely on threonine to maintain SAM production. When cells are starved of threonine, histone methylation is decreased, leading to a proliferation defect [28, 47].

1.3 Technical aspects of thesis

1.3.1 ChIP-seq

Chromatin immunoprecipitation and massive parallel sequencing (ChIP-seq) is a technique that can be used to interrogate where proteins are targeted to in the genome. It is particularly useful for studying chromatin-modifying enzymes, transcription factors, and other DNA-binding proteins. For example, ChIP-seq may be used to identify a motif within the genome that a transcription factor recognizes and binds to. Another application for ChIP has been described in the investigation of STAT-binding sites and epigenetic remodeling in Th1 and Th2 cells: STAT4 has many binding sites in Th1 cells (40% at promoters and 60% in intergenic regions), and STAT4 binding sites are associated with STAT4-dependent epigenetic modifications. Similarly, it was found that STAT6 plays a role in maintaining epigenetic structure in Th2 cells [12]. ChIP-seq may also be used to determine where histone modifications occur in a gene sequence or to demonstrate enrichment at particular loci and promoters by using the appropriate antibody.

To carry out ChIP-seq, first, the DNA/protein complex is cross-linked using formaldehyde. The DNA is sheared into fragments, with the protein or marker still physically associated. An antibody against the marker (protein of interest or histone modification) is employed for immunoprecipitation. After immunoprecipitation, the cross-link is reversed and DNA is isolated for sequencing using next-generation sequencing or mapping to a reference genome [12, 14].

There are multiple options downstream after DNA purification which vary in resolution, cost, and range. ChIP-PCR is a primer-based approach and ChIP-on-chip employs a microarray with pre-selected regions of the genome; these are useful for interrogating specific target genes or regions. ChIP-seq uses high-throughput next generation sequencing and thus has the highest resolution and greatest range [12].

1.3.2 T cell intracellular cytokine staining

Antigen presentation through MHC molecules or *in vitro* simulation of activation signals by anti-CD3 and anti-CD28 antibodies triggers T cell activation, leading to the induction of cytokine production. The enzyme-linked immunosorbent assay (ELISA) can be used to determine the concentration of secreted cytokine by collecting supernatants from T cells in culture. In contrast, intracellular cytokine staining (ICS) is a flow cytometry-based method that can be used to detect cytokine within activated cells after re-stimulation [49]. In addition, ICS can be used to examine other intracellular factors besides cytokines; these include transcription factors and histone marks. This method allows for quantification of cell populations by simultaneously analyzing both surface and intracellular markers in single cells by flow cytometry.

For optimal detection of intracellular cytokines, T cells are activated with phorbol myristate acetate (PMA), a protein kinase C (PKC) activator, and ionomycin, a Ca^{2+} ionophore, to stimulate cytokine production. These two agents are used together since PKC activation occurs downstream of

physiological TCR ligation and upon mobilization of intracellular calcium stores. Ionomycin acts synergistically with PMA to enhance PKC activity, which triggers phosphorylation of its targets and induces cytokine production [50, 51].

After treatment with PMA and ionomycin, T cells are treated with brefeldin A, which blocks cytokine secretion by impairing vesicular export [49]. Thus, cytokine is retained and accumulates within cells, allowing for detection by fluorochrome-conjugated antibodies [50]. Following treatment with PMA and ionomycin and brefeldin A, cells can be stained for surface markers, then fixed and permeabilized and stained for intracellular components.

ICS is a commonly used tool in studying T cell biology, but there are both advantages and disadvantages in the procedure. Re-stimulation with PMA and ionomycin results in increased cell death, increasing noise, and may also alter expression of some molecules on the cell surface. This is relevant to the work presented in this thesis as it was observed that CD4 expression decreases upon treatment with PMA and ionomycin; indeed, it has been documented in the literature that CD4 molecules are internalized. The increased cytokine in the cell caused by brefeldin A-induced retention improves the signal-to-noise ratio for flow cytometry. Brefeldin A may be used for the entire time of stimulation or it may be added at the end of culture for a limited duration to limit cellular toxicity.

Further caveats arise during sample processing after harvesting the cells from culture. Cell fixation may lead to epitope destruction or modification if cells are stained after fixing, preventing proper detection by flow antibodies. Fixing and permeabilizing cells also increases noise from non-specific binding of antibodies and auto-fluorescence. Moreover, for many cytokines, *in vitro* re-stimulation to induce cytokine production is an artificial signal and does not imply that detected cytokines would have been secreted [50]. Thus, data from flow cytometry may be confounded by more noise due to sample processing, but allows analysis of multiple parameters in single cells.

1.3.3 *In vivo* models

In vivo experiments are conducted to test hypotheses derived from observations from *in vitro* assays. Mouse models are commonly used due to rapid breeding and inbreeding of lab mice for nearly identical genotypes. In addition, the course of disease progression for mouse models of disease is generally predictable and well-documented, leading to fewer variables confounding the results of the experiment. Since mice are relatively simple to manipulate genetically, transgenic and knockout mice can be generated for mechanistic studies. *In vivo* experiments are more physiologically relevant than those done *in vitro* and are used to assess feasibility for translation to a clinical study [52]. For example, treatments for a disease may be tested in other species before being applied to a clinical trial with humans, or other therapeutic targets may be identified upon studying disease induction and pathogenesis.

The following sections of the thesis describe the model systems used in *in vivo* experiments: infection by *Listeria monocytogenes*, homeostatic proliferation in lymphocyte-deficient *Rag2*$^{-/-}$ mice, the development of colitis in *Rag2*$^{-/-}$ mice, and experimental autoimmune encephalomyelitis.

1.3.4 *Listeria monocytogenes* clearance by CD8$^+$ T cells

Listeria monocytogenes is a Gram-positive bacterium that causes listeriosis after ingestion of the food-borne pathogen. Listeriosis is a condition that may lead to gastroenteritis, meningitis and encephalitis in the brain, or infection of the fetus in pregnant women. *L. monocytogenes* is highly infectious, capable of infecting many cell types including non-phagocytic cells. Upon entry into cells, the bacterium replicates through direct cell-to-cell contact, infecting neighbouring host cells. Thus, due to its largely intracellular mechanism of replication, the complement system is ineffective against clearing this bacterial infection. In contrast, CD8$^+$ T cells can recognize and eliminate this intracellular pathogen through MHC class I presentation of bacterial antigen [53, 54].

Intravenous infection with *L. monocytogenes* is a model system *in vivo* used to evaluate host control and clearance of intracellular bacterial infection. In particular, it is useful for studying the $CD8^+$ T cell response and the generation of memory T cells that provide long-lasting protection. One of the advantages of this model system is the availability of both virulent and attenuated strains of the bacteria. The attenuated strain permits study of immunocompromised mice that may have weakened immune responses. Specifically, genetically manipulated immune gene knockout mice such as IFN-γ-deficient mice are able to clear attenuated *L. monocytogenes* [53]. In addition, the duration of infection can be controlled by administering antibiotics [54].

Another advantage is that *L. monocytogenes* has been engineered to express a well-known ovalbumin (OVA) epitope (designated Lm-OVA). Lm-OVA facilitates studies in C57BL/6 mice using transgenic OT-I T cells that have a T cell receptor that specifically recognizes $OVA_{257-264}$ [53]. Thus, it is possible to study clearance of *Listeria monocytogenes* by the endogenous host immune response or by the potent, specific activity of adoptively transferred OT-I T cells.

1.3.5 Induction of colitis in *Rag2*$^{-/-}$ mice

Although $CD4^+$ T cells play important roles in antigen-specific host immunity, they are also implicated in immune-mediated disease when loss of tolerance occurs. Th1 and Th17 $CD4^+$ T helper cells are drivers in a number of autoimmune diseases such as systemic lupus erythematosus and multiple sclerosis. Polymorphisms in STAT3, the signal transducer associated with Th17 cells, are linked to Crohn's disease susceptibility. Th2 cells may also play a role in autoimmune conditions because its signature cytokines are linked to atopic disease. Similarly, loss of T regulatory cells through mutations in the transcription factor FOXP3 also leads to systemic autoimmunity [12, 14].

Inflammatory bowel diseases (IBD) include ulcerative colitis and Crohn's disease and are characterized by inflammation of the intestine or colon [55, 56]. They exemplify an immune-mediated

disorder. Animal models are used to study IBD pathogenesis and assess therapeutic approaches via the induction of colitis in mice. Colitis can be chemically induced by the administration of dextran sodium sulfate (DSS) in the animals' drinking water [55, 57]. The specific model – acute, chronic, or relapsing – can be modulated by adjusting the dose of DSS. It is thought that DSS induces inflammation by damaging the epithelia of the large intestine, allowing intestinal bacteria to invade the underlying tissue. This murine model shares several similarities with human ulcerative colitis. However, DSS colitis development does not involve T and B lymphocytes and is instead more reliant on the role of the innate immune system [55].

Another method to induce colitis is by the adoptive transfer of $CD4^+$ $CD45RB^{hi}$ T cells into syngeneic lymphopenic mice [56-59]. The work presented in my thesis employs this method to study colitis in *Rag2*$^{-/-}$ mice. Cells are sorted by fluorescence-activated cell sorting and their transfer into hosts leads to onset of chronic colitis after 6-8 weeks [58].

RAG1 and RAG2 (encoded by the recombination activating genes) are the proteins that are responsible for the antigen specificity of T cells and B cells. During T and B cell development, V(D)J gene segments (V for variable, D for diversity, and J for joining) are shuffled, thus generating diversity for antigen recognition in a combinatorial process. The RAG enzymes activate recombination by recognizing the recombination signal sequences of the V(D)J gene segments, which is necessary for the formation of mature immunoglobulins and T cell receptors [60]. Loss of *Rag1* or *Rag2* leads to a deficiency of mature T and B lymphocytes, as development is arrested at the recombination phase [60, 61]. Without a functional T cell receptor, T cell precursors do not successfully undergo positive selection and are instead eliminated by apoptosis [61, 62].

Upon transfer into *Rag2*$^{-/-}$ hosts, naïve T cells undergo homeostatic expansion. Commensal enteric bacteria initiate and perpetuate chronic gut inflammation, which is mediated by T cells. Overall, chronic colitis develops since exposure to enteric antigen drives the differentiation of $CD4^+$ T cells to

Th1 and Th17 cells [56]. While Th1 and Th17 cells are pathogenic in colitis, Treg cells have a protective effect. Disease induced by transferred $CD4^+$ $CD45RB^+$ cells can be ameliorated by adoptive transfer of sort-purified regulatory T cells into colitic mice. The Treg cells promote resolution of intestinal inflammation caused by T cells, reversing colitis through the action of IL-10 [57]. The importance of IL-10 is demonstrated by the observation in a genetically susceptible model that colitis spontaneously develops in *Il10*$^{-/-}$ mice [56].

Colitis is evaluated by measuring the weight and length of colon at the time of sacrifice. Inflamed colons are shorter and heavier than colons from a healthy mouse; thus, the ratio of length-to-weight is indicative of disease [56]. In addition, colitis is associated with altered histological characteristics such as cellular infiltration of the lamina propria, decreased goblet cells, crypt abscesses, increased vasculature/hyperemia, thickened mucosa in the colon, and degradation of the epithelium [57].

1.3.6 Homeostatic proliferation assay

In normal physiological conditions, T cell numbers in peripheral lymphoid organs are maintained within a strict range to confer host protection without the unnecessary consumption of host resources. Cell number is controlled through regulating cell survival, death, and division. For example, survival of both $CD4^+$ and $CD8^+$ T cells is dependent on contact with self-MHC/peptide ligands. In lymphopenic conditions, in which the lymphocyte count is decreased, organisms have adapted to restore homeostatic T cell number through proliferation of naïve and memory T cells [63].

Homeostatic proliferation is a means by which organisms maintain peripheral T cell number. It can be modelled *in vivo* by lymphopenia-induced proliferation, in which naïve T cells introduced into a lymphopenic environment proliferate to populate the lymphocyte pool [64]. Genetic models with deficient lymphocyte generation such as SCID or *Rag2*$^{-/-}$ mice may be used for homeostatic proliferation assays or a lymphopenic environment may be produced artificially by sublethal irradiation of recipient

mice [64]. Following transfer of naïve ($CD44^{lo}$) T cells, the donated T cells exhibit two modes of growth. One group of cells spontaneously and rapidly proliferates and differentiates to memory cells in an IL-7-independent and TCR:MHC/self-dependent process. The other mode of growth is slow homeostatic proliferation, which is IL-7-dependent; in the absence of IL-7, survival and homeostatic proliferation of naïve cells are greatly diminished [10, 63, 65]. Depending on the lymphopenic model, transferred cells may favour one mode of growth over the other. Slow homeostatic proliferation dominates in the acute lymphopenia induced by sublethal irradiation, as the mice also exhibit endogenous T cell repopulation. Conversely, proliferation of naïve $CD4^+$ T cells transferred into *Rag*$^{-/-}$ mice is predominantly rapid and spontaneous.

The two growth patterns are also associated with differential expression of activation markers. In particular, CD44, a marker of activation, and CD62L, which is expressed on naïve T cells, are differentially expressed between the two groups. Rapidly dividing cells have high CD44 and low CD62L expression, while cells that had divided slowly have increased CD44 expression with each division and maintain high CD62L expression. CD62L is involved in mediating T cell homing to the peripheral lymph nodes, where homeostatic proliferation occurs, followed by lymph node egress to the spleen and blood [64]. In addition, spontaneous and homeostatic proliferation are marked by differential cytokine expression. Spontaneously proliferating cells exhibit increased capacity to produce cytokines such as IL-2 and IFN-γ [65].

Homeostatic proliferation has gained interest as it may have applications in cancer immunotherapy. Observations from mouse models demonstrate that following homeostatic proliferation, T cells are less prone to becoming anergic, and the process of homeostatic proliferation may reverse anergy. Thus, strategies in cancer immunotherapy have employed the induction of lymphopenia prior to adoptive T cell transfers [64].

1.3.7 Experimental autoimmune encephalomyelitis

Multiple sclerosis is an autoimmune disease of the central nervous system (CNS) characterized by inflammation of the brain and spinal cord, demyelination, and axonal degeneration. The disease is mediated by T lymphocytes that are specific for myelin self-antigens. After crossing the blood-brain barrier, these pathogenic T cells cause damage to the myelin sheath enrobing axons, slowing nerve conduction, and may eventually damage axons as well.

Experimental autoimmune encephalomyelitis (EAE) is an animal model of multiple sclerosis. It is induced by immunizing animals with a myelin antigen emulsified in complete Freund's adjuvant or through the adoptive transfer of activated myelin-specific $CD4^+$ T cells [18]. For example, one model of EAE is induced by myelin oligodendrocyte glycoprotein (MOG35-55) and is referred to as MOG-induced EAE [52, 66]. Like multiple sclerosis, EAE is mediated by T cells which are activated in peripheral lymphoid organs and migrate into the CNS by crossing the blood-brain barrier. Therefore, along with T cells, there is a particularly important role for dendritic cells in the pathogenesis of EAE as they guide T cell activity. DCs in peripheral lymphoid organs promote T cell proliferation and produce polarizing cytokines that induce naïve $CD4^+$ T cell differentiation to effector fates that drive the disease. In addition, DCs act in the perivascular space to facilitate infiltration of encephalitogenic T cells into the CNS [67]. Within the CNS, T cells are reactivated by local and infiltrating DCs and recruit other immune cells such as neutrophils, macrophages, and monocytes, leading to inflammation of the CNS and demyelination as observed in multiple sclerosis [18].

Th1 and Th17 cells are the pathogenic T lymphocytes that drive EAE [18, 67]. Greater EAE severity is linked to increased Th1 and Th17 cell infiltration of the CNS. Moreover, increased production of IL-1β as well as the polarizing cytokines, IL-6 and IL-12, which drive Th17 and Th1 differentiation, respectively, are found in animals more susceptible to EAE [67]. Conversely, *Il17*$^{-/-}$ mice or using a neutralizing anti-IL-17 antibody reduces EAE severity; *Il17*$^{-/-}$ mice exhibit delayed disease onset,

decreased disease scores, and early recovery. These observations highlight the significant impact of Th17 cells on EAE development and outcome, though Th1 cells can also induce EAE through adoptive transfer [18].

In contrast, regulatory T cells limit autoreactive T lymphocytes, including those that are specific for myelin antigen, and their activity is protective in EAE. Although T cells potentially specific for myelin self-antigen exist in normal individuals, they are normally kept in check by Treg cells. Treg counts are similar between healthy individuals and multiple sclerosis patients. Yet, *in vitro* suppression assays have shown that Tregs of MS patients have diminished function, particularly in controlling IL-17 [18]. Accordingly, EAE-susceptible animals have decreased IL-10 produced by anti-inflammatory Tregs, where IL-10 appears to be the mechanism through which Treg cells exert their suppressive activity since transfer of Tregs from *Il10*$^{-/-}$ mice fails to protect against EAE [18, 67]. Thus disease susceptibility and severity are determined by the balance between multiple T helper subsets.

Materials and Methods

Mice

C57BL/6 mice were purchased from Charles River Laboratories (Wilmington, MA) and OT-I mice were obtained from Dr. Martin Richer (McGill University, Canada). Mice were bred and maintained under specific pathogen-free conditions at McGill University under approved protocols. For *in vivo* methionine restriction experiments, animals were fed control diet (L-Amino Acid Rodent Diet with 10 kcal% Fat and 0.86% Methionine) or low methionine diet (L-Amino Acid Rodent Diet with 10 kcal% Fat and 0.12% Methionine) from Research Diets Inc. (New Brunswick, NJ). Animals were introduced to the diet 2 weeks prior to infection or disease induction and maintained on their respective diets until experimental endpoints. Experiments were performed on mice between 6 and 20 weeks of age.

T cell purification and culture

T cells ($CD3^+$, $CD4^+$, or $CD8^+$ depending on the assay) were purified from spleen and peripheral lymph nodes using a negative selection kit (StemCell Technologies, Vancouver, Canada). T cells were activated using platebound anti-CD3 (2 μg/ml) and anti-CD28 (1 μg/ml). Cells were grown in Iscove's Modification of DMEM (IMEM) (Wisent, St. Bruno, QC) supplemented with 10% FBS or 10% dialyzed FBS (Wisent, St. Bruno, QC), L-glutamine (Invitrogen, Chicago, IL), penicillin-streptomycin (Invitrogen), and 2-ME (Sigma-Aldrich, St. Louis, MO). For add-back experiments, cells were grown in custom IMEM supplemented with 10% dialyzed FBS, L-glutamine, penicillin-streptomycin, and 2-ME, adding back L-glutamine, D-glucose, L-serine, L-glycine, L-alanine, L-threonine, choline chloride, and sodium pyruvate to full nutrient medium concentrations, according to the manufacturer's website. L-methionine was added back to indicated concentrations (3 or 0 μM for methionine restriction conditions).

For differentiation assays, $CD4^+$ T cells were activated using platebound anti-CD3 (5 μg/ml) and anti-CD28 (2 μg/ml). Cells were cultured in Th17-polarizing medium containing IL-6 (20 ng/ml), TGF-

β (2 ng/ml), anti-IL-4 (2.5 µg/ml), anti-IFN-γ (2.5 µg/ml), and anti-IL-2 (2.5 µg/ml) for 3-5 days for long term methionine restrictions and 5 days for acute starvation. For Th1 polarization, cells were cultured in IL-2 (10 U/ml), IL-12 (5 ng/ml), and anti-IL-4 (5 µg/ml) for 3 days. For acute starvation experiments, cells were cultured in full nutrient medium with FBS, washed, and re-cultured for indicated periods of time in medium with dialyzed serum.

Immunoblotting

Cells were lysed in modified Laemmli lysis buffer (240 mM Tris/HCl pH 6.8, 40% glycerol, 8% SDS, 5% 2ME) supplemented with protease inhibitors and phosphatase inhibitors (Roche/Sigma-Aldrich). Protein from whole cell lysate was quantified by bicinchoninic acid assay (BCA assay) using Pierce BCA Protein Assay Kit (Thermo Fisher Scientific, Waltham, MA, USA). Lysates were resolved by SDS-PAGE, transferred to nitrocellulose, and incubated with primary antibodies to H3, H3K4me3, H3K9me3, H3K27me3, and H3K36me3 (Cell Signaling, Danvers, MA and Abcam, Cambridge, UK). HRP-conjugated anti-rabbit and anti-mouse secondary antibodies were obtained from Cell Signaling Technology.

Histology

Mouse tissue samples (colon and small intestine) were fixed in 4% paraformaldehyde overnight and embedded in paraffin. Samples were analyzed by Hematoxylin and Eosin (H&E) staining.

Flow cytometry

Single-cell suspensions were surface stained with fluorescently conjugated antibodies against CD3, CD4, CD8, CD44, CD25, CD62L, Ly6G (Gr-1), Ly6C, F4/80, CD11b, CD11c, NK1.1, KLRG1, CD127, Thy1.1, and CD45RB (eBioscience, San Diego, CA). Cell viability was assessed by using Fixable

Viability Dye eFluor 780 and eFluor 506 (eBioscience) according to the manufacturer's protocol. For intracellular cytokine staining (ICS) for IL-17, RORγt, IFN-γ, T-bet, FOXP3, and TNF-α, *in vitro* T cells were stimulated with PMA and ionomycin for 2 hours followed by treatment with Brefeldin A for 2 hours, or alternatively cells were cultured with PMA, ionomycin, and Brefeldin A together for 4 hours. After restimulation, cells were surface stained, fixed and permeabilized using FoxP3/Transcription Factor Staining Buffer Set (eBioscience), and stained intracellularly. Stained samples were analyzed by flow cytometry or sorted as indicated. Flow cytometry was performed using the LSR Fortessa (BD Biosciences) cytometer and analysis was performed on FlowJo (Tree Star). Fluorescence-activated cell sorting (FACS) was performed on an BD FACSAria Fusion cell sorter (BD Biosciences).

Infection with *L. monocytogenes*

5×10^3 OT-I T cells ($CD45.2^+$) were injected intravenously (tail vein) into $CD45.1^+$ mice. One day later, mice were immunized with a sublethal dose of recombinant attenuated *Listeria monocytogenes* (Lm) expressing OVA (LmOVA, 2×10^6 CFU). Splenocytes were isolated from mice 7 days post-infection and analyzed by flow cytometry for presence of OVA-specific $CD8^+$ T cells by MHC class I tetramer ($K^b/OVA_{257-264}$) for the endogenous response or CD45.2 for OT-I response. Cytokine production by $CD4^+$ and $CD8^+$ T cells was analyzed by ICS staining following peptide re-stimulation (OVA_{257} for $CD8^+$ T cells and LLO_{190} for $CD4^+$ T cells).

Induction of colitis and homeostatic proliferation in *Rag2*$^{-/-}$ mice

Rag2$^{-/-}$ mice were randomly divided into two groups and kept on control or low methionine diets for two weeks preceding adoptive transfer of naïve $CD4^+$ T cells. Naïve $CD4^+$ T cells were prepared by isolating $CD4^+$ T cells from spleen and peripheral lymph nodes of donor C57BL/6 mice and sorting for $CD4^+$ $CD45RB^{hi}$ $CD25^{lo}$ cells. 5×10^5 cells were injected (intraperitoneally) into $Rag^{-/-}$ mice. Mice were

weighed weekly and sacrificed at the clinical endpoint of 20% weight loss (from weight at time of injection). Mesenteric lymph nodes (MLNs) and spleens were collected and homogenized to a single cell suspension for surface staining and restimulated *in vitro* for intracellular staining for flow cytometry. Colon weights and lengths were recorded and analyzed by histology (H&E staining). Small intestines were also analyzed by histology.

For the homeostatic proliferation assay, *Rag2*$^{-/-}$ mice were maintained on the control or low methionine diet for two weeks, followed by injection of 1×10^6 naïve CD4$^+$ T cells stained with Violet Proliferation Dye (BD Biosciences, San Jose, CA, USA). One week post-transfer, spleens and MLNs were collected and analyzed by flow cytometry.

ELISA

CD4$^+$ and CD8$^+$ T cell supernatants were collected on indicated days from differentiation and growth curve assays. Cytokine production was quantified by sandwich ELISA for IL-17 (capture clone eBio17CK15A5, detection clone eBIO17B7) and IFN-γ (capture clone AN-18, detection clone XMG1.2), using antibodies (purified and biotin-conjugated) and standards from eBioscience.

qPCR

Total RNA was isolated from murine T cells using QIAzol (QIAGEN, Germantown, MD, USA). cDNA was synthesized from 250 ng to 1000 ng RNA using High-Capacity cDNA Reverse Transcription Kit (Applied Biosystems/ThermoFisher Scientific). Quantitative PCR (qPCR) was performed using SYBR Green with the following primer pairs:

Gene	Forward Primer	Reverse Primer
Il17	CTGGAGCATAACACTGTGAGAGT	TGCTGAATGGCGACGGAGTTC
Ifng	GATGCATTCATGAGTATTGCCAAGT	GTGGACCACTCGGATGAGCTC
Mat2a	AAGTGGCTTGTGAAACTGTTGCT	CTTGGGCAATATCTGGTGACTGTTG

Ogdh	AATGAGGAGAAGCGGACCTT	TCCACTCCATTTGCACTTGA
Rorc	CCGCTGAGAGGGCTTCAC	TGCAGGAGTAGGCCACATTACA
Tbp	ACCTTATGCTCAGGGCTT	GCCATAAGGCATCATTGG
Tbx21	CAACAACCCCTTTGCCAAAG	TCCCCCAAGCAGTTGACAGT

Metabolomics experiments

$CD4^+$ and total T cells were activated and expanded for 4 days. Cells were washed in methionine-free (for ^{13}C-methionine add-back) or serine-free (for ^{13}C-serine add-back) medium or full medium with dialyzed serum. Cells were re-cultured for indicated durations in ^{13}C-serine added back to normal medium concentrations or ^{13}C-methionine added back to indicated concentrations (Cambridge Isotope Laboratories).

For LC-MS, cells were plated at 10×10^6 cells per well in 6-well plates and for GC-MS, cells were plated at 2×10^6 cells per well in 24-well plates. For metabolite analysis of tissues, liver samples were snap frozen in liquid nitrogen at the time of sacrifice, and serum was collected by cardiac puncture and stored at -80°C. Solid tissue was ground with a mortar and pestle to a powder.

LC-MS

Liquid chromatography was performed using a 1290 Infinity ultra-performance LC system (Agilent Technologies, Santa Clara, CA, USA) equipped with a Scherzo 3µm, 3.0 × 150 mm SM-C18 column (Imtakt Corp, Japan). Column temperature was maintained at 10°C and the mobile phases A and B consisted of water containing 5 and 200 mM ammonium acetate with 20% ACN, respectively. The chromatographic gradient started at 100% mobile phase (A) with a 5 min gradient to 100% (B). This was followed by a 10 min hold time at 100% mobile phase B at a flow rate of 0.4 ml/min. A subsequent re-equilibration time (6 min) was performed before the next injection. Sample volumes of 5 µl were injected for LC-MS analysis. All LC-MS grade solvents (water, methanol, and formic acid) were purchased from

Fisher (Ottawa, Ontario, Canada). Authentic metabolite standards were purchased from Sigma-Aldrich (Oakville, Ontario, Canada).

LC-MS analysis was performed on an Agilent 6540 UHD Accurate-Mass Q-TOF mass spectrometer (Agilent Technologies, Santa Clara, CA, USA). Analyte ionization was accomplished using an electrospray ionization source (ESI) in positive polarity. The source operating conditions were set at 325°C and 9 L/min for gas temperature and flow, respectively, nebulizer pressure was set at 40 psi and capillary voltage was set at 4.0 kV. Reference masses 121.0509, 922.0099 were introduced into the source through a secondary spray nozzle to ensure accurate mass. MS data were acquired in full scan mode mass range: m/z 100-1000; scan time: 1.4s; data collection: centroid and profile. Retention times and accurate mass for each compound ere confirmed against authentic standards as well as matched unlabeled cell extracts grown under the same conditions were cells were undergoing SITA. Data were quantified by integrating the area underneath the curve of each compound using MassHunter Qual (Agilent Technologies, Santa Clara, CA, USA). Each metabolite accurate mass ion and subsequent isotopic ions were extracted (EIC) using a 0.02 Thomsons.

For targeted metabolite analysis and semi-quantitative concentration determination of amino acids, samples were injected into an Agilent 6430 Triple Quadrople (QQQ)-LC-MS/MS. Chromatography was done using a 1290 Infinity ultra-performance LC system (Agilent Technologies) consisting of vacuum degasser, autosampler and a binary pump. Chromatographic separation was performed on Scherzo SM-C18 column 3 μm, 3.0×150 mm (Imtakt Corp, Japan). For all LC-MS analyses, 5 μl of sample was injected. The column temperature was maintained at 10°C. Queued samples were maintained at 4°C. The chromatographic gradient started at 100% mobile phase A (0.2% formic acid in water) with a 2 min hold followed by a 6 min gradient to 80% B (0.2% formic acid in MeOH) at a flow rate of 0.4 ml/min. This was followed by a 5 min hold time at 100% mobile phase B and a subsequent re-equilibration time (6 min) before the next injection. The mass spectrometer was equipped

with an electrospray ionization (ESI) source operating in positive mode. Multiple reaction monitoring (MRM) transitions were optimized on standards for each metabolite quantified. Nitrogen temperature and flow were set at 350°C and 10 L/min, respectively, nebulizer pressure was set at 40 psi and capillary voltage was set at 3.5 kV. Relative concentrations were determined from external calibration curves. Data were quantified by integrating the area under the curve of each compound using MassHunter Quant (Agilent Technologies).

GC-MS

Gas chromatography coupled to mass spectrometry (GC-MS) was performed on T cells. Metabolites were extracted using cold 80% methanol and sonicated. D-myristic acid was added to supernatants (750 ng/sample) as an internal standard. Dried samples were dissolved in 30 µL methozyamine hydrochloride (10 mg/ml) in pyridine and derivatized as tert-butyldimethylsily (TBDMS) esters using 70 µL N-(*tert*-butyldimethylsilyl)-N-methyltrifluoroacetamide (MTBSTFA) [29].

For metabolite analysis, an Agilent 5975C GC/MS equipped with a DB-5MS+DG (30 m × 250 µm × 0.25 µm) capillary column (Agilent J&W, Santa Clara, CA, USA) was used. All data were collected by electron impact set at 70 eV. A total of 1 µL of the derivatized sample was injected in the GC in splitless mode with inlet temperature set to 280°C, using helium as a carrier gas with a flow rate of 1.5512 mL/min (rate at which myristic acid elutes at 17.94 min). The quadrupole was set at 150°C and the GC/MS interface at 285°C. The oven program for all metabolite analyses started at 60°C held for 1 min, then increasing at a rate of 10°C/min until 320°C. Bake-out was at 320°C for 10 min. Sample data were acquired both in scan (1-600 m/z) and selected ion monitoring (SIM) modes. Mass isotopomer distribution for cellular metabolites was determined using a custom algorithm developed at McGill University [29]. Briefly, the atomic composition of the TBDMS-derivatized metabolite fragments (M-57) was determined, and matrices correcting for natural contribution of isotopomer enrichment were

generated for each metabolite. After correction for natural abundance, a comparison was made between non-labeled metabolite abundances (^{12}C) and metabolite abundances which were synthesized from the ^{13}C tracer. Metabolite abundance was expressed relative to the internal standard (D-myristic acid) and normalized to cell number.

Statistical analysis

*, $p < 0.05$; **, $p < 0.001$; ***, $p < 0.0001$; ns = non-significant as determined by statistical analysis performed in GraphPad Prism. Data are presented as mean ± SEM for biological replicates or mean ± SD for technical replicates. For data presented in Tables 1-6, the data represent the mean ± SEM for biological replicates (n=4).

Results

SAM biosynthesis is enhanced upon T cell activation

One-carbon metabolism is involved in biosynthetic processes, redox balance, and epigenetic regulation and has been shown to support proliferation in cancer cells [39, 40]. Recent work from our group has shown that serine enters the folate cycle in T cells, leading to nucleotide biosynthesis and enhancing T cell proliferation [29]. This highlights that one-carbon metabolism promotes growth in T cells, analogous to its role in cancer cells. We hypothesized that one-carbon metabolism also has a role in epigenetic regulation in T cells, leading to changes in T cell growth and differentiation. We analyzed the expression of metabolites in naïve and activated $CD8^+$ OT-I T cells and identified S-adenosyl-L-methionine (SAM) upregulation in activated cells (Figure 7A). SAM is an intermediate of the methionine cycle, produced through the adenylation of methionine using an ATP molecule, and it is the universal methyl donor in cells (Figure 5). After donating a methyl group SAM is converted to SAH. Both of these metabolites are upregulated in T_{eff} cells (Figure 7B), suggesting that there is increased flux in methylation reactions. Although the total abundance of methionine is relatively unchanged upon activation (Figure 7C), the ratio of SAM to methionine is greatly increased (Figure 7D), indicating increased potential to methylate targets. Accordingly, protein levels of the enzyme that converts methionine to SAM, Mat2a, is also increased in activated T cells (Figure 7E).

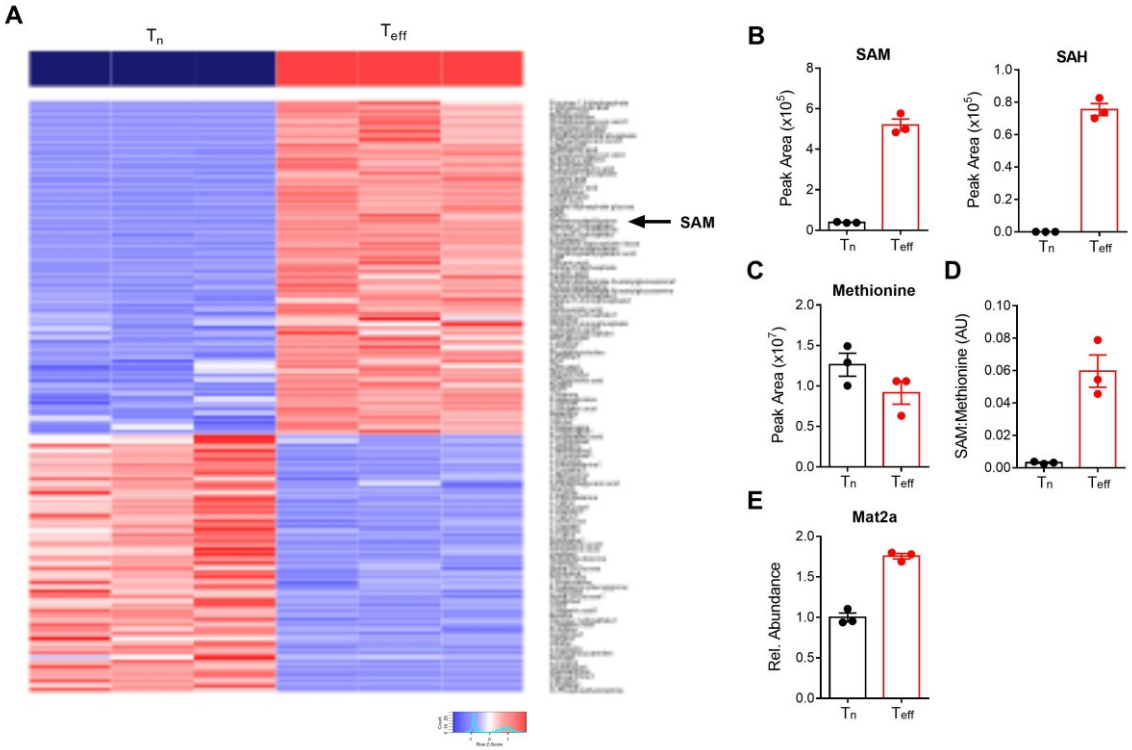

Figure 7: Differential metabolite expression between naïve and activated T cells

A) Heatmap of differentially expressed metabolites between naïve (T_n) and activated (T_{eff}) T cells after 3 days in culture. OT-I T cells were activated with OVA peptide and naïve T cells were maintained in culture with IL-7.

B) SAM and SAH levels in T_n and T_{eff} $CD8^+$ OT-I T cells after 3 days in culture as determined by LC-MS.

C) Total abundance of intracellular methionine in naïve (T_n) and activated (T_{eff}) $CD8^+$ OT-I T cells after 3 days in culture.

D) Ratio of SAM to methionine in T_n and T_{eff} OT-I T cells after 3 days in culture as determined by LC-MS.

E) Relative Mat2a protein abundance in T_n and T_{eff} $CD8^+$ OT-I T cells as determined by mass spectrometry.

Methionine cycle dynamics in T cells

We next sought to investigate the sources used to produce SAM in activated T cells. Activated T cells were cultured in methionine-free medium containing [$^{13}C_1$]-methionine added back to 200 μM (the concentration in full medium). Cells were harvested for gas chromatography-mass spectrometry (GC-MS) at 0 min, 15 min, 30 min, 1 h, and 2 h after plating in heavy-labeled methionine (data not shown for 2 h). The data show that extracellular methionine is rapidly taken up by T cells, nearly reaching equilibrium after 15 min and fully reaching steady state at 30 min (Figure 8A). This is consistent with the fact that T cells upregulate expression of the amino acid transporter SLC7A5 upon activation, leading to increased methionine intake [33].

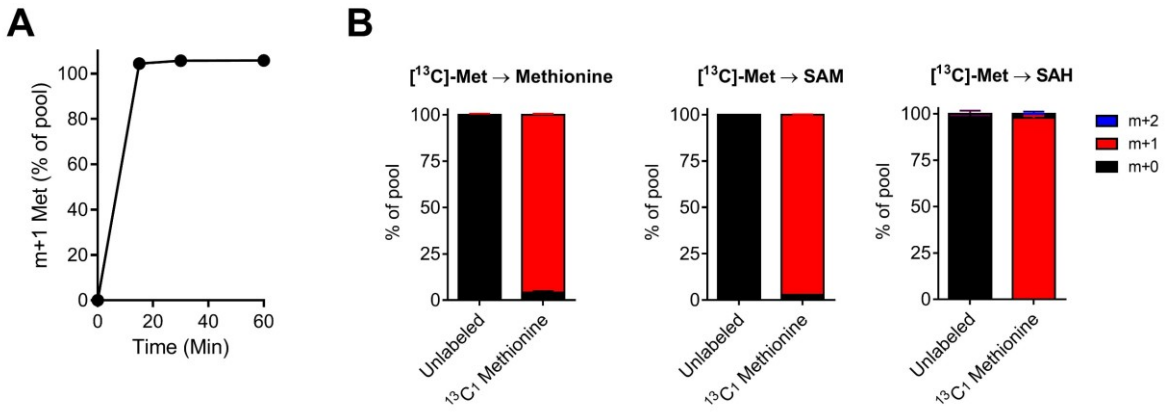

Figure 8: Extracellular methionine is rapidly incorporated into the methionine cycle

A) Time course of [$^{13}C_1$]-methionine uptake in total T_{eff} cells. T_{eff} cells were cultured for indicated times in medium containing [$^{13}C_1$]-methionine (200 μM). Intracellular methionine abundance (m+1 Met) was measured by GC-MS.

B) Mass isotopomer distribution (MID) for methionine, SAM, and SAH following ^{13}C-methionine tracing in T_{eff} cells. Total T cells were cultured for 6 hours in [$^{13}C_1$]-methionine. Incorporation into the methionine cycle (methionine, SAM, and SAH) was determined by LC-MS.

To determine whether methionine is incorporated into methionine cycle intermediates, we cultured T_{eff} cells in 200 μM [$^{13}C_1$]-methionine for 6 h. Cells were analyzed by liquid chromatography-mass spectrometry (LC-MS) to interrogate methionine, SAM, and SAH levels. Intracellular methionine in T cells was almost completely labeled (Figure 8B), demonstrating again that methionine is readily taken up by T cells. SAM and SAH were also highly labeled (>90%) (Figure 8B), indicating that methionine enters the methionine cycle, is converted to SAM, and is subsequently used to methylate various targets in the cell, thereby generating SAH.

Glucose and serine contribute to SAM production, but not methionine production

The folate and methionine cycles were previously thought to be bicyclic, coupled through the methylation of homocysteine to regenerate methionine (Figure 5). This one-carbon unit transfer can be accomplished by donation of a methyl group from 5-methyltetrahydrofolate, an intermediate of the folate cycle [1, 27]. However, previous work has shown that the folate and methionine cycles can be uncoupled in cells [28, 29]. Rather than direct incorporation of methyl groups from the folate cycle into methionine, the two cycles are linked due to the ATP-dependent biosynthesis of SAM. ATP produced from folate cycle purine nucleotide biosynthesis is incorporated into the methionine cycle because it is used to adenylate methionine in the step catalyzed by Mat2a (Figure 5).

We confirmed that the folate cycle does not directly contribute to methionine production, but does provide ATP for input into the methionine cycle. $CD8^+$ OT-I T cells or naïve T cells were cultured for 48h in uniformly labeled [^{13}C]-glucose. The lack of labeling in methionine from [^{13}C]-glucose indicates that glucose is not directly used to synthesize methionine, nor does it contribute one-carbon units for the remethylation of homocysteine (Figure 9A). However, m+5 labeling was detected in SAM (Figure 9A), suggesting that glucose-derived ATP is the route of entry for glucose-derived carbon into the methionine cycle.

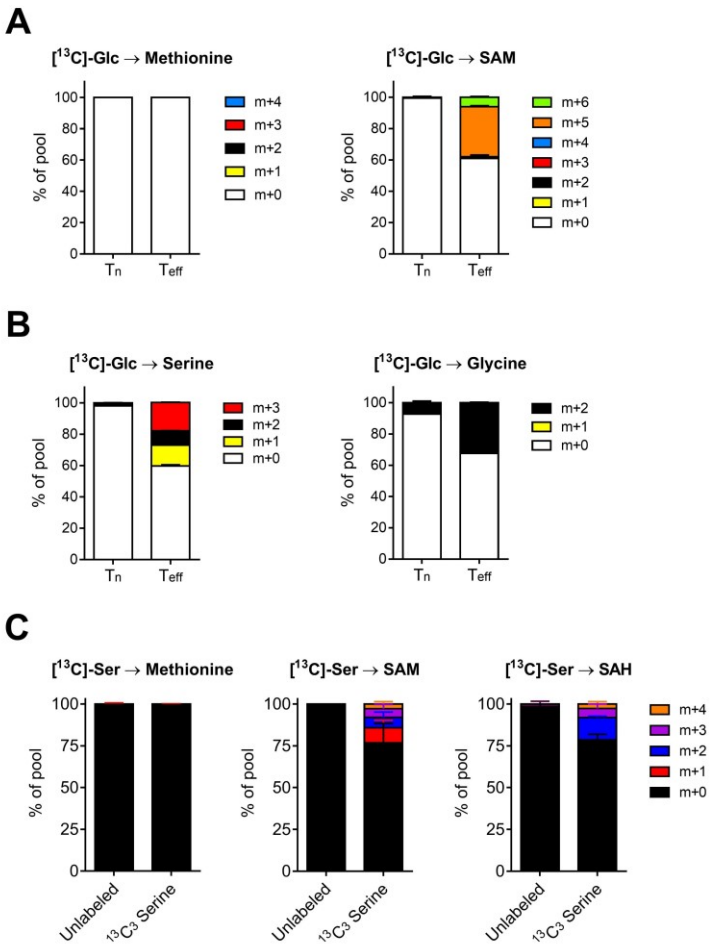

Figure 9: Glucose and serine are incorporated into SAM

A) Mass isotopomer distribution (MID) for methionine and SAM in naïve and activated $CD8^+$ OT-I T cells following U-[^{13}C]-glucose tracing. OT-I T cells were cultured for 48h in U-[^{13}C]-glucose and labeling into the methionine cycle was determined by LC-MS.

B) Mass isotopomer distribution (MID) for serine and glycine following U-[^{13}C]-glucose tracing. OT-I T cells were cultured for 48h in U-[^{13}C]-glucose and analyzed by LC-MS.

C) Total T cells were pulsed with [$^{13}C_3$]-serine for 6 hours, followed by LC-MS analysis to measure incorporation of extracellular serine into methionine, SAM, and SAH.

A proportion of glucose transported into T cells is partially metabolized through glycolysis and used to synthesize serine [1]. As predicted, glucose labeling is observed in serine (Figure 9B), including fully labeled m+3 serine, as well as m+1 and m+2 serine, indicative of serine and glycine interconversion. Accordingly, glycine is also labeled (Figure 9B). Thus, following serine biosynthesis from glucose, serine is converted to glycine by SHMT. In this reaction, serine donates a carbon to methylate 5-methyltetrahydrofolate, producing glycine and N^5,N^{10}-tetrahydrofolate. These products can be used to generate purine nucleotides through the folate cycle, including ATP. This explains the labeling from [^{13}C]-glucose into SAM through glucose-derived serine contributing to ATP production. Similar results were obtained when activated T cells were pulsed with [$^{13}C_3$]-serine for 6 hours. While serine does not contribute directly to methionine production, there is some labeling into SAM and SAH due to ATP incorporation (Figure 9C). Overall, these observations demonstrate that glucose is broken down to produce serine. Serine derived from extracellular serine or synthesized *de novo* is not directly incorporated into methionine, but does enter the methionine cycle by contributing to SAM synthesis.

Reduced SAM production under methionine restriction leads to decreased histone methylation

After confirming that T cells take up and use methionine to produce SAM, we measured the levels of intracellular methionine cycle metabolites following methionine restriction. Activated T cells were expanded in full complete medium (regular serum) for 4 days, then cultured acutely in varying concentrations of methionine. Cells were plated in no (0 μM), restricted (3 μM), or full (added back to 200 μM) methionine medium for 6 h and metabolite extracts were collected for LC-MS. The data show that acute methionine restriction greatly blunts methionine and SAM levels and reduces SAH levels as well (Figure 10A). This suggests that methionine is constantly being consumed by T_{eff} cells and needs to be continuously imported (since it is an essential amino acid), such that a 6 h starvation results in depleted

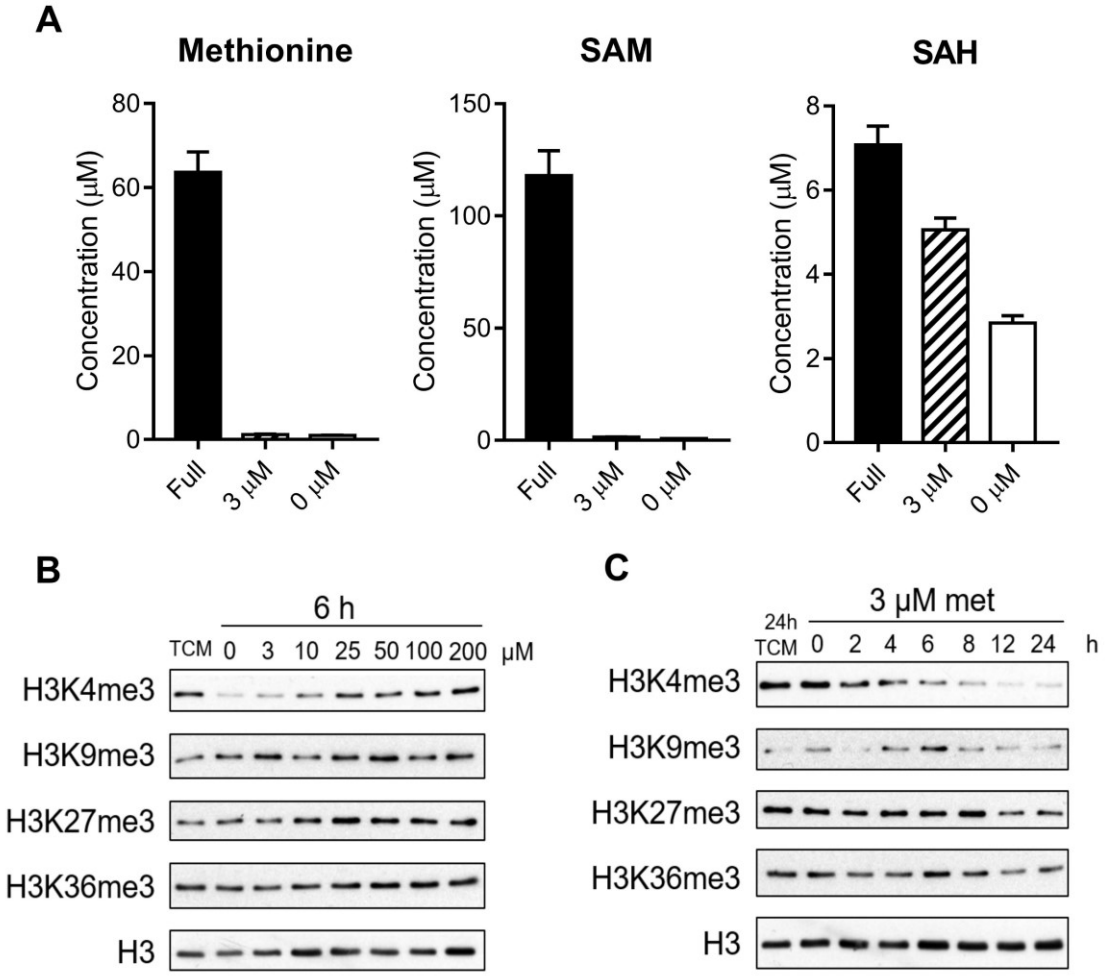

Figure 10: Methionine restriction decreases global histone methylation

A) Intracellular concentration of methionine, SAM, and SAH in T_{eff} cells. Activated total T cells were cultured in full, restricted (3 μM), or no (0 μM) methionine for 6 h and harvested to quantify methionine cycle metabolite abundances by LC-MS.

B) Immunoblot analysis of global histone H3 methylation in T_{eff} cells. Total T_{eff} cells were cultured for 6 h in varying extracellular concentrations of methionine. H3 is the loading control. TCM is full, complete T cell medium.

C) Global histone methylation of T_{eff} cells cultured in 3 μM methionine for 0 to 24 h.

intracellular methionine stores. SAM is also decreased due to the lack of methionine available to synthesize it.

SAM is the universal methyl donor in cells used by histone methyltransferases to add modifications onto histones. Given the extremely limited SAM in T cells upon methionine restriction and because the balance of SAM:SAH determines methyltransferase activity, we hypothesized that the cellular methylation capacity would be consequently impaired. We assessed global H3 histone methylation in total activated T cells cultured in methionine-restricted medium for 0 to 24 h or in varying concentrations of methionine for 6 h. We observed a decrease in histone methylation correlating with a decrease in methionine (Figure 10B), with H3K4me3 being the most labile of the marks and the most noticeable shift occurring between 10 μM and 25 μM methionine. There were very slight dose-dependent changes in H3K27me3 and H3K36me3 as well, while H3K9me3 appeared variable with methionine concentration. In Figure 10C, we show that H3K4me3 marks are susceptible to loss with methionine restriction over time, with gradual decreases in methylation apparent as soon as 2 hours following methionine restriction. H3K27me3 exhibited less dramatic changes, though there was a decrease in methylation between 8 and 12 h, while H3K36me3 and H3K9me3 levels appeared variable. Interestingly, our data demonstrate that some histone methylation marks are affected more than others – particularly H3K4me3, a permissive mark – which suggests differential sensitivity of histone methyltransferases for SAM.

Methionine restriction impairs T cell growth

We next investigated how T cells respond in methionine-limited conditions by performing growth curves. T_{eff} cells grown in full complete T cell medium were replated for 3 days of growth in a dose range (0 to 200 μM) of methionine. For both $CD4^+$ and $CD8^+$ T cells, cell number is proportional to methionine concentration (Figure 11A). Cells in 0 μM and 3 μM methionine exhibited very little growth over the

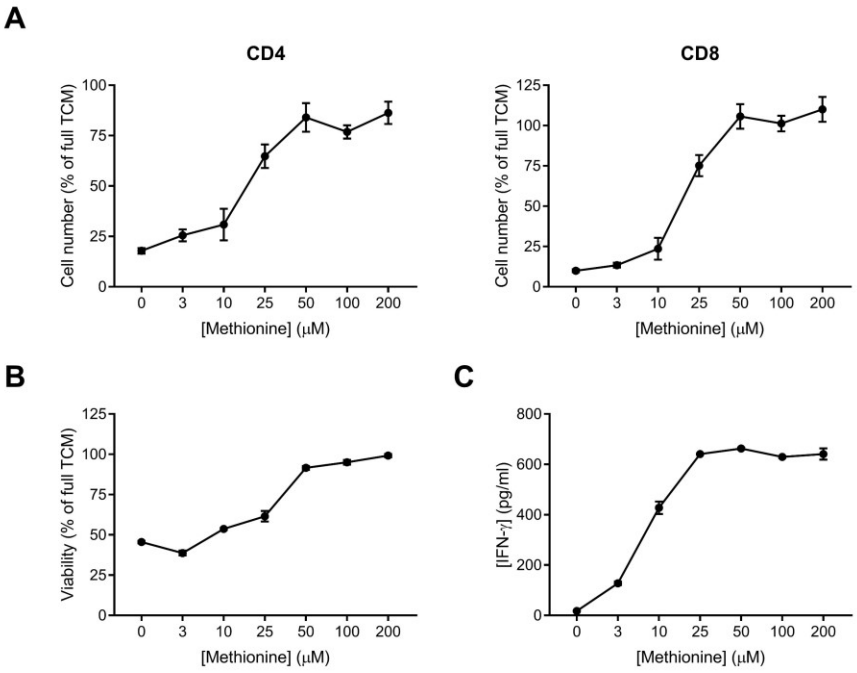

Figure 11: Impaired T cell growth and cytokine production in low methionine

A) T_{eff} cells were cultured in different concentrations of methionine over 3 days. $CD4^+$ (left) and $CD8^+$ (right) T cell numbers from 3-day cultures of T_{eff} cells are presented. Cell numbers are expressed relative to average live cell count of cells grown in full T cell medium.

B) Viability of total T cells measured by flow cytometry expressed as a percentage of the viability of T cells grown in full T cell medium.

C) ELISA of supernatants collected on day 3, measuring IFN-γ content.

course of 3 days, while T cells in 10 μM methionine grew only slightly better. 25 μM methionine marks a substantial shift, almost restoring normal growth, as cells grew similarly in methionine containing 25 μM up to 200 μM methionine (data recorded from days 0 to 2 not shown). Cell viability follows the same pattern as proliferation, though within a slightly smaller range (Figure 11B). For viability, the shift between low and high viability occurs between 25 and 50 μM methionine. Due to reduced cell number,

less cytokine was secreted into the medium by cells grown in low methionine as measured by enzyme-linked immunosorbent assay (ELISA) (Figure 11C). Cells grown in 25 μM methionine and above exhibited similar IFN-γ production. Thus, we establish that T cell growth is limited in low methionine (0 and 3 μM), while approximately 25 μM methionine is sufficient for normal T cell activity.

Differentiation in low methionine limits lineage-specific factors in Th17 cells

Having established that T cell growth is impaired under conditions of methionine restriction *in vitro,* we next examined whether low methionine affects T cell differentiation. Naïve $CD4^+$ T cells were grown in high or low methionine medium containing polarizing cytokines to induce differentiation to the Th17 lineage. After 3 days of differentiation, cells in restricted methionine (3 μM) were given a bolus of methionine (or no additional methionine as a negative control) to add-back to full condition for 2 h before the 4 h restimulation. The purpose of this was to determine whether methionine is involved with transcriptional or translation regulation of gene expression, where a defect in translation due to limited methionine availability would be corrected by the add-back of methionine to the culture medium. Following restimulation with PMA and ionomycin and treatment with Brefeldin A to retain cytokines intracellularly, cells were analyzed by flow cytometry.

Each T helper subset is associated with particular signature cytokines and a lineage-specific transcription factor. Thus, for Th17 cells, differentiation status was assessed by evaluating IL-17 and RORγt expression, the signature cytokine and master regulator transcription factor, respectively. We found that $CD4^+$ T cells polarized in low extracellular methionine had a reduced capacity to differentiate, illustrated by the decreased percentage of $ROR\gamma t^+$ and $IL\text{-}17^+$ cells in 3 μM methionine (Figure 12A and 12B). Cells grown in 3 μM methionine but given methionine at the point of restimulation yielded the same percentage of $ROR\gamma t^+$ and $IL\text{-}17^+$ cells as cells cultured in 3 μM methionine without the add-back, suggesting that although methionine is required for protein synthesis, methionine restriction plays only

a minimal role in translational regulation and likely acts at the transcriptional level to alter differentiation capacity. The geometric mean, which describes the degree of expression of IL-17, is higher for 3 μM + add-back than either the full or restricted methionine conditions (Figure 12B), suggesting that for cells that have already differentiated, additional methionine can boost translation of available transcripts. Surprisingly, there was no difference in viability between cells differentiated in full or low methionine (Figure 12C). As an additional confirmation of the flow cytometry data, we performed an ELISA to measure IL-17 levels, which revealed decreased IL-17 production from cells that had been differentiated in low methionine (Figure 12D). Gene expression analysis showed that while differences in *Il17* and *Rorc* (which encodes RORγt) between full and restricted methionine are modest, there was a dramatic increase in *Mat2a* mRNA levels (Figure 12E). The increased *Mat2a* expression in low methionine may be a compensatory upregulation for cells to capture as much methionine as possible for methylation reactions.

In contrast, Th1 differentiation in full or restricted methionine led to opposite results. The percentages of T-bet$^+$ and IFN-γ$^+$ cells are higher when naïve CD4$^+$ T cells were differentiated in low methionine (Figure 12F and 12G). The geometric mean is slightly higher for 3 μM conditions, including the add-back, compared to full methionine (Figure 12G). High methionine during the restimulation process, such as in the full and 3 μM + add-back conditions, seems to have a negative effect on viability (Figure 12H). However, despite having more T-bet$^+$ and IFN-γ$^+$ cells, ELISA data indicate that Th1 cells in low methionine produced less cytokine (Figure 12I). In addition, transcript levels of *Ifng* appeared mildly decreased in restricted methionine Th1 cells, and the reduction is even greater for *Tbx21* transcript levels. *Mat2a* upregulation in low methionine is an unvaried observation (Figure 12J). The unexpected results from flow cytometry may be due to Th1 cells failing to grow well in dialyzed serum.

Thus, differentiation in low methionine limits Th17 polarization, which is shown by decreased lineage-specific transcription factor expression and signature cytokine production. Th1 polarization in

low methionine leads to decreased transcript levels of lineage-associated factors and a reduction in secreted cytokine in low methionine, though results are inconclusive. For both cell types, methionine restriction leads to *Mat2a* upregulation.

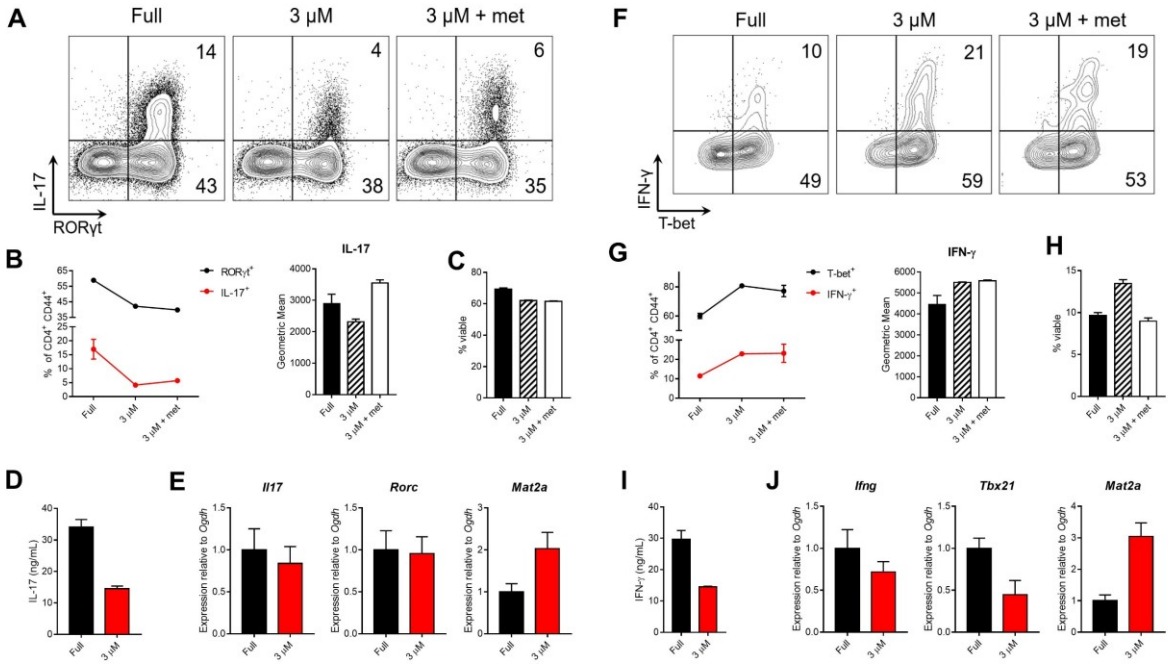

Figure 12: Low extracellular methionine reduces capacity to differentiate to Th17 lineage

A) Differentiation status of Th17 cells polarized in full or low methionine confirmed by flow cytometry. $CD4^+$ T cells were cultured in Th17-polarizing conditions for 3 or 5 days in full or 3 μM methionine. For 3 μM cultures, methionine was added back to full (200 μM) for the final 6 hours in culture, designated 3 μM + met. Flow plots are gated on activated $CD4^+$ T cells. Representative plots are from Day 3.

B) Summary of flow cytometry data. Percentage of RORγt- and IL-17-expressing cells (left) and geometric mean for IL-17 expression (right).

C) Viability of cells as determined by flow cytometry.

D) Cytokine production measured by ELISA. Supernatants were collected from Day 5 Th17 cells grown in full or 3 μM methionine to measure IL-17 production.

E) Expression of key Th17 genes and *Mat2a* as determined by qPCR. RNA was collected from Day 5 Th17 cultures grown in full or 3 μM methionine. Expression is relative to *Ogdh* mRNA levels and normalized to full condition.

F) Differentiation status of Th1 cells polarized in full or restricted methionine confirmed by flow cytometry. $CD4^+$ T cells were cultured in Th1-polarizing conditions for 3 days in full or 3 μM methionine. Methionine was added back to full condition (200 μM) for 3 μM cultures for the final 6 hours in culture, designated 3 μM + met. Plots are gated on activated $CD4^+$ cells.

G) Summary of flow cytometry data. Percentage of T-bet- and IFN-γ-expressing cells (left) and geometric mean for IFN-γ expression (right).

H) Viability of cells differentiated in full or 3 μM methionine as determined by flow cytometry.

I) Cytokine production was determined by ELISA. Supernatants from Day 3 Th1 cultures were collected to measure IFN-γ production.

J) Gene expression of key Th1 genes and *Mat2a* was measured by qPCR. RNA was collected from Th1 cultures on Day 3 and transcript levels were determined relative to *Ogdh* and normalized to full condition.

Acute methionine restriction decreases cytokine production, but not lineage identity

Since there are many reports that differentiated T cells exhibit plasticity in response to environmental stimuli [4], we sought to test whether modulating methionine levels had an impact after $CD4^+$ T cells were terminally differentiated. Naïve $CD4^+$ T cells were differentiated to the Th17 or Th1 lineage in full medium (containing undialyzed serum) for 3 days and subsequently replated in medium with methionine added back to 0 μM, 3 μM, or 200 μM. Th17 cells were subjected to acute methionine restriction for 6, 12, and 24 h. At each timepoint (data not shown for 12 and 24 h), low methionine (0 or 3 μM) led to fewer cells expressing signature cytokine IL-17, while the percentage of cells expressing the cell fate-associated transcription factor RORγt was unchanged (Figure 13A and 13B). This indicates that acute methionine restriction did not impact lineage identity (expression of master regulator RORγt) but the proportion of differentiated cells that can produce cytokine was decreased, along with the degree of

expression of cytokine as shown by the geometric mean (Figure 13B). Similar results were obtained by measuring IL-17 in the supernatant by ELISA; cytokine production was reduced in acutely starved cells compared to cells in full methionine (Figure 13D). Consistent with the other findings, mRNA transcript levels for *Rorc* (which encodes RORγt) were relatively unchanged between the cells grown in different concentrations of methionine, but *Il17* transcript levels dropped in a step-wise fashion proportional to methionine reduction (Figure 13E). Cell viability was not affected by acute methionine restriction (Figure 13C).

Likewise, for Th1 cells, data from flow cytometry indicate that the percentage of cells expressing the signature cytokine IFN-γ was decreased in conditions of methionine restriction and the lineage-specific transcription factor T-bet was not affected (Figure 13F and 13G). Both the decrease in percentage and degree of expression indicated by the geometric mean correlated with methionine concentration (Figure 13G). Less IFN-γ was secreted by cells cultured in low methionine (Figure 13I). For Th1 cells, the transcript levels of both *Ifng* and *Tbx21* (encoding T-bet) were unchanged (Figure 13J). Methionine restriction did not impact cell viability in any of the conditions (Figure 13H). Overall, like Th17 cells, acute methionine restriction on terminally differentiated Th1 cells can modulate cytokine expression without altering lineage identity.

Taken together, these data suggest that if the effect of methionine restriction on terminally differentiated T helper cells is mediated by epigenetic regulation, the remodeling occurs at the loci that encode signature cytokines, while the lineage-associated transcription factors are unchanged under conditions of acute methionine withdrawal. Cell fate is not altered but the efficacy of the cells may be impaired when acutely starved of methionine.

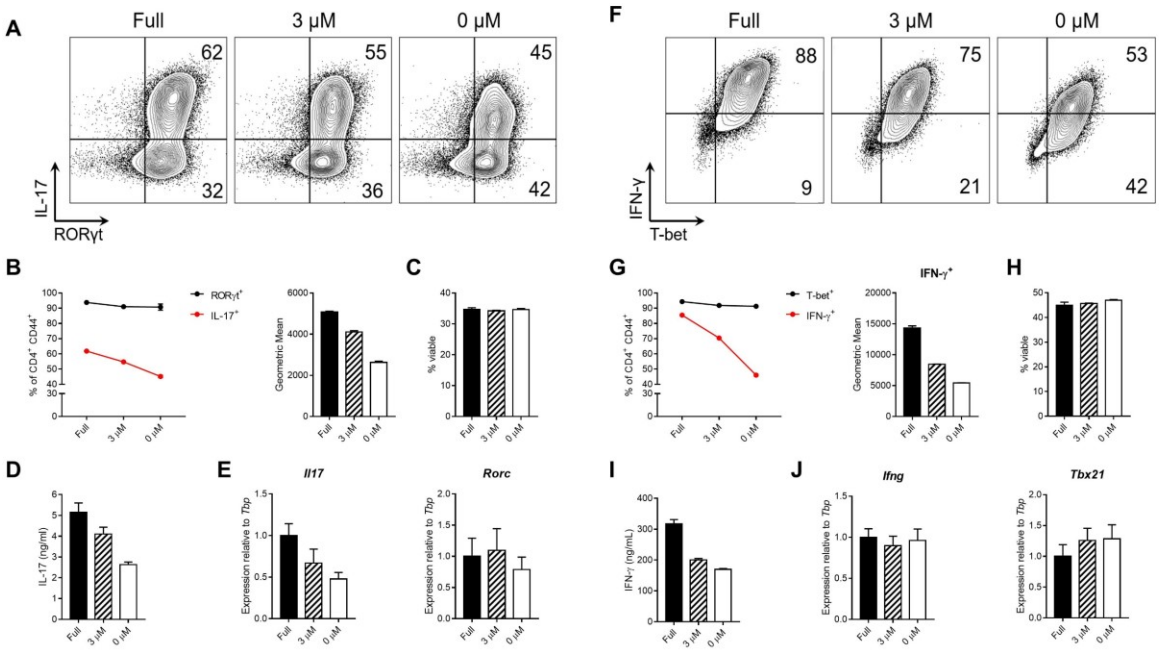

Figure 13: Acute methionine restriction impairs production of lineage-specific cytokines

A) Flow cytometry plots of acute methionine restriction of Th17 cells. Naïve $CD4^+$ T cells were polarized to the Th17 lineage for 5 days in complete medium, then replated in indicated concentrations of methionine for 6, 12, or 24 h. Representative flow plots are from 6 h methionine restriction, gated on activated $CD4^+$ cells.

B) Summary of flow cytometry data. Percentage of $ROR\gamma t^+$ and $IL\text{-}17^+$ cells (left) and geometric mean for IL-17 expression (right).

C) Viability following 6 h methionine restriction as determined by flow cytometry.

D) ELISA measurement of cytokine production. Supernatants from Th17 cells were collected following methionine restriction at each timepoint. Data shown are from 6 h methionine restriction.

E) Gene expression analysis of key Th17 genes determined by qPCR. RNA from Th17 cells was collected after duration of methionine restriction. Data shown are from 6 h.

F) Representative flow plots of Th1 cells acutely starved of methionine for 6 h. $CD4^+$ T cells were differentiated to the Th1 lineage for 3 days in full complete medium, followed by methionine starvation for 6 h. Gated on activated $CD4^+$ cells.

G) Summary of flow cytometry data. Percentage of T-bet- and IFN-γ-expressing cells (left) and geometric mean for IFN-γ expression (right).

H) Viability following methionine restriction as determined by flow cytometry.

I) Cytokine production measured by ELISA. Supernatants from Th1 cultures were collected at each timepoint after methionine restriction and analyzed for IFN-γ production.

J) Gene expression analysis of key Th1 genes was determined by qPCR. RNA was collected from Th1 cells following methionine restriction.

Dietary methionine affects the serum levels of methionine cycle metabolites

Given our observations that methionine restriction impairs *in vitro* T cell proliferation and $CD4^+$ T cell differentiation to the Th17 lineage, we next tried to determine whether methionine availability affects T cell responses *in vivo.* Recent work from our lab has shown that keeping mice on a low serine/glycine diet is sufficient to manipulate serum levels of serine and glycine, without affecting other amino acids [29]. Similarly, it has been reported that diet can alter SAM levels [23]. Thus, to restrict methionine *in vivo,* we used a pair of research diets: the control feed contained 0.86% methionine while the low methionine diet contained 0.12% methionine; both contained 10 kcal% fat. C57BL/6 mice were maintained on the diet for 8 weeks and analyzed every 2 weeks by collecting serum by cardiac puncture and liver by dissection (n = 4 per group per timepoint).

Tissue concentrations of methionine, SAM, and SAH were determined by LC-MS. We found that the low methionine diet reduced serum methionine (Figure 14A). Serum SAM and SAH were also reduced (Figure 14A), likely due to the decreased input into the methionine cycle. Mice on the low methionine diet also had decreased methionine, SAM, and SAH in the liver, though the difference was not as prominent for SAM (Figure 14B). Overall, this dietary regimen can reduce circulating levels and liver concentrations of methionine cycle metabolites in 2 weeks.

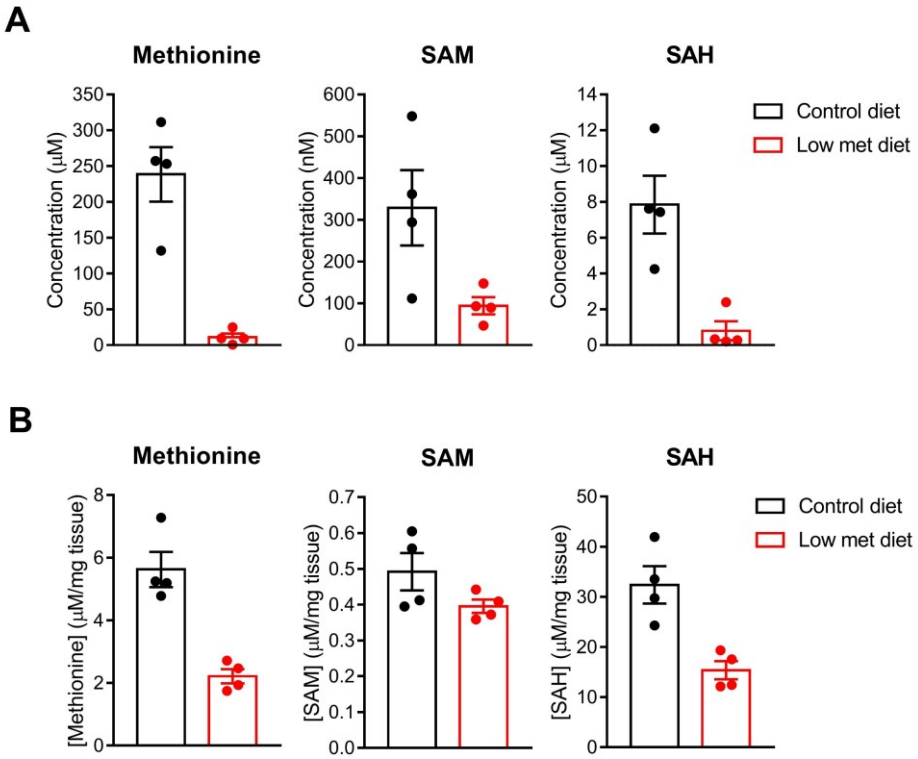

Figure 14: Circulating methionine levels are decreased on low methionine diet

A) Methionine, SAM, and SAH concentrations as measured by LC-MS from mice maintained on control or low methionine diet for 2 weeks.

B) Concentration of methionine, SAM, and SAH in the liver after 2 weeks on the control or low methionine diet. Tissue was collected from mice at time of sacrifice, weighed, and analyzed by LC-MS.

Low methionine diet does not alter immune cell proportions in secondary lymphoid organs

In the same experiment as in Figure 14, we collected the spleen, peripheral lymph nodes, and mesenteric lymph nodes from mice at the time of sacrifice to assess if the diets induced changes in immune cell composition. Flow cytometry revealed no significant difference in the percentage of $CD4^+$ and $CD8^+$ T cells, B cells, and NK cells in each organ at week 2 (Figure 15A). For innate immune cells, there was no difference in the percentage of dendritic cells, macrophages, monocytes, and neutrophils between the two feeds, though there was a decrease in eosinophil frequency in mice on the low methionine diet (Figure 15B). Thus, diet did not impact the proportions of most of the immune cells we assessed.

Considering cell numbers, the splenic T cell populations were unchanged between the control and low methionine feed. However, the average cell number for total homogenized organs differed between the two groups; the spleen cellularity was unchanged but the peripheral and mesenteric lymph nodes contained fewer cells for mice given low dietary methionine. This is shown by the decreased number of cells for a given cell type despite the unchanged percentage (Figure 15A). Cell numbers for each immune cell subset are shown in Tables 1-6. Thus, mice on the low methionine feed exhibited smaller immune compartments (PLN and MLN) than the control group, but the immune cell composition expressed as a percentage was not altered.

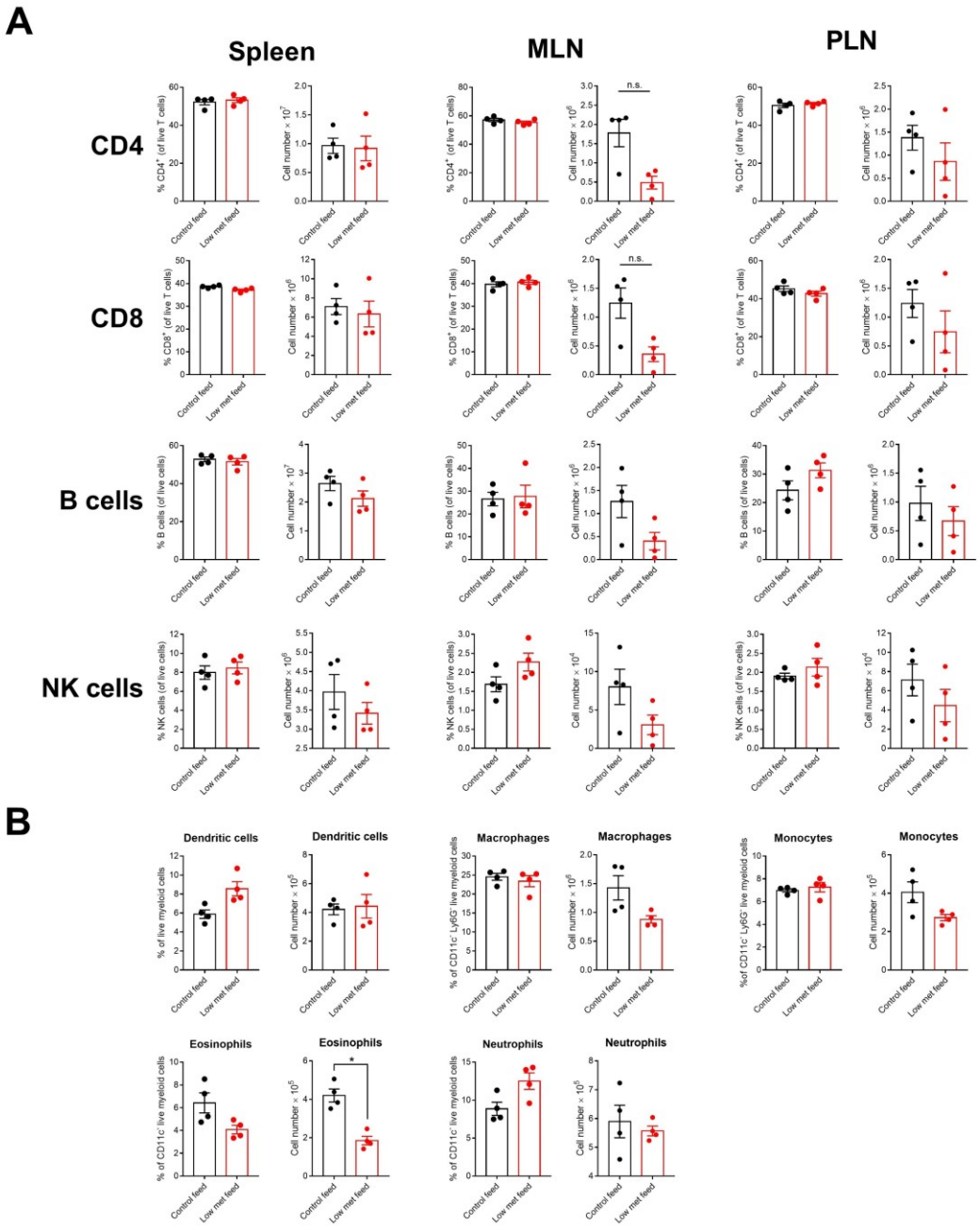

Figure 15: Low methionine diet does not alter immune cell composition in secondary lymphoid organs

A) Adaptive immune cell populations as determined by flow cytometry and cell counts. Percentage and number of $CD4^+$ and $CD8^+$ T cells, B cells, and NK cells in spleen, mesenteric lymph nodes (MLN), and peripheral lymph nodes (PLN) in mice fed a control or low methionine diet for 2 weeks. Data represent the mean ± SEM, n = 4, analyzed by Welch's t-test.

B) Innate immune cell populations from flow cytometry and cell counts. Percentage and number of dendritic cells, macrophages, monocytes, eosinophils, and neutrophils from spleen, MLN, and PLN after 2 weeks on control or low methionine diet. Data represent the mean ± SEM, n = 4, analyzed by unpaired Welch's t-test.

Low methionine *in vivo* does not attenuate OT-I response to *L. monocytogenes*

Since we observed that methionine leads to a proliferation defect for T cells *in vitro* (Figure 11) we questioned whether there would be a diminished proliferative response *in vivo.* We used *Listeria monocytogenes* as a model to measure the murine host response to bacterial infection. While this induces both $CD4^+$ and $CD8^+$ responses, the $CD8^+$ T cell response is particularly important for host protection. Mice were introduced to the control or low methionine diet approximately 2 weeks prior to adoptive transfer of $CD8^+$ OT-I T cells. These T cells have a transgenic T cell receptor that specifically recognizes OVA peptide on OVA-expressing *L. monocytogenes* (Lm-OVA) [53]. The next day, Lm-OVA were injected into mice intravenously. Mice were maintained on the diet for the duration of the experiment until analysis 7 days post-infection (Figure 16A). To track antigen-specific or host T cell cytokine production, we used the Thy1.1 and Thy1.2 markers, which are expressed by the transgenic OT-I T cells and endogenous T cells, respectively. We measured methionine, SAM, and SAH levels from serum collected from the mice on the day of sacrifice and found that methionine was decreased in mice on the low methionine diet (Figure 16B), which is similarly shown in Figure 14. However, SAM and SAH were the same between control and low methionine feed animals (Figure 16B), possibly due to physiological fluctuations in SAM and SAH when maintained on the control diet.

The data show that the $Thy1.1^+$ OT-I T cell population frequency was the same between the control and low methionine groups, both in percentage, cell number, and OT-I expression (Figure 16B

and 16C). This indicates that the cells did not demonstrate impaired proliferation in a low methionine environment. These cells produced IFN-γ, but there was no difference between the two groups in percentage, cell number, and expression (Figure 16E and 16F). The endogenous response made very minimal contributions to overall pathogen clearance and cytokine production (data not shown), likely because the antigen-specific T cells rapidly cleared the infection.

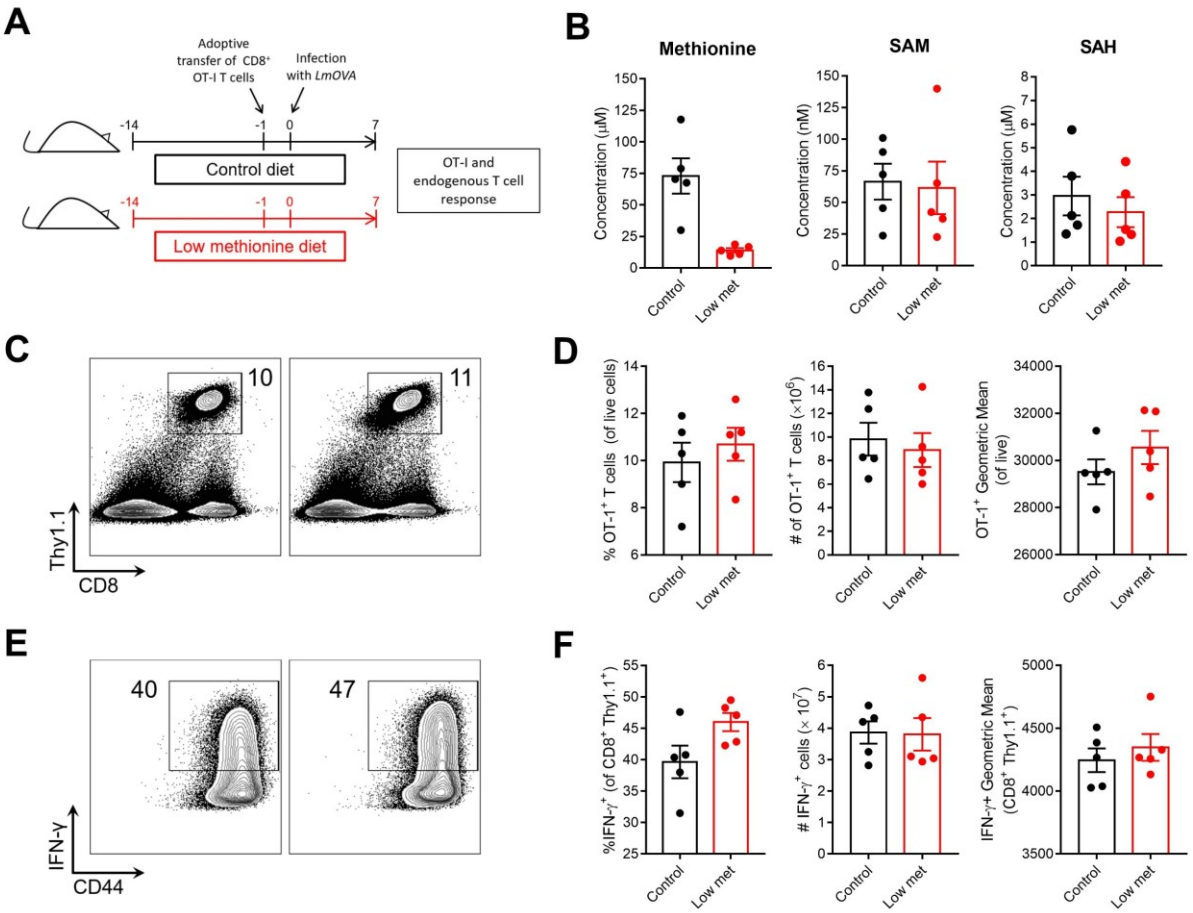

Figure 16: *In vivo* CD8$^+$ T$_{eff}$ response to *L. monocytogenes* is not impaired in low methionine

A) Schematic of the experiment. Mice were maintained on the control or low methionine feed for 2 weeks (starting Day -14). At Day -1, CD8$^+$ OT-I T cells were injected into mice. At Day 0, *L. monocytogenes* was inoculated into the host mice. The immune response was assessed 7 days post-infection.

B) Concentration of methionine, SAM, and SAH in the serum. Serum was collected from mice at time of sacrifice and analyzed by LC-MS.

C) Flow cytometry analysis of adoptively transferred OT-I T cells. Gated on live cells.

D) Bar graphs summarizing the OT-I population gated in C. Percentage (left), cell count (middle), and geometric mean (right) were determined by flow cytometry and cell counts.

E) Cytokine production was assessed by flow cytometry. Plots are gated on $CD8^+$ $Thy1.1^+$.

F) Summary of the IFN-γ producing population gated in E, showing percentage (left), cell count (middle), and geometric mean (right).

Low dietary methionine led to earlier clinical endpoints in colitic *Rag2*$^{-/-}$ mice

We next investigated a murine model primarily involving T helper cells. We assessed the induction of colitis in *Rag2*$^{-/-}$ mice, a disease driven by pathogenic Th1 and Th17 cells. Naïve ($CD4^+$ $CD45RB^{hi}$ $CD25^{lo}$) cells were obtained by cell sorting and injected intraperitoneally into recipient *Rag2*$^{-/-}$ mice. Mouse weights were tracked over the course of the experiment to monitor the clinical endpoint. We observed a reduction in mouse weight following initiation of the diet; mice had already diverged in weight prior to adoptive T cell transfer (Figure 17A). Mice on the low methionine diet lost weight over the course of 4 weeks following disease induction, while control mice maintained or only slightly increased in weight by the termination of the experiment. Change in weight was measured at least twice weekly until sacrifice at the clinical endpoint of 20% loss of body weight (from week 0) (Figure 17B). At the time of sacrifice, colon weight and length were measured (Figure 17C), revealing that the low dietary methionine group had shorter colons that weighed less. Expressed as a ratio, there was no difference between the groups in colon weight-to-length (Figure 17D), although this ratio has been used to indicate disease [56].

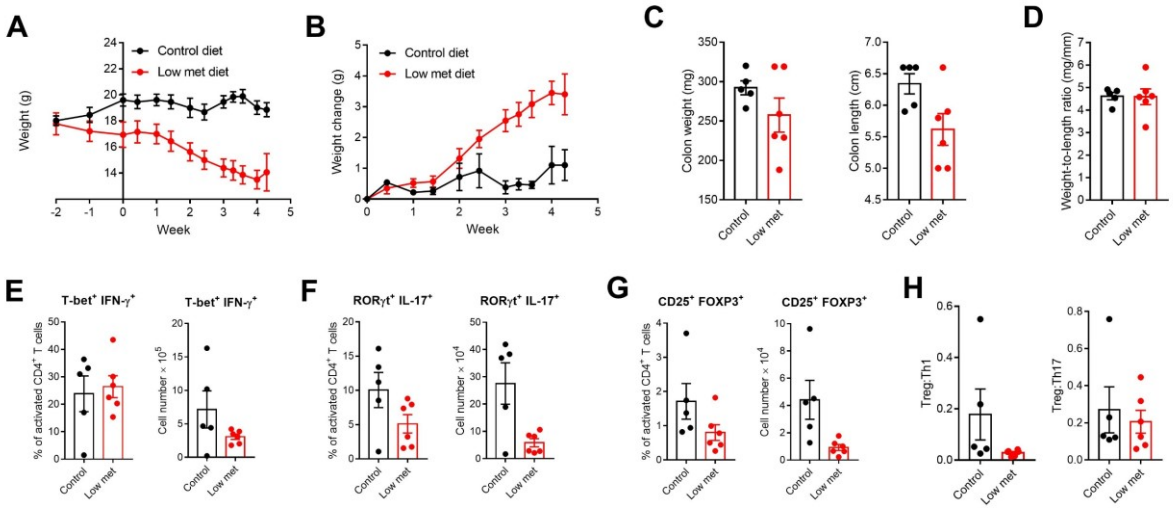

Figure 17: Induction of colitis in *Rag2*$^{-/-}$ mice

A) Mouse weight tracked through course of experiment. Mice were introduced to control or low methionine diet at Week -2, injected with $CD4^+$ $CD45RB^{hi}$ $CD25^{lo}$ T cells at Week 0, and sacrificed (due to clinical endpoint) at approximately Week 4.

B) Change in mouse weight from weight at Week 0.

C) Measurement of mouse colon weight (left) and colon length (right).

D) Ratio of colon weight to length, from B.

E) Immunophenotyping of mesenteric lymph nodes for T-bet^+ IFN-γ^+ (Th1 cells), showing percentage of cells (left) and cell number (right).

F) Analysis of MLN RORγt^+ IL-17^+ (Th17 cells) for percentage (left) and number (right).

G) Analysis of MLN $CD25^+$ $FoxP3^+$ (Treg cells) for percentage (left) and number (right).

H) Ratio of Treg to Th1 cells (left) and of Treg to Th17 cells (right) based on E-G.

At endpoint, we collected the spleen and mesenteric lymph nodes for immunophenotyping. We analyzed the immune cells for disease-inducing Th1 and Th17 cells as well as Treg cells, which play a protective role in colitis. Immunophenotyping revealed a comparable percentage of T-bet^{+} IFN-γ^{+} Th1 cells (Figure 17E), and decreased RORγt^{+} IL-17^{+} Th17 and CD25^{+} FoxP3^{+} Treg cells (Figure 17F and 17G) in mice fed the low methionine diet. However, taking cell numbers into account, all of these populations are smaller in the low methionine group, indicating a change in the size of the immune compartment (mesenteric lymph node) (Figure 17E-G).

The difference in MLN cell number from the colitis experiment prompted examination of growth of adoptively transferred CD4^{+} T cells through a homeostatic proliferation assay. Since T cells proliferate to fill a gap in the immune compartment, this assay tested the proliferative capacity of the adoptively transferred cells in environments of varying methionine concentration. As with the other *in vivo* experiments, *Rag2*$^{-/-}$ mice were maintained on the experimental diets for 2 weeks.

As observed in the colitis experiment, mice on the low methionine diet gradually began to lose weight upon initiating the diet (Figure 18A). Naïve (CD44^{lo}) CD4^{+} T cells were labeled with Violet Proliferation Dye (VPD) and purified by cell sorting, injected intravenously into recipient *Rag2*$^{-/-}$ mice, and then retrieved one week after adoptive transfer. We observed increased mesenteric and peripheral lymph node counts in mice on the low methionine diet, but comparable splenocyte counts (Figure 18B). Furthermore, the data show different proliferation patterns depending on the immune organ. In the spleen, cells had fully divided in both the control and low methionine groups. In the peripheral and mesenteric lymph nodes, the cells exhibited two modes of growth, as previously described [65] (Figure 18C). Homeostatically proliferating cells had undergone fewer divisions and expressed CD62L, but not activation markers (Figure 18E), while the spontaneous and rapidly proliferating cells had diluted out the VPD completely within the week and expressed CD44, CD25, and CD62L (Figure 18C and 18E). Surprisingly, a greater percentage of cells from mice on the low methionine diet were fully divided,

compared to more cells from the control diet group having undergone fewer divisions (Figure 18D). These data are contrary to the findings from the colitis experiment as well as *in vitro* growth curves; in particular, mesenteric lymph nodes yielded higher cell counts in the low methionine compared to the control group in this assay.

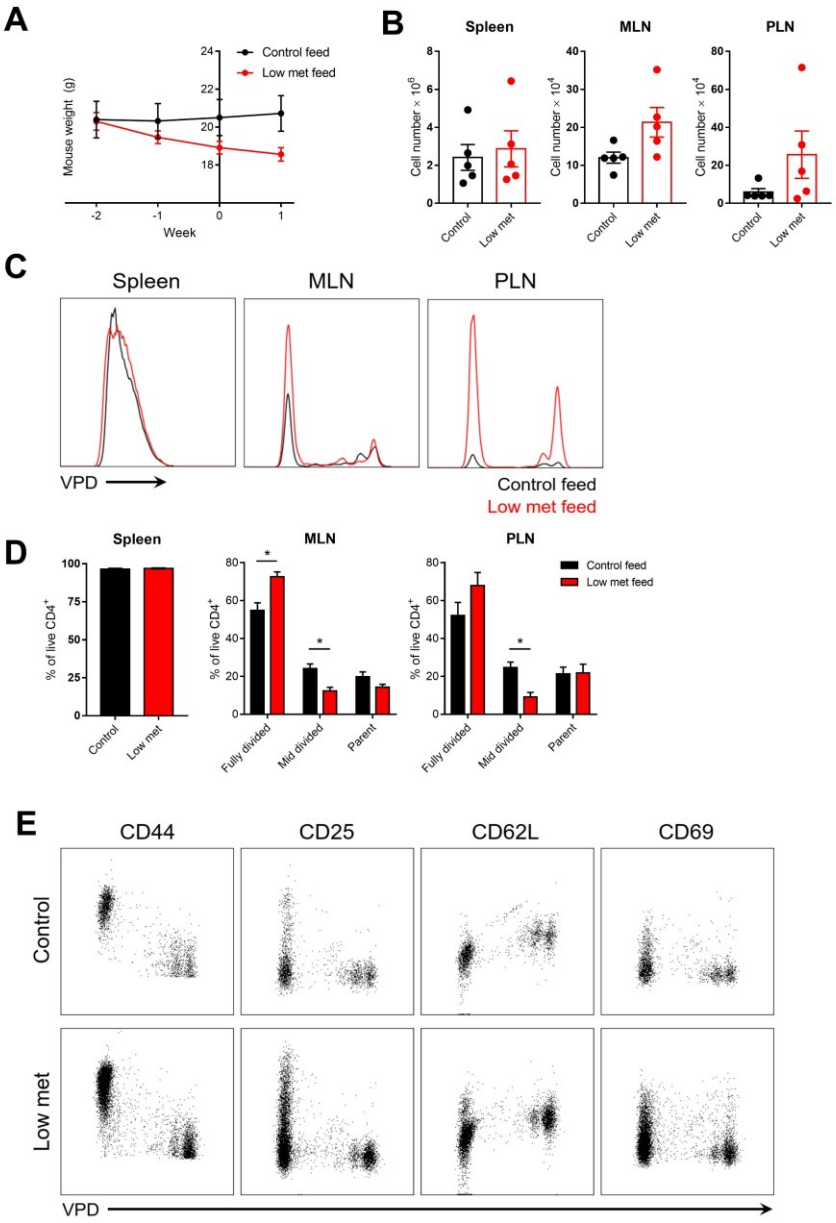

Figure 18: Homeostatic proliferation assay in *Rag2*$^{-/-}$ mice

A) Mouse weights tracked through course of experiment.

B) Cell counts from the spleen, mesenteric lymph nodes, and peripheral lymph nodes.

C) Flow plots depicting proliferation of adoptively transferred naïve CD4^{+} T cells. 1 × 10^{6} CD44^{lo} CD4^{+} T cells stained with Violet Proliferation Dye were transferred into Rag$^{-/-}$ mice maintained on control or low methionine diet. Proliferation of adoptively transferred cells was assessed one week after injection.

D) Percentage of dividing cells as determined by flow cytometry. (mean ± SEM, n = 5, analyzed by unpaired Welch's t-test)

E) Expression of activation markers determined by flow cytometry. Spleen, peripheral lymph nodes, and mesenteric lymph nodes were dissected from *Rag2*$^{-/-}$ mice one week after adoptive transfer of CD44^{lo} CD4^{+} T cells. CD4^{+} T cells were analyzed for activation markers versus proliferation.

Low dietary methionine is protective for experimental autoimmune encephalomyelitis

To further investigate the role of methionine on Th1 and Th17 cell-mediated pathogenesis, we employed the experimental autoimmune encephalomyelitis model. Using the same experimental design, mice were kept on either the control or the low methionine diet for 2 weeks prior to immunization with CFA/MOG to induce EAE. The experiment was continued for 30 days post-immunization (Figure 19A). At day 15, 2 mice from each group were analyzed for infiltrate in the central nervous system. Cell counts from the lymph nodes and spleen revealed smaller immune compartments in animals in the low methionine group, as well as fewer infiltrating cells in the central nervous system (Figure 19B). The clinical score was evaluated by examining mice daily for motor symptoms; mice on the low methionine diet had a lower clinical score, indicating lower disease severity (Figure 19C). Moreover, 7 out of 10 animals were asymptomatic in the methionine restriction group, compared to 3 out of 10 animals in the control group (Figure 19D). Thus, methionine restriction is protective in EAE, leading to lower disease incidence and severity.

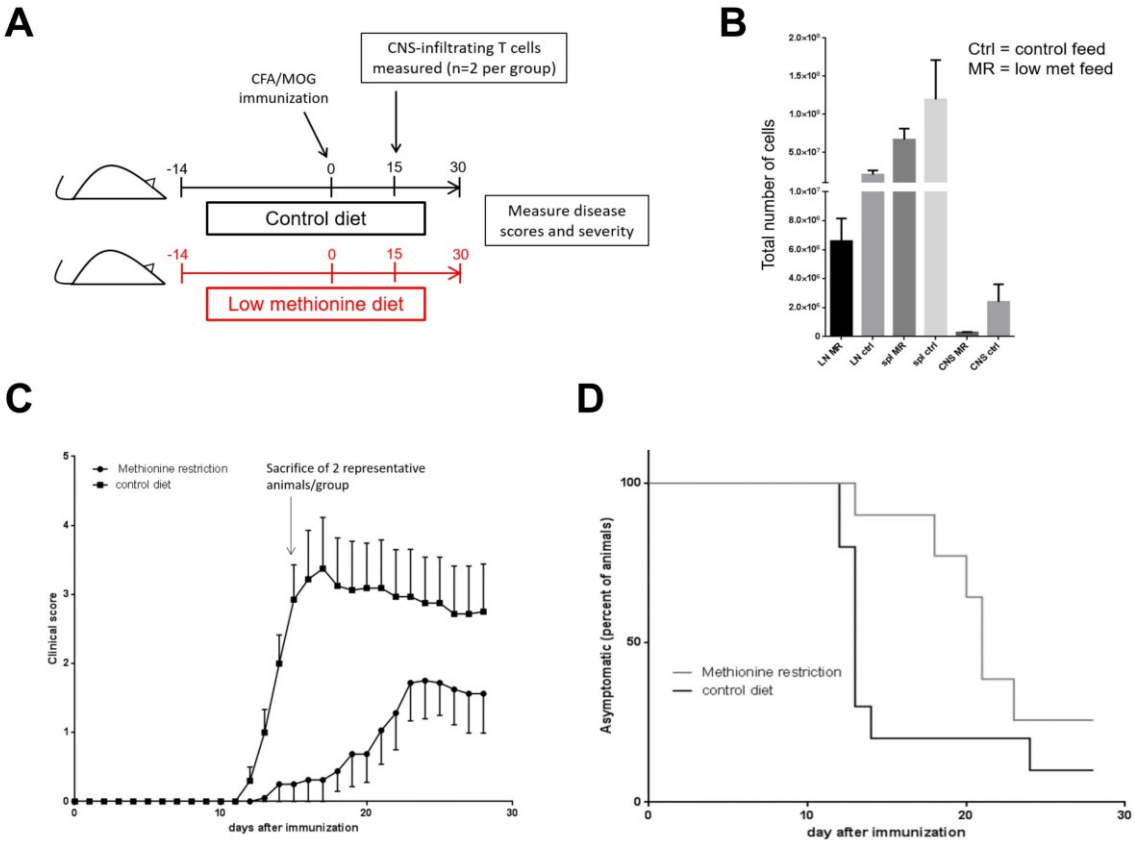

Figure 19: Reduced EAE severity in mice on low methionine diet

A) Schematic of experiment. Mice were maintained on control or low methionine diet for two weeks then immunized with CFA/MOG to induce experimental autoimmune encephalomyelitis. Disease severity was measured after 30 days, and a preliminary measurement of T cell infiltrate was made at day 15.

B) T cell infiltrate was measured at day 15 in the lymph nodes, spleen, and central nervous system.

C) Clinical score determined by daily assessment of motor symptoms.

D) Percent of animals that were asymptomatic after disease induction.

Discussion

In conclusion, I have shown that extracellular methionine is rapidly taken up by activated T cells and incorporated into the methionine cycle. Methionine is used to synthesize SAM, which is converted to SAH after donating a methyl group. Other metabolites such as glucose and serine also contribute to SAM synthesis via the production of ATP. Methionine restriction leads to decreased methionine and SAM in T cells. Due to the decreased substrate for methylation reactions, there is reduced global histone methylation for certain histone marks, particularly H3K4me3, that directly correlates with methionine concentration. Furthermore, low extracellular methionine decreases T cell proliferation, viability, and cytokine production. Similarly, polarization of naïve $CD4^+$ T cells to the Th17 lineage is impaired in low methionine, leading to cells with attenuated expression of RORγt and IL-17. This phenotype is not rescued by the addition of methionine during the restimulation step, suggesting that methionine availability may affect the cells at the transcriptional level. Acute methionine restriction in Th17 and Th1 cells shows that methionine needs to be present even after terminal differentiation to maintain signature cytokine expression, but acute withdrawal is not sufficient to change lineage identity (Figure 20).

I have shown that manipulating dietary methionine by feeding mice a control or low methionine diet leads to decreased circulating methionine. For some of the *in vivo* experiments, circulating SAM and SAH are also reduced due to the diet. However, the effect *in vivo* is not prominent in a $CD8^+$ T cell model as shown by infection with *Listeria monocytogenes*; adoptively transferred cells show no difference in proliferation nor cytokine production between the two groups. However, methionine appears to impact $CD4^+$ T cell models of disease, including the induction of colitis in *Rag2*$^{-/-}$ mice and EAE. In the colitis model, mice on the low methionine feed exhibited a more rapid loss of body weight which may be indicative of disease, as well as decreased colon length and weight without a change in the ratio. Immunophenotyping of mesenteric lymph nodes revealed a decreased percentage of Treg and Th17 cells

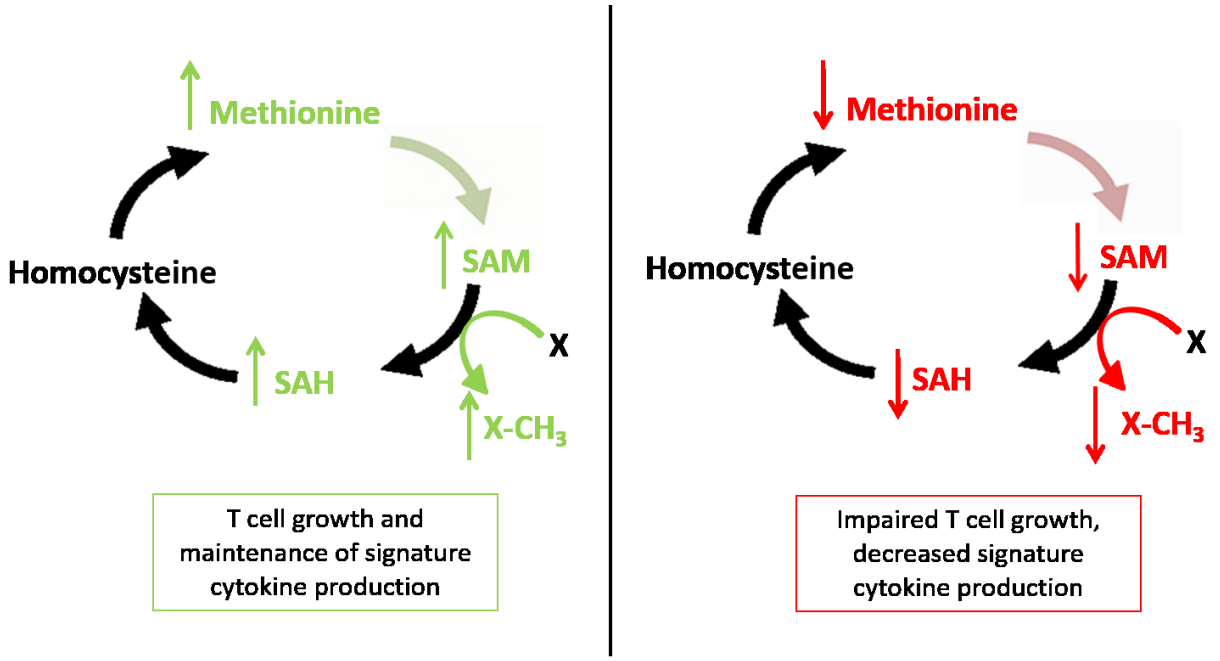

Figure 20: Summary of the effect of methionine cycle dynamics on T cell function

(Left) In sufficient methionine, there is increased flux to SAM leading to production of SAH and greater histone methylation. This promotes T cell growth and differentiation, shown by expression of signature cytokines and lineage-associated transcription factors.

(Right) When methionine is limiting, there is decreased intracellular SAM, leading to reduced histone methylation and less SAH produced. This correlates with impaired T cell proliferation, dampened expression of signature cytokines in differentiated cells, as well as decreased capacity to differentiate.

in the low methionine group, though overall MLN cell count was decreased. In contrast, in the EAE model, low dietary methionine had a protective effect and led to decreased disease severity and incidence.

Serine and methionine feed different pools for one-carbon metabolism

Evidence from the literature states that serine contributes to the methionine cycle both through remethylating homocysteine to regenerate methionine and through ATP synthesis after entry into the

folate cycle [1, 28]. My work confirms that the folate cycle and methionine cycle are uncoupled in T cells as serine labeling (from extracellular ^{13}C-serine or derived from ^{13}C-glucose) is not detected in methionine. This provides evidence against serine contributing to remethylating homocysteine to regenerate methionine and instead supports that it generates ATP for SAM synthesis. Rather than being used to regenerate methionine, homocysteine could instead be entering the transsulfuration pathway to generate glutathione to help T cells respond to oxidative stress. To test this hypothesis, we would pulse T cells with ^{13}C-methionine and examine the labeling patterns in homocysteine, cysteine, and glutathione, which are components of the transsulfuration pathway. If the hypothesis is true, we expect to see that methionine contributes to these molecules.

Methionine availability influences T cell epigenetics

T cells adapt their metabolic profile upon activation and largely rely on glucose, glutamine, and serine for growth. I provide evidence for methionine as another nutrient that impacts T cell activity as T cell proliferation and differentiation are impaired in limiting extracellular methionine. Methionine may be involved in transcriptional regulation to bring about these observations. In the Th17 long-term differentiation assay in full or 3 μM methionine, methionine is added back to the restricted condition prior to restimulation. Yet the add-back does not restore cytokine production, hinting that methionine may play roles in both translational and epigenetic regulation. In other words, despite its important role in protein synthesis, methionine may have an equivalently large impact on transcriptional regulation of T cell differentiation.

My data suggest that methionine availability may have a role in epigenetic remodeling in T cell differentiation. When a naïve CD4$^+$ T cell transitions to a differentiated state, repressive epigenetic marks need to be removed or permissive marks need to be established at loci encoding STAT proteins, cytokines, and cooperating transcription factors in order to induce and maintain the lineage. I have shown

that methionine restriction results in reduced intracellular SAM, leading to decreased global histone methylation. This could potentially prevent the opening of loci required for differentiation, preventing transcription machinery from accessing the DNA and thereby limiting gene expression. In particular, I have shown that H3K4me3 is decreased in low extracellular methionine. Loss of this permissive mark may be implicated in my observations.

Interestingly, I observed the greatest dose-dependent response of methionine on H3K4me3, compared to another mark such as H3K27me3 which is only affected slightly by methionine restriction. This is explained by the differential affinity for SAM between histone methyltransferases, which is quantitatively expressed as the Km. A lower Km indicates that a particular histone methyltransferase (HMT) has a greater affinity for SAM, which would mean that the marks it produces are more stable and more likely to be retained in methionine-restricted medium compared to those regulated by HMTs with higher Km. For example, MLL1 is a H3K4me3 methyltransferase with a higher Km than that of EZH2, a H3K27me3 methyltransferase, so one would predict a greater shift in H3K4me3 [27]. Accordingly, H3K4me3 is the more labile modification as shown in my data. In addition, this is also exemplified in mouse embryonic stem cells that require threonine catabolism to maintain histone methylation. Threonine restriction specifically decreases H3K4me2 and H3K4me3, while other marks such as H3K4me1, H3K9me3, H3K27me3, H3K36me3, and H3K79me3 were largely unchanged [47]. Thus genes regulated by specific marks may be more liable to display a shift in expression in response to methionine restriction.

Using methionine restriction as a strategy for manipulating SAM and histone methylation to induce changes in T cell activity poses other questions. Given that methionine is an essential amino acid, methionine restriction may have effects in the cell beyond decreasing histone methylation. It has been shown in human stem cells that these other effects include activation of a stress response, apoptotic pathways, and differentiation pathways [27]. This issue can be addressed by using a method that depletes

SAM in place of methionine restriction. One option is the overexpression of nicotinamide N-methyltransferase (NNMT); this enzyme methylates nicotinamide using SAM as a methyl donor to produce 1-methylnicotinamide. NNMT serves as a sink for SAM, depleting intracellular stores and shifting the SAM:SAH ratio to prevent HMT SAM usage [68].

Regulation of SAM biosynthesis in T cells

I observed a dramatic increase of *Mat2a* expression in long-term methionine restriction differentiation experiments. The upregulation in low methionine environment may help cells to pick up as much methionine as possible to maintain SAM production. This suggests that MAT2A may be a target for depleting intracellular SAM. Thus, another approach to the experiments in lieu of methionine starvation is to develop a *Mat2a* hairpin to knockdown this enzyme. This should decrease SAM production, leading to decreased H3K4me3 methylation. A caveat to this is the fact that SAM is a universal methyl donor, so methylation of other substrates could also be impaired by SAM depletion. A HMT inhibitor would be useful for targeting histone methylation specifically. Since the different histone marks have corresponding writers/readers/erasers [27], it would be informative to know which are the marks of interest to target. For example, EZH2 is a H3K27 methyltransferase and is known to bind to the *Il4/Il13* locus in Th1 cells, suppressing expression of Th2 cytokines [14]. Inhibiting EZH2 specifically would perhaps be a more effective way to target Th2 differentiation.

Conversely, rather than loss of function experiments, another objective might be to show that SAM is sufficient to restore T cell proliferation and differentiation in the absence of methionine. If successful, this would support that my observations were dependent on SAM/methylation reactions, strengthening the epigenetic argument. These experiments might involve performing a methionine starvation but adding back a SAM analog that can be taken up by cells. Another approach might be to overexpress the enzyme that converts SAH to homocysteine. The increased rate of hydrolysis of SAH

would enhance overall SAH clearance, thereby relieving product inhibition of methylation reactions. This also increases the SAM:SAH ratio and is expected to increase methylation [47].

The presence of different HMTs for different histone marks implies that there is competition for a finite amount of SAM, and maintenance of some marks will be favoured over others especially when SAM is limiting. This is determined by the Km of the HMTs. Moreover, there is also competition in the activities of HMTs and KDMs. Since histone methylation is a dynamic process, one may wish to study the interplay between histone lysine demethylases (KDMs) and HMTs (Figure 21). Methionine

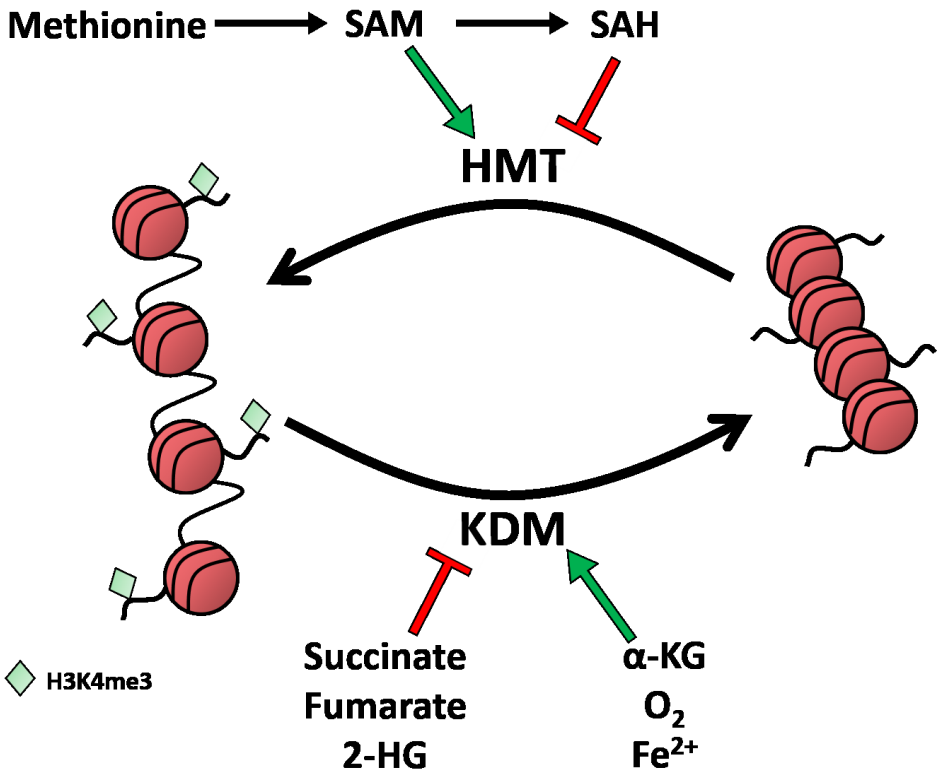

Figure 21: Balance between HMT and KDM activity regulates chromatin epigenetic state

Metabolic status is integrated into epigenetic regulation through HMT or KDM reliance on metabolites as cofactors and substrates. The interplay of HMT and KDM activity, or the addition and removal of histone methylation marks, contributes to the epigenetic landscape and conformation of chromatin.

restriction leading to decreased H3K4me3 methylation indicates that high SAM flux is needed to maintain this mark as it is also constantly being removed. Thus, there are two factors: the rate of H3K4me3 addition and the rate of its removal. To determine the relative rates of adding and removing marks, one could use inhibitors of HMTs and KDMs. KDMs require α-KG, O_2, and Fe^{2+} as cofactors, and are inhibited by succinate and fumarate. Since several of these are TCA cycle intermediates, TCA cycle flux can inhibit KDMs by the accumulation of succinate and fumarate or by the depletion of α-KG. HMTs require SAM as a substrate and are product inhibited by SAH. Inhibiting both enzymes and observing the methylation status may give an idea of the balance between HMTs and KDMs.

Methionine availability and control of T cell epigenetics

Although I observed varying degrees of global changes in histone methylation when total T cells were deprived of methionine, it remains to be elucidated which loci in particular are being epigenetically regulated. This question can be answered by performing a chromatin immunoprecipitation (ChIP) experiment. ChIP on differentiated cells will inform on where the histone methylation marks are located in the genome. Analyzing the precipitated DNA sequences bound to histone marks will identify which genes are in a poised or repressed state based on chromatin accessibility inferred by the epigenetic mark. I hypothesize that histone modifications will be grouped around key lineage genes. For example, for a Th17 differentiation, genes of interest would be IL-17 and RORγt. These may be marked by activating histone marks H3K4me3 in the promoter region, by H3K4me1 in the enhancer region, and throughout the gene body by H3K36me3. Based on reports in the literature, I expect that there will be repressive H3K27me3 marks at the loci encoding signature cytokines of alternate fates. For example, the *Ifng* or *Il4* loci may be repressed by H3K27me3 in Th17 cells. At the loci for master regulators of other cell fates, there may be bivalence – both H3K4me3 and H3K27me3 will be present at the *Tbx21* or *Foxp3* loci. Under methionine restriction, since I observed the greatest change in H3K4me3, I expect that this mark

at the *Il17* and *Rorc* promoters will be decreased, explaining their reduced expression. For an acute methionine restriction, since RORγt was unaffected but IL-17 was sensitive to the methionine starvation, I expect that the decrease in H3K4me3 will be specifically localized at the *Il17* promoter with minimal effect at the *Rorc* locus. Alternatively, the decrease in H3K4me3 could be equal at both sites, with additional epigenetic modifications mediating continued RORγt expression.

One further question is the relative contribution of different epigenetic marks. So far, I have focused on histone methylation, although other epigenetic marks can influence gene expression. Threonine tracing shows that it is incorporated into folate metabolism as 5-methyltetrahydrofolate, which supports SAM production through ATP availability. It is also used to synthesize acetyl-CoA that enters the TCA cycle [28, 47]. It is possible that this acetyl-CoA could be exerting an effect on the chromatin itself through histone acetylation. There are multiple examples of acetyl-CoA generation, which could potentially contribute to epigenetic regulation. For example, memory T cell generation of acetyl-CoA from fatty acid oxidation can be used for histone acetylation. Similarly, rapidly proliferating T_{eff} cells oxidize glucose to pyruvate; if the pyruvate is not converted to lactate, it can enter the mitochondria and be converted to acetyl-CoA. This provides a substrate for acetylating enzymes, but may also be involved for epigenetic regulation to reinforce T cell activity [7].

Dietary methionine availability and immune responses

Based on the results of Figure 16, the response to Lm-OVA infection in animals maintained on methionine-restricted diets is not hampered by the decreased serum methionine. Minimal endogenous response was detected, which may be due to a smaller immune compartment (MLN and PLN) in mice fed a low methionine diet, but this is unlikely. It is more probable that because the OT-I cells are antigen-specific, the immune response is robust and pathogen clearance is rapid despite being transferred into a

low methionine environment. The CD8 response is not impaired, but CD4 models suggest that diseases relating to T helper cell differentiation are more sensitive to methionine restriction.

Methionine restriction from manipulating diet may not be specific to T cells. Since other immune cells such as dendritic cells, monocytes, macrophages, and neutrophils are involved disease pathogenesis, we need to further investigate whether methionine restriction affects the activity of other immune cell subsets. Further studies in EAE using mice on specific feeds may take into consideration the impact of control versus low methionine diet on these other cells. Both Th1 and Th17 cells can induce and contribute to EAE. However, other immune cells contribute to the disease in concert with pathogenic T lymphocytes. For example, Th1 cells promote expression of chemokines that attract monocytes and macrophages into the CNS. Similarly, IL-23-polarized T cells (Th17 cells) promote expression of chemokines to attract neutrophils into the brain. Thus, Th1 and Th17 cells cooperate in EAE pathogenesis by recruiting other immune cells into the central nervous system [18]. DCs play an important role since they induce differentiation of $CD4^+$ T cells to the lineages that drive disease (Th1 and Th17), promote proliferation, and guide infiltration of the CNS [67]. There may also be a role for B cells because there is a correlation between oligoclonal IgG (produced by B cells) in cerebral spinal fluid and disease progression in multiple sclerosis. Like DCs, B cells are antigen-presenting cells. Moreover, differentiated B cells can produce cytokines to induce T cell differentiation and modulate the immune response by secreting IL-10 [52]. Innate lymphoid cells (ILCs) regulate intestinal immunity by promoting antimicrobial peptides and preventing bacterial infection by maintaining the integrity of the epithelial barrier [57], highlighting a potential role in colitis. Moreover, ILCs are also regulated by many of the same molecular players as T helper cells, indicating that dietary methionine is non-specific.

T cell plasticity is involved in disease pathogenesis, which is thought to involve epigenetic remodeling. Th1 and Th17 cells are thought to drive EAE and colitis, but a population of cells that are $ROR\gamma t^+$ $T\text{-}bet^+$ and produce both IL-17 and IFN-γ accumulate in the CNS for EAE and in the intestine

for colitis. Epigenetic modulators affecting the transition from Th17 cells to Th1 cells are observed in these diseases, which can impact disease progression [18, 67]. As such, since methionine can influence the epigenetic landscape, it may similarly impact disease progression. This provides the rationale for therapeutic targeting of the methionine cycle. Similarly, evidence from literature presents DNA methylation as a target in immune disorders such as rheumatoid arthritis and systemic lupus erythematosus [46]. To identify further targets, methylome mapping may be used to compare the epigenetic landscape between healthy and autoimmune disease cases in immune cells. Differences in key genes and pathways indicate therapeutic targets and epigenetic biomarkers [13].

Concluding Thoughts

In conclusion, we have found that extracellular methionine largely contributes to the intracellular methionine pool in T cells and is used to produce SAM and SAH. Methionine availability is directly linked to histone methylation, in particular H3K4me3, and in limiting methionine (< 25 μM), T cell growth and differentiation to the Th17 cell fate are impaired. Moreover, methionine is required after terminal differentiation of Th17 cells to maintain production of signature cytokine IL-17. We have observed *in vivo* that lowered dietary methionine does not attenuate the $CD8^+$ T cell response to Lm-OVA infection and has inconclusive effects in a $CD4^+$ T cell-mediated colitis model. However, low dietary methionine may be protective in EAE, as it led to lower clinical scores and more asymptomatic animals compared to the control group. Our next steps in this project are to use a MAT2A inhibitor or to knock down *Mat2a* using shRNAs to avoid the broad cellular impact of methionine restriction. This will allow us to specifically probe the role of SAM in modulating T cell epigenetics and its effect on T cell differentiation and function.

Table 1: Splenic immune cell composition by cell number for mice on control or low methionine feed

Week 2	**Control feed**		**Low met feed**		
Cell type	# cells	SEM	# cells	SEM	Significance
CD4 ($\times 10^7$)	0.96425675	0.13225216	0.91773975	0.21457320	ns
CD8 ($\times 10^6$)	7.1001775	0.833323013	6.32680325	1.343616833	ns
B cells ($\times 10^7$)	2.640505	0.248737633	2.117005	0.265417367	ns
NK cells ($\times 10^6$)	3.968075	0.454564526	3.41188	0.28220969	ns
Eosinophils ($\times 10^5$)	4.197581	0.337965413	1.849153	0.220682375	*
Neutrophils ($\times 10^5$)	5.89622075	0.564198564	5.5677215	0.170506997	ns
Macrophages ($\times 10^6$)	1.4261565	0.210928257	0.878217	0.063534975	ns
Monocytes ($\times 10^5$)	4.046958	0.544129989	2.72680125	0.161333653	ns
Dendritic cells ($\times 10^5$)	4.21190375	0.376549786	4.42529575	0.819774738	ns
Week 4	**Control feed**		**Low met feed**		
Cell type	# cells	SEM	# cells	SEM	Significance
CD4 ($\times 10^7$)	1.32245825	0.07604621	0.97107000	0.15802326	ns
CD8 ($\times 10^6$)	9.43159	0.398529941	6.640102	0.789921596	ns
B cells ($\times 10^7$)	3.860175	0.238391136	2.93973	0.276908774	ns
NK cells ($\times 10^6$)	4.51146	0.164150872	4.33989	0.314157075	ns
Eosinophils ($\times 10^5$)	5.5232465	0.957441407	6.392278	1.580517745	ns
Neutrophils ($\times 10^5$)	13.67082	0.823974488	7.3451285	0.64575904	*
Macrophages ($\times 10^6$)	1.51915225	0.037888157	1.39165825	0.106330453	ns
Monocytes ($\times 10^5$)	5.75109275	0.947106617	3.5009025	0.311202492	ns
Dendritic cells ($\times 10^5$)	4.76194025	0.22758319	4.70401625	0.630787612	ns
Week 6	**Control feed**		**Low met feed**		
Cell type	# cells	SEM	# cells	SEM	Significance
CD4 ($\times 10^7$)	1.16500000	0.05780715	1.17400000	0.19158810	ns
CD8 ($\times 10^6$)	7.86469475	0.683214234	8.28072175	1.134780949	ns
B cells ($\times 10^7$)	3.2153	0.237303524	3.66254	0.454508876	ns
NK cells ($\times 10^6$)	4.46138	0.465608579	5.940945	0.696759315	ns
Eosinophils ($\times 10^5$)	4.4148705	0.711026463	5.33452675	0.466882346	ns
Neutrophils ($\times 10^5$)	10.052197	1.263519507	9.9778405	1.524533569	ns
Macrophages ($\times 10^6$)	1.02361725	0.127427112	1.31517725	0.181522422	ns
Monocytes ($\times 10^5$)	3.1723075	0.473257561	3.353749	0.538447188	ns
Dendritic cells ($\times 10^5$)	3.0895215	0.262854785	3.758521	0.499707778	ns
Week 8	**Control feed**		**Low met feed**		
Cell type	# cells	SEM	# cells	SEM	Significance
CD4 ($\times 10^7$)	1.29280450	0.21208481	1.15813350	0.06159041	ns
CD8 ($\times 10^6$)	8.67707725	1.378079397	7.83999975	0.530802259	ns
B cells ($\times 10^7$)	3.241755	0.337256795	3.56998	0.800373704	ns
NK cells ($\times 10^6$)	5.07067	0.431876883	5.66925	0.853581812	ns
Eosinophils ($\times 10^5$)	4.946225	0.520740696	4.33336025	0.579093422	ns
Neutrophils ($\times 10^5$)	12.75573	1.354650612	10.034664	1.710800971	ns
Macrophages ($\times 10^6$)	1.3891605	0.090956188	1.40678325	0.225945113	ns
Monocytes ($\times 10^5$)	3.96512425	0.615251067	3.64690775	0.869217761	ns
Dendritic cells ($\times 10^5$)	2.7725555	0.35531253	3.0624555	0.742413469	ns

Table 2: Splenic immune cell composition by percentage for mice on control or low methionine feed

Week 2	**Control feed**		**Low met feed**		
Cell type	% of parent	SEM	% of parent	SEM	Significance
CD4 ($\times 10^7$)	52.175	1.429087704	53.225	1.247246968	ns
CD8 ($\times 10^6$)	38.625	0.286865241	37.125	0.40901304	ns
B cells ($\times 10^7$)	52.775	1.180660126	51.475	1.70361136	ns
NK cells ($\times 10^6$)	7.975	0.701694378	8.46	0.624312956	ns
Eosinophils ($\times 10^5$)	6.425	0.880165704	4.075	0.375555145	ns
Neutrophils ($\times 10^5$)	8.855	0.873522562	12.4975	1.084668728	ns
Macrophages ($\times 10^6$)	24.525	0.91047149	23.375	1.460236853	ns
Monocytes ($\times 10^5$)	6.985	0.144712358	7.265	0.413047616	ns
Dendritic cells ($\times 10^5$)	5.88	0.444597196	8.5525	0.756244835	ns
Week 4	**Control feed**		**Low met feed**		
Cell type	% of parent	SEM	% of parent	SEM	Significance
CD4 ($\times 10^7$)	52.025	0.989423233	51.7	1.547578754	ns
CD8 ($\times 10^6$)	37.2	0.801040989	35.925	0.597738795	ns
B cells ($\times 10^7$)	54.3	1.53785565	54.65	0.929605651	ns
NK cells ($\times 10^6$)	6.38	0.271661554	8.14	0.396316372	*
Eosinophils ($\times 10^5$)	7.6475	1.050106145	10.7975	2.03990349	ns
Neutrophils ($\times 10^5$)	19.15	0.983615779	12.7	0.871779789	*
Macrophages ($\times 10^6$)	29.575	2.119109483	31.8	1.775293403	ns
Monocytes ($\times 10^5$)	10.9175	1.334655855	7.98	0.453835506	ns
Dendritic cells ($\times 10^5$)	6.22	0.28777885	7.4	0.707542696	ns
Week 6	**Control feed**		**Low met feed**		
Cell type	% of parent	SEM	% of parent	SEM	Significance
CD4 ($\times 10^7$)	51.35	1.178629147	49.125	0.716908874	ns
CD8 ($\times 10^6$)	34.375	0.862530193	35.125	0.640800281	ns
B cells ($\times 10^7$)	54.7	0.267706307	56.725	0.601906693	ns
NK cells ($\times 10^6$)	7.555	0.465501522	9.235	0.297839442	ns
Eosinophils ($\times 10^5$)	8.0975	1.067023703	8.3625	0.608911255	ns
Neutrophils ($\times 10^5$)	18.4	0.524404424	15.3	1.283874345	ns
Macrophages ($\times 10^6$)	25.55	1.540833108	26.675	2.324641549	ns
Monocytes ($\times 10^5$)	7.89	0.428135493	6.7225	0.40905124	ns
Dendritic cells ($\times 10^5$)	5.4375	0.364036972	5.46	0.38839413	ns
Week 8	**Control feed**		**Low met feed**		
Cell type	% of parent	SEM	% of parent	SEM	Significance
CD4 ($\times 10^7$)	51.075	0.996138377	51.025	1.168599589	ns
CD8 ($\times 10^6$)	34.4	0.550757055	34.45	0.673918887	ns
B cells ($\times 10^7$)	52.575	1.314264687	54.625	3.29276353	ns
NK cells ($\times 10^6$)	8.33	0.600805016	8.975	0.736404554	ns
Eosinophils ($\times 10^5$)	7.8375	0.353797847	7.11	0.525372883	ns
Neutrophils ($\times 10^5$)	20.225	0.654949107	16.2	1.017349497	*
Macrophages ($\times 10^6$)	30.95	0.673918887	29.725	3.335009995	ns
Monocytes ($\times 10^5$)	8.69	0.819725564	7.4625	0.784457084	ns
Dendritic cells ($\times 10^5$)	4.24	0.51128922	4.5525	0.501653516	ns

Table 3: Peripheral lymph node immune cell composition by cell number for mice on control or low methionine feed

Week 2	**Control feed**		**Low met feed**		
Cell type	# cells	SEM	# cells	SEM	Significance
CD4 ($\times 10^6$)	1.379472	0.269129	0.86051	0.405804	ns
CD8 ($\times 10^6$)	1.237198	0.243151	0.744711	0.363263	ns
B cells ($\times 10^6$)	0.976215	0.297113	0.66805	0.251635	ns
NK cells ($\times 10^4$)	7.1218	1.64972	4.45651	1.686417	ns
Week 4	**Control feed**		**Low met feed**		
Cell type	# cells	SEM	# cells	SEM	Significance
CD4 ($\times 10^6$)	1.781247	0.323744	0.908387	0.367039	ns
CD8 ($\times 10^6$)	1.489815	0.281729	0.758984	0.274726	ns
B cells ($\times 10^6$)	1.613425	0.32754	0.769603	0.260812	ns
NK cells ($\times 10^4$)	7.637075	1.588296	3.942275	1.377094	ns
Week 6	**Control feed**		**Low met feed**		
Cell type	# cells	SEM	# cells	SEM	Significance
CD4 ($\times 10^6$)	1.317781	0.314106	1.02788	0.17604	ns
CD8 ($\times 10^6$)	1.08057	0.257512	0.842998	0.101293	ns
B cells ($\times 10^6$)	1.068065	0.171737	0.726118	0.177353	ns
NK cells ($\times 10^4$)	6.60975	1.365184	4.4375	0.972907	ns
Week 8	**Control feed**		**Low met feed**		
Cell type	# cells	SEM	# cells	SEM	Significance
CD4 ($\times 10^6$)	1.239988	0.139932	1.106313	0.196286	ns
CD8 ($\times 10^6$)	0.951393	0.146926	0.90528	0.193731	ns
B cells ($\times 10^6$)	0.914348	0.120669	1.061553	0.302678	ns
NK cells ($\times 10^4$)	5.2713	0.246377	7.3026	1.573911	ns

Table 4: Peripheral lymph node immune cell composition expressed as a percentage for mice on control or low methionine feed

Week 2	**Control feed**		**Low met feed**		
Cell type	% of parent	SEM	% of parent	SEM	Significance
CD4 ($\times 10^6$)	50.45	1.1736695	51.45	0.6020797	ns
CD8 ($\times 10^6$)	45.25	1.4608787	42.65	1.3079883	ns
B cells ($\times 10^6$)	24.3	3.3254072	31.325	2.5840456	ns
NK cells ($\times 10^4$)	1.9025	0.0739792	2.135	0.2320381	ns
Week 4	**Control feed**		**Low met feed**		
Cell type	% of parent	SEM	% of parent	SEM	Significance
CD4 ($\times 10^6$)	51.875	0.6485561	48.775	0.9259005	ns
CD8 ($\times 10^6$)	43.075	1.6479153	43.675	2.2521749	ns
B cells ($\times 10^6$)	31.875	1.9508011	30.975	2.0531987	ns
NK cells ($\times 10^4$)	1.47	0.073598	1.5925	0.0625	ns
Week 6	**Control feed**		**Low met feed**		
Cell type	% of parent	SEM	% of parent	SEM	Significance
CD4 ($\times 10^6$)	50	0.7106335	51.85	1.1109305	ns
CD8 ($\times 10^6$)	40.875	2.3924795	43.4	1.0977249	ns
B cells ($\times 10^6$)	30.825	2.5335663	26.25	1.7153717	ns
NK cells ($\times 10^4$)	1.865	0.1678044	1.62	0.0701189	ns
Week 8	**Control feed**		**Low met feed**		
Cell type	% of parent	SEM	% of parent	SEM	Significance
CD4 ($\times 10^6$)	52.825	0.9885806	48.65	2.413331	ns
CD8 ($\times 10^6$)	39.8	2.1809784	38.725	1.3393873	ns
B cells ($\times 10^6$)	28.325	1.0225581	31.675	3.0310545	ns
NK cells ($\times 10^4$)	1.7125	0.2174617	2.36	0.2965074	ns

Table 5: Mesenteric lymph node immune cell composition by cell number for mice on control or low methionine feed

Week 2	**Control feed**		**Low met feed**		
Cell type	# cells	SEM	# cells	SEM	Significance
CD4 ($\times 10^6$)	1.777806	0.357558	0.485145	0.166415	ns
CD8 ($\times 10^6$)	1.242956	0.263209	0.35645	0.12699	ns
B cells ($\times 10^6$)	1.260088	0.350372	0.400209	0.190272	ns
NK cells ($\times 10^4$)	8.005225	2.297792	3.055288	1.2807	ns
Week 4	**Control feed**		**Low met feed**		
Cell type	# cells	SEM	# cells	SEM	Significance
CD4 ($\times 10^6$)	2.190345	0.192874	1.732525	0.331765	ns
CD8 ($\times 10^6$)	1.537837	0.185199	1.223362	0.182031	ns
B cells ($\times 10^6$)	1.71877	0.186152	1.365988	0.278356	ns
NK cells ($\times 10^4$)	7.811575	1.053207	6.630875	1.010933	ns
Week 6	**Control feed**		**Low met feed**		
Cell type	# cells	SEM	# cells	SEM	Significance
CD4 ($\times 10^6$)	1.759331	0.184327	1.517076	0.335842	ns
CD8 ($\times 10^6$)	1.207028	0.111369	1.107245	0.26392	ns
B cells ($\times 10^6$)	1.189445	0.189522	1.178758	0.314353	ns
NK cells ($\times 10^4$)	6.232125	0.901132	7.807475	1.743599	ns
Week 8	**Control feed**		**Low met feed**		
Cell type	# cells	SEM	# cells	SEM	Significance
CD4 ($\times 10^6$)	1.704291	0.235041	1.096902	0.230222	ns
CD8 ($\times 10^6$)	1.147354	0.156568	0.72105	0.124458	ns
B cells ($\times 10^6$)	1.196678	0.299763	0.82318	0.197327	ns
NK cells ($\times 10^4$)	6.552075	1.468068	5.39845	1.018607	ns

Table 6: Mesenteric lymph node immune cell composition expressed as a percentage for mice on control or low methionine feed

Week 2	**Control feed**		**Low met feed**		
Cell type	% of parent	SEM	% of parent	SEM	Significance
CD4 ($\times 10^6$)	57.075	1.1513579	55.3	0.9398581	ns
CD8 ($\times 10^6$)	39.65	1.1086779	40.575	0.9222933	ns
B cells ($\times 10^6$)	26.55	2.9485872	27.675	4.9498106	ns
NK cells ($\times 10^4$)	1.685	0.1961505	2.27	0.2350886	ns
Week 4	**Control feed**		**Low met feed**		
Cell type	% of parent	SEM	% of parent	SEM	Significance
CD4 ($\times 10^6$)	56.675	0.8929119	55.625	1.2658166	ns
CD8 ($\times 10^6$)	39.375	0.748749	40.35	1.179336	ns
B cells ($\times 10^6$)	30.05	0.9596006	29.35	2.4339611	ns
NK cells ($\times 10^4$)	1.3525	0.0690863	1.485	0.0504149	ns
Week 6	**Control feed**		**Low met feed**		
Cell type	% of parent	SEM	% of parent	SEM	Significance
CD4 ($\times 10^6$)	56.825	1.0217428	55.475	0.7542933	ns
CD8 ($\times 10^6$)	39.1	0.8878814	40.1	0.8831761	ns
B cells ($\times 10^6$)	27.225	3.0001042	28.65	1.3431927	ns
NK cells ($\times 10^4$)	1.42	0.110227	1.97	0.0924662	*
Week 8	**Control feed**		**Low met feed**		
Cell type	% of parent	SEM	% of parent	SEM	Significance
CD4 ($\times 10^6$)	57.475	0.4269563	57.075	1.0804127	ns
CD8 ($\times 10^6$)	38.7	0.341565	38.475	1.24591	ns
B cells ($\times 10^6$)	27.25	2.357435	28.95	2.0645823	ns
NK cells ($\times 10^4$)	1.515	0.1310534	1.9775	0.1552619	ns

References

1. Yang, M. and K.H. Vousden, *Serine and one-carbon metabolism in cancer.* Nat Rev Cancer, 2016. **16**(10): p. 650-62.
2. Lee, C.G., A. Sahoo, and S.H. Im, *Epigenetic regulation of cytokine gene expression in T lymphocytes.* Yonsei Med J, 2009. **50**(3): p. 322-30.
3. Zhang, Y. and D. Reinberg, *Transcription regulation by histone methylation: interplay between different covalent modifications of the core histone tails.* Genes Dev, 2001. **15**(18): p. 2343-60.
4. Nakayamada, S., et al., *Helper T cell diversity and plasticity.* Curr Opin Immunol, 2012. **24**(3): p. 297-302.
5. Chaplin, D.D., *Overview of the immune response.* J Allergy Clin Immunol, 2010. **125**(2 Suppl 2): p. S3-23.
6. Parkin, J. and B. Cohen, *An overview of the immune system.* Lancet, 2001. **357**(9270): p. 1777-89.
7. Pearce, E.L., et al., *Fueling immunity: insights into metabolism and lymphocyte function.* Science, 2013. **342**(6155): p. 1242454.
8. Sallusto, F. and A. Lanzavecchia, *The instructive role of dendritic cells on T-cell responses.* Arthritis Res, 2002. **4 Suppl 3**: p. S127-32.
9. Blagih, J., et al., *The energy sensor AMPK regulates T cell metabolic adaptation and effector responses in vivo.* Immunity, 2015. **42**(1): p. 41-54.
10. Almeida, L., et al., *Metabolic pathways in T cell activation and lineage differentiation.* Semin Immunol, 2016. **28**(5): p. 514-524.
11. Noble, A., et al., *The balance of protein kinase C and calcium signaling directs T cell subset development.* J Immunol, 2000. **164**(4): p. 1807-13.
12. O'Shea, J.J., et al., *Genomic views of STAT function in CD4+ T helper cell differentiation.* Nat Rev Immunol, 2011. **11**(4): p. 239-50.
13. Tripathi, S.K. and R. Lahesmaa, *Transcriptional and epigenetic regulation of T-helper lineage specification.* Immunol Rev, 2014. **261**(1): p. 62-83.
14. Hirahara, K., et al., *Helper T-cell differentiation and plasticity: insights from epigenetics.* Immunology, 2011. **134**(3): p. 235-45.
15. Usui, T., et al., *GATA-3 suppresses Th1 development by downregulation of Stat4 and not through effects on IL-12Rbeta2 chain or T-bet.* Immunity, 2003. **18**(3): p. 415-28.
16. Li, P., et al., *Complex interactions of transcription factors in mediating cytokine biology in T cells.* Immunol Rev, 2014. **261**(1): p. 141-56.
17. Brucklacher-Waldert, V., et al., *Tbet or Continued RORgammat Expression Is Not Required for Th17-Associated Immunopathology.* J Immunol, 2016. **196**(12): p. 4893-904.
18. Fletcher, J.M., et al., *T cells in multiple sclerosis and experimental autoimmune encephalomyelitis.* Clin Exp Immunol, 2010. **162**(1): p. 1-11.
19. Han, L., et al., *Th17 cells in autoimmune diseases.* Front Med, 2015. **9**(1): p. 10-9.
20. Hegazy, A.N., et al., *Interferons direct Th2 cell reprogramming to generate a stable GATA-3(+)T-bet(+) cell subset with combined Th2 and Th1 cell functions.* Immunity, 2010. **32**(1): p. 116-28.
21. Zhou, X., et al., *Instability of the transcription factor Foxp3 leads to the generation of pathogenic memory T cells in vivo.* Nat Immunol, 2009. **10**(9): p. 1000-7.
22. Goldberg, A.D., C.D. Allis, and E. Bernstein, *Epigenetics: a landscape takes shape.* Cell, 2007. **128**(4): p. 635-8.
23. Lu, C. and C.B. Thompson, *Metabolic regulation of epigenetics.* Cell Metab, 2012. **16**(1): p. 9-17.

24. Rosl, F., et al., *The effect of DNA methylation on gene regulation of human papillomaviruses.* J Gen Virol, 1993. **74 (Pt 5)**: p. 791-801.
25. Dantas Machado, A.C., et al., *Evolving insights on how cytosine methylation affects protein-DNA binding.* Brief Funct Genomics, 2015. **14**(1): p. 61-73.
26. Hirahara, K., et al., *Mechanisms underlying helper T-cell plasticity: implications for immune-mediated disease.* J Allergy Clin Immunol, 2013. **131**(5): p. 1276-87.
27. Mentch, S.J. and J.W. Locasale, *One-carbon metabolism and epigenetics: understanding the specificity.* Ann N Y Acad Sci, 2016. **1363**(1): p. 91-8.
28. Maddocks, O.D., et al., *Serine Metabolism Supports the Methionine Cycle and DNA/RNA Methylation through De Novo ATP Synthesis in Cancer Cells.* Mol Cell, 2016. **61**(2): p. 210-21.
29. Ma, E.H., et al., *Serine Is an Essential Metabolite for Effector T Cell Expansion.* Cell Metab, 2017. **25**(2): p. 345-357.
30. Wang, R. and D.R. Green, *Metabolic reprogramming and metabolic dependency in T cells.* Immunol Rev, 2012. **249**(1): p. 14-26.
31. Maddocks, O.D., et al., *Serine starvation induces stress and p53-dependent metabolic remodelling in cancer cells.* Nature, 2013. **493**(7433): p. 542-6.
32. Andrejeva, G. and J.C. Rathmell, *Similarities and Distinctions of Cancer and Immune Metabolism in Inflammation and Tumors.* Cell Metab, 2017. **26**(1): p. 49-70.
33. Sinclair, L.V., et al., *Control of amino-acid transport by antigen receptors coordinates the metabolic reprogramming essential for T cell differentiation.* Nat Immunol, 2013. **14**(5): p. 500-8.
34. Chen, H., et al., *Cellular metabolism on T-cell development and function.* Int Rev Immunol, 2015. **34**(1): p. 19-33.
35. Wang, R., et al., *The transcription factor Myc controls metabolic reprogramming upon T lymphocyte activation.* Immunity, 2011. **35**(6): p. 871-82.
36. Michalek, R.D., et al., *Cutting edge: distinct glycolytic and lipid oxidative metabolic programs are essential for effector and regulatory CD4+ T cell subsets.* J Immunol, 2011. **186**(6): p. 3299-303.
37. van der Windt, G.J., et al., *Mitochondrial respiratory capacity is a critical regulator of CD8+ T cell memory development.* Immunity, 2012. **36**(1): p. 68-78.
38. Griss, T., et al., *Metformin Antagonizes Cancer Cell Proliferation by Suppressing Mitochondrial-Dependent Biosynthesis.* PLoS Biol, 2015. **13**(12): p. e1002309.
39. Locasale, J.W., *Serine, glycine and one-carbon units: cancer metabolism in full circle.* Nat Rev Cancer, 2013. **13**(8): p. 572-83.
40. Labuschagne, C.F., et al., *Serine, but not glycine, supports one-carbon metabolism and proliferation of cancer cells.* Cell Rep, 2014. **7**(4): p. 1248-58.
41. Davis, S.R., et al., *Tracer-derived total and folate-dependent homocysteine remethylation and synthesis rates in humans indicate that serine is the main one-carbon donor.* Am J Physiol Endocrinol Metab, 2004. **286**(2): p. E272-9.
42. Xiao, M., et al., *Inhibition of alpha-KG-dependent histone and DNA demethylases by fumarate and succinate that are accumulated in mutations of FH and SDH tumor suppressors.* Genes Dev, 2012. **26**(12): p. 1326-38.
43. Wellen, K.E., et al., *ATP-citrate lyase links cellular metabolism to histone acetylation.* Science, 2009. **324**(5930): p. 1076-80.
44. Rossetto, D., N. Avvakumov, and J. Cote, *Histone phosphorylation: a chromatin modification involved in diverse nuclear events.* Epigenetics, 2012. **7**(10): p. 1098-108.
45. Kinnaird, A., et al., *Metabolic control of epigenetics in cancer.* Nat Rev Cancer, 2016. **16**(11): p. 694-707.

46. Li, H., et al., *Targeting methionine cycle as a potential therapeutic strategy for immune disorders.* Expert Opin Ther Targets, 2017: p. 1-17.
47. Shyh-Chang, N., et al., *Influence of threonine metabolism on S-adenosylmethionine and histone methylation.* Science, 2013. **339**(6116): p. 222-6.
48. Mentch, S.J., et al., *Histone Methylation Dynamics and Gene Regulation Occur through the Sensing of One-Carbon Metabolism.* Cell Metab, 2015. **22**(5): p. 861-73.
49. Schmidt, T. and M. Sester, *Detection of antigen-specific T cells based on intracellular cytokine staining using flow-cytometry.* Methods Mol Biol, 2013. **1064**: p. 267-74.
50. Yin, Y., A. Mitson-Salazar, and C. Prussin, *Detection of Intracellular Cytokines by Flow Cytometry.* Curr Protoc Immunol, 2015. **110**: p. 6.24.1-18.
51. Chatila, T., et al., *Mechanisms of T cell activation by the calcium ionophore ionomycin.* J Immunol, 1989. **143**(4): p. 1283-9.
52. Robinson, A.P., et al., *The experimental autoimmune encephalomyelitis (EAE) model of MS: utility for understanding disease pathophysiology and treatment.* Handb Clin Neurol, 2014. **122**: p. 173-89.
53. Condotta, S.A., et al., *Probing CD8 T cell responses with Listeria monocytogenes infection.* Adv Immunol, 2012. **113**: p. 51-80.
54. Khan, S.H. and V.P. Badovinac, *Listeria monocytogenes: a model pathogen to study antigen-specific memory CD8 T cell responses.* Semin Immunopathol, 2015. **37**(3): p. 301-10.
55. Chassaing, B., et al., *Dextran sulfate sodium (DSS)-induced colitis in mice.* Curr Protoc Immunol, 2014. **104**: p. Unit 15.25.
56. Ostanin, D.V., et al., *T cell transfer model of chronic colitis: concepts, considerations, and tricks of the trade.* Am J Physiol Gastrointest Liver Physiol, 2009. **296**(2): p. G135-46.
57. Brasseit, J., et al., *CD4 T cells are required for both development and maintenance of disease in a new mouse model of reversible colitis.* Mucosal Immunol, 2016. **9**(3): p. 689-701.
58. Ostanin, D.V., et al., *T cell-induced inflammation of the small and large intestine in immunodeficient mice.* Am J Physiol Gastrointest Liver Physiol, 2006. **290**(1): p. G109-19.
59. Song-Zhao, G.X. and K.J. Maloy, *Experimental mouse models of T cell-dependent inflammatory bowel disease.* Methods Mol Biol, 2014. **1193**: p. 199-211.
60. Shinkai, Y., et al., *RAG-2-deficient mice lack mature lymphocytes owing to inability to initiate V(D)J rearrangement.* Cell, 1992. **68**(5): p. 855-67.
61. Mombaerts, P., et al., *RAG-1-deficient mice have no mature B and T lymphocytes.* Cell, 1992. **68**(5): p. 869-77.
62. Surh, C.D. and J. Sprent, *T-cell apoptosis detected in situ during positive and negative selection in the thymus.* Nature, 1994. **372**(6501): p. 100-3.
63. Tan, J.T., et al., *IL-7 is critical for homeostatic proliferation and survival of naive T cells.* Proc Natl Acad Sci U S A, 2001. **98**(15): p. 8732-7.
64. Schuster, K., et al., *Homeostatic proliferation of naive CD8+ T cells depends on CD62L/L-selectin-mediated homing to peripheral LN.* Eur J Immunol, 2009. **39**(11): p. 2981-90.
65. Min, B., et al., *Spontaneous and homeostatic proliferation of CD4 T cells are regulated by different mechanisms.* J Immunol, 2005. **174**(10): p. 6039-44.
66. Bittner, S., et al., *Myelin oligodendrocyte glycoprotein (MOG35-55) induced experimental autoimmune encephalomyelitis (EAE) in C57BL/6 mice.* J Vis Exp, 2014(86).
67. Yen, J.H., et al., *Higher susceptibility to experimental autoimmune encephalomyelitis in Muc1-deficient mice is associated with increased Th1/Th17 responses.* Brain Behav Immun, 2013. **29**: p. 70-81.
68. Wong, C.C., Y. Qian, and J. Yu, *Interplay between epigenetics and metabolism in oncogenesis: mechanisms and therapeutic approaches.* Oncogene, 2017. **36**(24): p. 3359-3374.